Search for Rare and Forbidden Dilepton Decays of D^+, D_s^+ and D^0

David Sanders

Abstract:

We report the results of a search for flavor-changing neutral-current (FCNC), lepton number violating (LNV) and lepton family violating (LFV) decays of D^+, D_s^+ and D^0 (and their antiparticles) into modes containing muons and electrons. The results come from Fermilab charm hadroproduction experiment E791. For D^+ we examined the decay modes $D^+ \to \pi\ell\ell$ and $D^+ \to K^+\ell^\pm\ell^\mp$. For D_s^+ we examined the decay modes $D_s^+ \to K\ell\ell$ and $D_s^+ \to \pi\ell\ell$. For D^0 we examined the decay modes $D^0 \to \ell^\pm\ell^\mp$. We present upper limits on the branching fractions at the 90% confidence level. These upper limits provide significant improvements over published results.

Offline_doc_393

Version 3.7

May 19, 1999

Table of Contents:

Introduction

This analysis is a continuation of work started by others in this collaboration[1-2]. This current method uses a "blind" or "closed box" technique where first one optimizes the cuts while excluding the data signal region and then later one opens the "box". The original code was incorporated in a substrip package called SELECT_REGULAR[1]. There is one major change, the use of the muon quality and distance cuts described by Chong Zhang[3] to improve muon identification by using more of the TDC information. There were also a few minor changes to the original cuts and some additional cuts that were suggested at previous collaboration meetings. These changes to the SELECT_REGULAR code were implemented in my Ntuple writing package SELECT_NTUP, which was based on SELECT_REGULAR. To set my cuts I used Monte Carlo "signal" and wing-data (outside the "box") background and then optimized the Monte Carlo "signal" versus the square root of the background e.g. $MC/\sqrt{Bkgnd}$.

The decay modes (and those of their antiparticles) that were examined are described in Table 1. The two underlined modes have already been published by E791. See Figure 1, Figure 2, and Figure 3 for the Feynman Diagrams.

Table 1: Decay Modes Examined

FCNC	**LFV**	**LNV**
$\underline{D^+ \to \pi^+ \mu^+ \mu^-}$	$D^+ \to \pi^+ \mu^\pm e^\mp$	$D^+ \to \pi^- \mu^+ \mu^+$
$\underline{D^+ \to \pi^+ e^+ e^-}$	$D^+ \to \pi^- \mu^+ e^+$	$D^+ \to \pi^- e^+ e^+$
$D^+ \to K^+ \mu^+ \mu^-$	$D^+ \to K^+ \mu^\pm e^\mp$	$D_s^+ \to K^- \mu^+ \mu^+$
$D^+ \to K^+ e^+ e^-$	$D_s^+ \to K^+ \mu^\pm e^\mp$	$D_s^+ \to K^- e^+ e^+$
$D_s^+ \to K^+ \mu^+ \mu^-$	$D_s^+ \to K^- \mu^+ e^+$	$D_s^+ \to \pi^- \mu^+ \mu^+$
$D_s^+ \to K^+ e^+ e^-$	$D_s^+ \to \pi^+ \mu^\pm e^\mp$	$D_s^+ \to \pi^- e^+ e^+$
$D_s^+ \to \pi^+ \mu^+ \mu^-$	$D_s^+ \to \pi^- \mu^+ e^+$	
$D_s^+ \to \pi^+ e^+ e^-$	$D^0 \to \mu^\pm e^\mp$	
$D^0 \to \mu^+ \mu^-$		
$D^0 \to e^+ e^-$		

History and Status

History

Other issues that were brought up at the July and April meetings have also been addressed. The issues that were brought up at the April meeting are the following:

- Cut out tracts that passed through the pair plane holes in the Čerenkov mirror midplanes.
- Cut out all category 3 tracks.
- Set the cut on PTB.
- Study possible reflections/misidentifications of $\pi \to \mu$ as a source of systematic background.
- Study the muon TDCs and the muon quality and distance cuts from Offline_doc_219.

And the issues that were brought up at the July meeting are the following:

- Check and plot Z of the primary vertex versus Z of the secondary vertex to ensure that there were no secondary vertices occurring in the targets.
- Tighten the ϕ mass cut for the $D_s \to \phi\pi^+$ normalization.
- Finalize the muon quality and distance cuts.
- Use asymmetric cuts for decays involving electrons to account for the bremsstrahlung tail sticking out of a symmetric box.
- Tighten the kaon Čerenkov probability cuts to above *a priori* for D^+ and D^0 decays.

At the September meeting other issues were raised. They include the following:

- Show the kinematics distributions of the data and Monte Carlo events.
- Make a final check on which muon categories to use, e.g., whether or not to use the X-wall information or only the Y-wall hits.
- What is the relative efficiency without the particle ID cuts for the $\ell^+\ell^-$ modes relative to the normalization modes?
- The cut on 10 D_s^+ lifetimes for those decays seemed too loose.
- For the background, it was suggested that using real data would give more reliable estimates of background (misidentification rates) for these modes.
- Rebin the histograms from 4 MeV/c^2 per bin to 10 MeV/c^2 per bin.

Status

The status so far is that I:

- Generated Monte Carlo events for the modes described above.
- Filtered the Monte Carlo events using the KSU microstrip and the SELECT_ REGULAR substrip.
- Ran the SELECT_REGULAR substrip on data from the KSU microstrip.
- Made cut for hole in the Čerenkov mirror midplane[4].
- Removed all category 3 tracks.
- Set cut on PTB to <0.35 GeV/c. (See Figure 4.) I also checked setting the cut to either <0.30 GeV/c or <0.20 GeV/c but since I found no significant increase in the signal-to-noise ratio I decided to stick with the loosest cut.
- The SDZ cut was set to >12 in the SELECT_REGULAR package so that was the minimum I could set it. For both D_s and D^0 decay modes I relied on the previous work[1]. For the D^+ modes I checked the

signal-to-noise ratio for the SDZ range from 12 to 20. (See Table 2 below.) Given these results I will stick with SDZ>20.

- Set asymmetric cuts at 1/2 the mass window width above and 3/2 the width below the mass for decays involving electrons to account for the bremsstrahlung tail, rather than 1/2 the width above and 1/2 the width below for dimuon decays. Because the bremsstrahlung tail sticks out of a symmetric "box" a solution must be found to preserve the method of "blind" analysis. My solution is to extend the lower limit of the mass window to cover the tail and then recalculate the background for all the cuts and preliminary results*. (See Figure 5.)

- Produced Ntuples of both Data and Monte Carlo based on the select substrip, but using Chong's muon quality and distance cuts[3].
- Performed background studies of possible reflections/misidentifications of $\pi \to \mu$.
- Plotted z-primary versus z-secondary to ensure that no secondary vertices occur within the target (See Figure 6). I also plotted z-primary to locate the source of events with apparent primary vertices located between the targets (See Figure 7). This lead to an investigation of the effects from the 4-target runs. When I properly read in the new target positions for each different run, the ratio of the number of D^+ events with a primary vertex within 3σ of a target versus all D^+ events was the same (98%) for both the 4-target and 5-target. Even though the 4-target runs account for only 5% of the total data, I will keep all the 4-target runs.
- Produced preliminary results with the "box" still closed by assuming a "signal" equal to the square-root of the estimated background.

From the September Meeting I have:

- Produced plots of the kinematics variables DIP, SDZ, and PTB. (See Figure 8 and Figure 9 for D^+, Figure 10 and Figure 11 for D_s^+, and Figure 12 and Figure 13 for D^0). These plots are the summed histograms of all the decay modes for a particular parent (D^+, D_s^+ or D^0). They have all the same cuts as in Figure 17, Figure 20, and Figure 25 for MC and Figure 34, Figure 38, and Figure 43 for data. That is except to the variable plotted itself. So the PTB plot for D^+ is the sum of the PTB for each D^+ decay mode with the standard cuts for SDZ, DIP, DZTARG, etc., including a cut on the "box" (MC inside and data outside the box).
- I have checked the muon quality categories for $D^+ \to \pi^+\mu^+\mu^-$ with different cuts to determine the best categories to use and determine what information from the X-wall is useable.
- In light of remarks made by Milind on the problems of making cuts with low statistics I have reexamined the PTB cut.
- I rebinned the histograms to 10 MeV/c^2 per bin but I found that they were too course so I set the binning to 5 MeV/c^2 per bin.
- I determined the electron and muon efficiencies in the Monte Carlo events.
- I reduced the cut on the D_s^+ lifetime from 5 ps to 3 ps.
- I examined reflection background from the D^+ and D_s^+ normalization decay modes.

---

* "…but I didn't inhale."

Cuts

Variable Definitions

SDZ: The significance of spatial separation from the primary vertex of the secondary vertex, along the beam direction.

DZTARG: The number of sigmas the secondary vertex is outside the target.

TRKXIS: The maximum of the fit χ^2 of the reconstructed tracks.

VITXIS: The maximum χ^2 fit of the reconstructed vertex.

XYZVTX: The position along the beam (z-coordinate) direction of the secondary vertex in cm.

τ: The lifetime of the parent particle in picoseconds (ps).

PTB: The component of the parent particle momentum perpendicular to the line joining the primary and secondary vertices, in GeV/c.

DIP: The transverse impact parameter of the parent particle with respect to the primary vertex, in mm.

RATIO: The product, for each reconstructed track in the vertex, of the ratio of the distance between the track and the secondary vertex and of the distance between the track and the primary vertex. Set to $10^{-nprong}$ where nprong is the number of tracks/vertex.

EMPROB: The probability of that track being an electron in percent.

SIGMAS: The number of sigmas a projected muon track was from a hit ion the muon scintillator wall.

mucat: The muon track quality. See below under muon cuts.

dist: The "distance" from the center-line to the point $\left(x(cts), y(cm)\right)$ in a plot of TDC counts (translated to "*x*") versus projected *y* position in units of approximately TDC counts. Also see below under muon cuts.

Kinematics Cuts

The minor changes to the final cuts from Offline_Doc_234 are underlined in the following list. They are increasing the kaon Čerenkov Probability cut from >0.10 to >0.13 for D^+ and D^0 decays, loosening the mass window for D^+ from $1.85\ \mathrm{GeV/c^2} < M\left(D^+\right) < 1.89\ \mathrm{GeV/c^2}$ to $1.84\ \mathrm{GeV/c^2} < M\left(D^+\right) < 1.90\ \mathrm{GeV/c^2}$, tightening the vertex χ^2 cut from <10 to <6, and tightening the ϕ mass cut D^+ from $0.99\ \mathrm{GeV/c^2} < M\left(\phi\right) < 1.05\ \mathrm{GeV/c^2}$ to $1.01\ \mathrm{GeV/c^2} < M\left(\phi\right) < 1.03\ \mathrm{GeV/c^2}$. Also the D_s^+ lifetime cut was reduced from 5 to 3 ps. Note the number in parenthesis for the "box" is the lower extent of the asymmetric "box" to cover the bremsstrahlung tail.

Offline_Doc_234 Final D^+ Cuts:

Mass window: 1.72 GeV/c^2 < $M(D^+)$ < 2.12 GeV/c^2
SDZ>20
DZTARG>5
TRKXIS<5
VITXIS<6
XYZVTX<-0.4 cm
τ<5 ps
DIP<0.040 mm
RATIO<0.001
"Box": (1.78)1.84 GeV/c^2 < $M(D^+)$ < 1.90 GeV/c^2
K-Čerenkov Prob. >0.10 ($D^+ \to K^-\pi^+\pi^+$ for $D^+ \to \pi\ell\ell$ modes)
K-Čerenkov Prob. >0.13 ($D^+ \to K^-\pi^+\pi^+$ for $D^+ \to K^+\ell^\pm\ell^\mp$ modes)
EMPROB>90 (electrons)
SIGMAS<1.00 (muons)

Offline_Doc_234 Final D_s^+ Cuts:

Mass window: 1.72 GeV/c^2 < $M(D_s)$ < 2.12 GeV/c^2
SDZ>12
DZTARG>5
TRKXIS<5
VITXIS<6
XYZVTX<-0.4 cm
τ<3 ps
DIP<0.040 mm
RATIO<0.001
"Box": (1.91)1.95 GeV/c^2 < $M(D_s)$ < 1.99 GeV/c^2
Mass window: (1.01 GeV/c^2 < $M(\phi)$ < 1.03 GeV/c^2)
K-Čerenkov Prob. >0.18
(K-Čerenkov Prob. >0.18 for same charge K from $D_s^+ \to \phi\pi^+$ D K^+K^-)
K-Čerenkov Prob. >0.10 ($D_s^+ \to \phi\pi^+$ for $D_s^+ \to \pi\ell\ell$ modes)
EMPROB>90 (electrons)
SIGMAS<1.00 (muons)

Offline_Doc_234 Final D^0 Cuts:

Mass window: 1.715 GeV/c^2 < $M(D^0)$ < 2.015 GeV/c^2
SDZ>12
DZTARG>5
TRKXIS<5
VITXIS<6
XYZVTX<-0.4 cm
τ<3 ps
DIP<0.040 mm
RATIO<0.01
"Box": (1.76)1.83 GeV/c^2 < $M(D^0)$ < 1.90 GeV/c^2
K-Čerenkov Prob. >0.13 ($D^0 \to K^-\pi^+$)
EMPROB>90 (electrons)
SIGMAS<1.00 (muons)

The SDZ cut for the D^+ modes for the SDZ range from 12 to 20 using the summed histograms for all the decay modes.

Table 2: SDZ Results for D^+

	SDZ>20	**SDZ>18**	**SDZ>16**	**SDZ>14**	**SDZ>12**
Monte Carlo	14628±121	15479	16374	17260	18039
Background	136±12	156	172	206	254
$S/\sqrt{B}$	**1254**±55	1239	1249	1203	1132

In light of remarks made by Milind on the problems of making cuts with low statistics I have reexamined the PTB cut. I tested it using background data and Monte Carlo events for the $D^+ \to \pi^+\mu^+\mu^-$ decay mode. Table 3 shows the results for 3 values of PTB.

Table 3: $D^+ \to \pi^+\mu^+\mu^-$ PTB Cuts

Cut		**<0.35 GeV/c**	**<0.25 GeV/c**	**<0.20 GeV/c**
Tight: (1) above	MC	3136	3022±55	2916
	data	48	43±7	40
	$MC/\sqrt{B}$	453	**461**±36	**461**
Loose: (6) above with no muon cuts	MC	4338	4027±63	3744
	data	309	226±15	188
	$MC/\sqrt{B}$	247	268±10	**273**

I have also plotted PTB for $D^+ \to K^-\pi^+\pi^+$, $D_s^+ \to \phi\pi^+$ and $D^0 \to K^-\pi^+$ data and Monte Carlo and the ratio of data/Monte Carlo in Figure 14, Figure 15 and Figure 16, respectively. After removing the reflections we decided to recheck the PTB cut on D^+ by summing all the modes. The results are given in Table 4.

Table 4: D^+ PTB Cuts After Reflection Cuts

Cut		<0.25 GeV/c	<0.20 GeV/c	<0.175 GeV/c
$D^+ \to \pi ll$ only	MC	8961	8522±92	8182
	data	20	20±5	16
	$MC/\sqrt{B}$	2004	**1906**±214	**2046**
$D^+ \to \pi ll$ and $D^+ \to Kll$	MC	12525	11959±109	11531
	data	27	27±5	22
	$MC/\sqrt{B}$	2410	**2302**±223	**2458**

Given these results and the PTB distributions shown in below in the plots Figure 8 and Figure 9, I will set the PTB cut at PTB<0.20 GeV/c, since the significance similar to the rather tight cut of PTB<0.175 GeV/c for D^+. However, given some concerns about the loss of significance for D_s^+, I reexamined the plots in Figure 8 through Figure 13. The PTB distributions in the Monte Carlo plots of D_s^+ and D^0 seemed broader that the plot for D^+. I the calculated $MC/\sqrt{B}$ for different values of PTB for both D_s^+ and D^0, using the summed histograms for all the decay modes. The results are shown in Table 5.

Table 5: Summed D_s^+ and D^0 PTB Cuts

Mode		<0.35 GeV/c	<0.30 GeV/c	<0.25 GeV/c	<0.20 GeV/c
D_s^+	MC	3238	3138±56	2925	2613
	data	92	81±9	72	58
	$MC/\sqrt{B}$	339	**348±20**	347	341
D^0	MC	11143	10548±103	9638	8394
	data	70	59±8	55	45
	$MC/\sqrt{B}$	1332	**1373±90**	1299	1249

After removing the reflections I also reexamined the PTB cuts for the D_s^+ and D^0 modes. The final PTB cuts will be as follows:

PTB<0.20 GeV/c for D^+
PTB<0.25 GeV/c for D_s^+
PTB<0.30 GeV/c for D^0.

Muon Cuts (Offline_Doc_219 Final Cuts):

There was a cut on the muon track momentum of $|\mathbf{P}_\mu|$>8 GeV/c and, for dimuon events, no two muon tracks may share the same Y-paddle.

- The recommended cuts from Offline_Doc_219 were *mucat* = 3 or (*mucat* ≥ 6 and *dist* <10.0).

Muon Quality Category

To generate the following table, one starts with good muon candidates, that is a TDC hit in either a X or Y-Paddle or both a X and Y-Paddle, but only one hit per X or Y. A hit is defined as when a muon candidate track is projected to hit within a candidate paddle. The number of sigma is the distance of a projected track from the candidate paddle edge divided by the muon multiple scattering distance (from the calorimeters, steel and concrete). The variable *mucat* (muon category) is thus illustrated (the boldface numbers are the ones being used) in Table 6. The full text of the subroutine used to calculate mucat and dist can be found in the Appendix.

Table 6: *mucat*, the Muon Quality Category

x-hit / y-hit	Hit X-Paddle	$\leq 1\sigma_x$	$>1\sigma_x$
Hit Y-Paddle	**9**	**8**	**7**
$\leq 1\sigma_y$	**6**	5	4
$>1\sigma_y$	**3**, 2	1	0

To check the muon quality categories for $D^+ \to \pi^+\mu^+\mu^-$ with different cuts in order to determine the best categories to use and determine what information from the X-wall is useable I used a series of cuts. The different cuts I used are:

(1) *dist* <10 cut on first muon, the offline_doc_219 final muon category cuts on second muon, and the final kinematics cuts,
(2) no *dist* cut on first muon, the offline_doc_219 final muon category cuts on second muon, and the final kinematics cuts,
(3) *dist* <10 cut on first muon, the offline_doc_219 final muon category cuts on second muon, and loose kinematics cuts,
(4) no *dist* cut on first muon, the offline_doc_219 final muon category cuts on second muon, and loose kinematics cuts,
(5) *dist* <10 cut on first muon, any muon category cuts on second muon, and loose kinematics cuts,
(6) no *dist* cut on first muon, any muon category cuts on second muon, and loose kinematics cuts,
(7) Chong's $K^{*0}\mu^+\nu_\mu$ data from offline_doc_219.

The $D^+ \to \pi^+ \mu^+ \mu^-$ Monte Carlo and data numbers for different cuts are given Table 7:

Table 7: Muon Quality Category

Cut		9	8	7	6	5	4	3
(1)	MC	1993	161	245	444	48	62	293
	data	17	2	17	6	1	10	6
	$MC/\sqrt{B}$	483	114	59	181	48	20	120
(2)	MC	2000	161	248	445	48	66	293
	data	19	2	26	10	1	25	6
	$MC/\sqrt{B}$	459	114	49	141	48	13	120
(3)	MC	2681	229	328	589	70	87	395
	data	31	2	29	17	4	23	17
	$MC/\sqrt{B}$	482	162	61	143	35	18	96
(4)	MC	2690	230	333	590	70	94	395
	data	36	2	44	21	4	51	17
	$MC/\sqrt{B}$	448	163	50	129	35	13	96
(5)	MC	2778	241	339	612	73	88	413
	data	56	3	60	23	6	46	32
	$MC/\sqrt{B}$	372	139	44	128	30	13	73
(6)	MC	2798	242	344	613	73	95	413
	data	66	4	105	35	6	96	32
	$MC/\sqrt{B}$	344	121	34	104	30	10	73
(7)	RS	728	56	727	345	72	822	228
	WS	142	17	375	146	42	489	85
	$(\mathrm{RS}-\mathrm{WS})/\sqrt{\mathrm{WS}}$	49	9	18	16	5	15	16

One should note that the X-wall is roughly 10' x 20' and the Y-wall is only roughly 8' x 10'. Therefore, we need to consider the *mucat*=3 tracks.

I then combined these categories for the some of the cuts described above and a:

(8) combination of Monte Carlo "signal" from cut (1) with "data" which is the same Monte Carlo "signal" weighted with the ratio of WS/RS from cut (7).

The resulting "signal-to-noise" ratios are given in Table 8:

Table 8: Muon Quality Category

Cut		3-9	3, 6-9	6-9	3, 7-9	7-9	6-9, 4, 3
(1)	MC	3251	3141±56	2847	2696	2402	3203
	data	59	48±7	42	42	36	58
	$MC/\sqrt{B}$	423	**453±34**	439	416	400	421
(6)	MC	4578	4410±66	3997	3797	3384	4505
	data	344	242±16	210	207	175	338
	$MC/\sqrt{B}$	247	**283±10**	276	264	256	245
(8)	MC	3251	3141±56	2847	2696	2402	3203
	"data"	927	863±29	753	674	565	900
	$MC/\sqrt{B}$	107	**107±3**	104	104	101	107
(7)	RS	2978	2084±46	1856	1739	1511	2906
	WS	1296	765±28	680	619	534	1254
	$(\mathrm{RS}-\mathrm{WS})/\sqrt{\mathrm{WS}}$	47	**48±1**	45	45	42	47

As one can see, the original muon category cuts determined in offline_doc_219 are the best cuts; therefore, for this analysis they are the final cuts to be used.

- Where $dist = \left| \frac{(m \cdot \mathrm{tdc}_\mu + b) - X_{\mathrm{Proj}}}{\sqrt{m^2+1}} \right|$ in units of ~10 cm

  and *m* is the slope and *b* the intercept for the global TDCs and when:
  1) Run Number < 1000, *m*=-9.8, *b*=9011
  2) 1000 ≤ Run Number < 1400, *m*=-10.0, *b*=9150
  3) Run Number ≥ 1400, *m*=-9.8, *b*=8971

To determine the TDC cut, *dist*, I tested it using background data and Monte Carlo events for the $D^+ \to \pi^+\mu^+\mu^-$ decay mode. Table 9 shows the results for 7 values of *dist*.

Table 9: Muon TDC Distance Cuts

Cut		*dist*<10	*dist*<8	*dist*<6	*dist*<5.5	*dist*<5	*dist*<4.5	*dist*<4
Tight: (1) above, except *mucat*>6 cut on first muon	MC	3161	3132	3075±55	3050	3004	2915	2814
	data	22	21	17±4	17	16	16	16
	$MC/\sqrt{B}$	674	684	746±91	740	**751**	729	704
Loose: (6) above except *mucat*>6 cut on first muon	MC	4668	4662	5444±74	4502	4432	4307	4167
	data	115	101	88±9	79	75	72	71
	$MC/\sqrt{B}$	435	464	**580±32**	507	512	508	495

Given these results I will set the TDC *dist* cut at *dist*<6, a cut of 60 cm in spatial coordinates.

The Monte Carlo program mistakenly defined the muon X-wall efficiencies as 100% and not the 69% measured[5]. This discrepancy can be corrected for because the individual category is available for each muon track. The correction would involve weighting the each of muon category 6 and 3 tracks by the true efficiency (69%) for the Monte Carlo events with muon tracks. This is about a 10-15% effect.

Monte Carlo Studies

The number of Monte Carlo events generated and passing cuts is shown in the following table. Note the underlined modes have already been published[2].

Table 10: Monte Carlo Yields

	Mode	# Generated	# Passed Cuts	% Yield	Min Tag	% Yield
A	$D^+ \to K^-\pi^+\pi^+$	250,000	2,653(2,050)	1. 06(0.82)	Same	NA
B	$\underline{D^+ \to \pi^+\mu^+\mu^-}$	250,000	2,706	1.08	3974	1.59
C	$\underline{D^+ \to \pi^+e^+e^-}$	250,000	816	0.33	1183	0.47
D	$D^+ \to \pi^+\mu^\pm e^\mp$	250,000	1,272	0.51	1746	0.70
E	$D^+ \to \pi^-\mu^+\mu^+$	250,000	2,088	0.84	2853	1.14
F	$D^+ \to \pi^-e^+e^+$	250,000	701	0.28	1078	0.43
G	$D^+ \to \pi^-\mu^+e^+$	250,000	976	0.39	1274	0.51
V	$D^+ \to K^+\mu^+\mu^-$	250,000	1206	0.48	1722	0.69
W	$D^+ \to K^+e^+e^-$	250,000	453	0.18	665	0.27
X	$D^+ \to K^+\mu^\pm e^\mp$	250,000	664	0.27	914	0.37
H	$D^+ \to K^-\mu^+\mu^+$	250,000	1,214	0.49	1781	0.71
I	$D^+ \to K^-e^+e^+$	250,000	421	0.17	609	0.24
J	$D^+ \to K^-\mu^+e^+$	250,000	683	0.27	943	0.38
K	$D_s^+ \to \phi\pi^+$	250,000	1,225(1,152){1491}	0.49(0.46){0.60}	Same	NA
L	$D_s^+ \to K^+\mu^+\mu^-$	250,000	647	0.26	970	0.39
M	$D_s^+ \to K^+e^+e^-$	250,000	244	0.10	357	0.14
N	$D_s^+ \to K^+\mu^\pm e^\mp$	250,000	388	0.16	540	0.22
O	$D_s^+ \to K^-\mu^+\mu^+$	250,000	686	0.27	1036	0.41
P	$D_s^+ \to K^-e^+e^+$	250,000	257	0.10	365	0.15
Q	$D_s^+ \to K^-\mu^+e^+$	250,000	381	0.15	511	0.20
Y	$D_s^+ \to \pi^+\mu^+\mu^-$	250,000	1725	0.69	2514	1.01
Z	$D_s^+ \to \pi^+e^+e^-$	250,000	565	0.23	825	0.33
AA	$D_s^+ \to \pi^+\mu^\pm e^\mp$	250,000	809	0.32	1428	0.57
AB	$D_s^+ \to \pi^-\mu^+\mu^+$	250,000	1588	0.69	2156	0.86
AC	$D_s^+ \to \pi^-e^+e^+$	250,000	528	0.23	771	0.31
AD	$D_s^+ \to \pi^-\mu^+e^+$	250,000	911	0.32	1200	0.48
R	$D^0 \to K^-\pi^+$	250,000	4,535	1.81	Same	NA
S	$D^0 \to \mu^+\mu^-$	250,000	5,297	2.12	6569	2.63
T	$D^0 \to e^+e^-$	250,000	1,577	0.63	2133	0.85
U	$D^0 \to \mu^\pm e^\mp$	250,000	2983	1.19	3821	1.53

Note that Minimum Tagging implies *emprob*>80% for electrons and no *mucat* or *dist* cuts for muons. A comparison of the difference in the yields between "Minimum Tagging" and the "Number that Passed Cuts" is used to examine the systematic effects of making minimal versus the standard particle ID cuts.

This gives a handle on the effect of differences in the kinematics between the dilepton modes and the normalization modes

The difference in the yield is due to the detection efficiencies of the various particles involved. Generally electrons have a lower efficiency than muons and kaons have a lower efficiency than pions. See Figure 17, Figure 18 and Figure 19 for D^+ decay modes, Figure 20, Figure 21, Figure 22, Figure 23, and Figure 24 for D_s^+ decay modes and, Figure 25 and Figure 26 for D^0 decay modes.

To check the relative yields of the Monte Carlo events above, I compared the four modes $D^+ \to \pi^+\mu^+\mu^-$, $D^+ \to \pi^+e^+e^-$, $D_s^+ \to K^+\mu^+\mu^-$, and $D_s^+ \to K^+e^+e^-$. While examining the Monte Carlo e/μ and K/π relative efficiencies, I made the following observations. The first was that there was (1) a difference in the total number of events reconstructed and written to the DST tape. The second was (2) that the bremsstrahlung tail was responsible for a significant difference in the number of events within the mass windows. The third was (3) that there was an excess of antiparticles produced and reconstructed by the Monte Carlo. Observation (1) indicated that there were about 20% more D^+ than D_s^+ events and about 15% more dimuon than di-electron events. Observation (2) determined that there was a loss of about 20% of the di-electron events that were outside of the mass window, while an even higher percentage (about 33%) are outside the "box". Observation (3) may account in part for the difference in the number of D^+ and D_s^+ events produced and reconstructed by the Monte Carlo due to leading-particle enhanced production of D^+.

To perform this check of the relative yields of the Monte Carlo events, I used an independent program with the standard kinematics cuts and filled histograms. These histograms were filled within a mass window described above for the offline_doc_234 cuts with 3-prong vertices with either no particle ID or with simple lepton tagging. I used 40,000 events from my Monte Carlo DST tapes for each mode. I filled the masses of the three tracks for each of the possible mass combinations and then averaged the number of events still within the mass window for the "No ID" results. The tagging was to match two muon candidates to two tracks for $D^+ \to \pi^+\mu^+\mu^-$ and $D_s^+ \to K^+\mu^+\mu^-$ or find two tracks with *emprob*>50 (and also 90) for $D^+ \to \pi^+e^+e^-$ and $D_s^+ \to K^+e^+e^-$. I also plotted the electron events down to a mass of 1.3 GeV/c^2 to examine the losses due to the bremsstrahlung tail. The results are given in Table 11 (the numbers for cuts most similar to those used in this analysis are shown in boldface).

Table 11: Relative Muon and Electron Efficiencies for Monte Carlo Events

	Cut	**Mode**			
		$D^+ \to \pi^+\mu^+\mu^-$	$D^+ \to \pi^+e^+e^-$	$D_s^+ \to K^+\mu^+\mu^-$	$D_s^+ \to K^+e^+e^-$
a	No ID	6578	4415	3131	2324
b	Tagged, no K-Čerenkov cut	**4969**	2079	2963	1491
c	*emprob*>90		**996**		725
d	Tagged + K-Čerenkov>0.18			**1196**	**641**
e	No ID with Tails		5993		3980
f	Tagged with Tails		2591		1899
g	*emprob*>90 with Tails		1188		891

I have used these numbers to calculate the electron and muon efficiencies. The average muon efficiency ($\sqrt{\mathbf{b}/\mathbf{a}}$) is 92%. The average electron efficiency ($\sqrt{\mathbf{c}/\mathbf{a}}$) is 52%. These numbers are consistent with other documents[1,6]. The relative effective ratio (those events within the mass window) of $ee/\mu\mu$ ($(\mathbf{c}/\mathbf{a})_e/(\mathbf{b}/\mathbf{a})_\mu$) is thus about 32%. This would give an approximate decay mode ratio for $\mu\mu$:μe:ee of

6:3:2. The decay mode ratios **B**:**D**:**C**, **E**:**G**:**F**, **H**:**J**:**I**, **L**:**N**:**M**, **O**:**Q**:**P**, and **S**:**U**:**T** from Table 10 are all fairly consistent with this ratio of 6:3:2.

I also calculated the kaon Čerenkov efficiency for the D_s^+ decay modes (**d**/**b**). I found that the average Kaon Čerenkov efficiency was a somewhat low 42%. Since the average kaon momentum for the Monte Carlo D_s^+ events was about 36 GeV/c, this low efficiency is consistent with earlier documents[7] for a kaon Čerenkov cut at 0.18. (The average pion momentum for the Monte Carlo D^+ events was about 29 GeV/c.) The ratios of decay modes **L**:**B** and **O**:**E**, when adjusted for the 20% deficit in reconstructed events between D_s^+ and D^+ (1), agree with this number.

The kaon momenta for both data and Monte Carlo events from D^+ and D_s^+ normalization decay modes are shown in Figure 27. The ratio of decay modes **H**:**E** is 55%, which is consistent with the kaon Čerenkov efficiency for a cut at 0.13 for kaons in the momentum range of 20-30 GeV/c.

Background Studies

Reflection Background

After seeing the D_s^+ lifetime paper I decided that I should examine $K \leftrightarrow \pi$ reflections in D^+ and D_s^+ normalization modes. To examine the $D^+ \to K^-\pi^+\pi^+$ reflected into $K^-K^+\pi^+$ with a mass consistent with D_s^+ I filled the same sign kaon's four-vector in the $D_s^+ \to \phi\pi^+$ decay mode with a pion mass. I then applied a mass cut to this recalculated invariant mass of $1.84\ \mathrm{GeV/c^2} < M < 1.90\ \mathrm{GeV/c^2}$ along with a cut on the lifetime of τ>1.5 ps. This left only 21 events (1.9%) to be subtracted from the $D_s^+ \to \phi\pi^+$ mass plot, Figure 40. For the case where $D_S^+ \to K^-K^+\pi^+$ reflects to $K^-\pi^+\pi^+$, with a mass consistent with D^+, I filled one of the same sign pions' four-vectors from the $D^+ \to K^-\pi^+\pi^+$ decay mode with a kaon mass. I then applied a mass cut of $1.95\ \mathrm{GeV/c^2} < M < 1.99\ \mathrm{GeV/c^2}$ and a *K*-Čerenkov probability cut to this "kaon". I had 1770 events (7.9%) to subtract from the $D^+ \to K^-\pi^+\pi^+$ mass plot with the *K*-Čerenkov probability cut of >0.13 (1377 events (6.1%) with a cut of >0.18) rather than 10543 events (47%) with no *K*-Čerenkov probability cut. See Figure 28.

To examine possible reflections from normal charm hadron decays for the dilepton modes, the tracks were refit with deliberately wrong particle mass for each event. This produced a "reflection" into one of the following possible hadron decays. For 3-prong events:

(1) $D^+ \to \pi^+\pi^-\pi^+$ with a mass window of $1.84\ \mathrm{GeV/c^2} < M(D^+) < 1.90\ \mathrm{GeV/c^2}$

(2) $D_s^+ \to \pi^+\pi^-\pi^+$ with a mass window of $1.95\ \mathrm{GeV/c^2} < M(D_s) < 1.99\ \mathrm{GeV/c^2}$

(3) $D^+ \to K^-\pi^+\pi^+$ with a mass window of $1.84\ \mathrm{GeV/c^2} < M(D^+) < 1.90\ \mathrm{GeV/c^2}$

(4) $D_s^+ \to K^+\pi^+\pi^-$ with a mass window of $1.95\ \mathrm{GeV/c^2} < M(D_s) < 1.99\ \mathrm{GeV/c^2}$

(5) $D^+ \to K^+K^-\pi^+$ with a mass window of $1.84\ \mathrm{GeV/c^2} < M(D^+) < 1.90\ \mathrm{GeV/c^2}$

(6) $D_s^+ \to K^+K^-\pi^+$ with a mass window of $1.95\ \mathrm{GeV/c^2} < M(D_s) < 1.99\ \mathrm{GeV/c^2}$

(7) $\Lambda_c^+ \to pK^-\pi^+$ with a mass window of $2.260\ \mathrm{GeV/c^2} < M(\Lambda_c^+) < 2.310\ \mathrm{GeV/c^2}$

For 2-prong events:

(1) $D^0 \to \pi^+\pi^-$ with a mass window of $1.83\ \mathrm{GeV/c^2} < M(D^0) < 1.90\ \mathrm{GeV/c^2}$

(2) $D^0 \to K^-\pi^+$ with a mass window of $1.83\ \mathrm{GeV/c^2} < M(D^0) < 1.90\ \mathrm{GeV/c^2}$

Then the event was tagged if they were within a mass window of the proposed reflections. The percentage of tagged events for each decay mode is shown in Table 12.

Table 12: The percentage of events that are within the mass window of the reflections.

Reflection	**1**		**2**		**3**		**4**		**5**		**6**		**7**	
Mode	**MC**	**Data**	**MC**	**Data**	**MC**	**Data**	**MC**	**Data**	**MC**	**Data**	**MC**	**Data**	**MC**	**Data**
$D^+ \to \pi^+\mu^+\mu^-$	83%	2%	0%	2%	0	73%	7%	8%	0	0	0	0	0	2%
$D^+ \to \pi^+e^+e^-$	47%	11%	6%	11%	0	44%	6%	11%	0	0	0	0	0	0
$D^+ \to \pi^+\mu^\pm e^\mp$	59%	0	5%	0	0%	75%	8%	0	0	0	0	0	0	0
$D^+ \to \pi^-\mu^+\mu^+$	84%	0	0%	0	0	63%	12%	13%	0	0	0	0	0	0
$D^+ \to \pi^-e^+e^+$	46%	67%	7%	33%	0	0	9%	0	0	0	0	0	0	0
$D^+ \to \pi^-\mu^+e^+$	60%	33%	4%	0	0	0	10%	0	0	0	0	0	0	33%
$D^+ \to K^+\mu^+\mu^-$	0%	0	0	0	16%	39%	0%	9%	1%	21%	9%	9%	2%	4%
$D^+ \to K^+e^+e^-$	3%	0	0%	0	16%	25%	4%	25%	0%	0	6%	0	1%	25%
$D^+ \to K^+\mu^\pm e^\mp$	2%	0	0%	0	10%	0	3%	0	1%	25%	7%	0	2%	25%
$D^+ \to K^-\mu^+\mu^+$	0%	0	0	0	94%	31%	10%	0	0	25%	7%	6%	9%	19%
$D^+ \to K^-e^+e^+$	4%	0	0%	0	47%	0	8%	0	0	0	7%	0	8%	0
$D^+ \to K^-\mu^+e^+$	3%	0	0	0	61%	20%	8%	0	0	0%	7%	0	8%	20%
$D_s^+ \to K^+\mu^+\mu^-$	20%	0	0	0	13%	29%	71%	4%	0	18%	1%	14%	1%	4%
$D_s^+ \to K^+e^+e^-$	28%	0	0	0	7%	0	28%	0	0	13%	1%	0	0%	13%
$D_s^+ \to K^+\mu^\pm e^\mp$	23%	0	1%	0	11%	13%	42%	0	0	13%	0	13%	1%	25%
$D_s^+ \to K^-\mu^+\mu^+$	17%	0	0	0	0	22%	12%	0	0	22%	0	22%	5%	22%
$D_s^+ \to K^-e^+e^+$	21%	0	2%	50%	0	0	9%	0	0	0	0	0	5%	0
$D_s^+ \to K^-\mu^+e^+$	22%	0	1%	0	0	10%	10%	10%	0	0	0	0	4%	10%
$D_s^+ \to \pi^+\mu^+\mu^-$	0	3%	68%	0	0	69%	0	5%	0	0	0	3%	0	3%
$D_s^+ \to \pi^+e^+e^-$	0	17%	34%	17%	0	50%	0	17%	0	0	0	0	0	0
$D_s^+ \to \pi^+\mu^\pm e^\mp$	0	14%	45%	0	0	57%	0	14%	0	0	0	0	0	0
$D_s^+ \to \pi^-\mu^+\mu^+$	0	0	67%	0	0	50%	0	14%	0	0	0	0	0	0
$D_s^+ \to \pi^-e^+e^+$	0	0	33%	0	0	0	0	0	0	0	0	0	0	0
$D_s^+ \to \pi^-\mu^+e^+$	0	25%	44%	0	0	50%	0	25%	0	0	0	0	0	25%
$D^0 \to \mu^+\mu^-$	95%	6%	0	73%										
$D^0 \to e^+e^-$	72%	0	3%	25%										
$D^0 \to \mu^\pm e^\mp$	80%	0	2%	50%										

The conclusion form examining these results is that for $D^+ \to \pi\ell\ell$ events the $D^+ \to K^-\pi^+\pi^+$ reflection should be cut, for $D^+ \to K^-\ell^+\ell^+$ the $D^+ \to K^+K^-\pi^+$should be cut, for $D_s^+ \to K\ell\ell$ both the $D^+ \to K^+K^-\pi^+$ and $D_s^+ \to K^+K^-\pi^+$ reflections should be cut, and for $D^0 \to \ell^+\ell^-$ the $D^0 \to K^-\pi^+$ reflection should be cut. The final decision is as follows:

- For $D^+ \to \pi\ell\ell$ events, all reflections except $D^+ \to \pi^+\pi^-\pi^+$ should be cut.
- For $D^+ \to K^-\ell^+\ell^+$ events, all reflections except $D^+ \to K^-\pi^+\pi^+$ should be cut.
- For $D^+ \to K^+\ell^-\ell^+$ events, all reflections except $D^+ \to K^-\pi^+\pi^+$ should be cut.
- For $D_s^+ \to K\ell\ell$ events, all reflections except $D^+ \to \pi^+\pi^-\pi^+$ and $D_s^+ \to K^+\pi^+\pi^-$ should be cut.
- For $D_s^+ \to \pi\ell\ell$ events, all reflections except $D_s^+ \to \pi^+\pi^-\pi^+$ should be cut.
- For $D^0 \to \ell^+\ell^-$ events, the $D^0 \to K^-\pi^+$ reflection should be cut.

Pion Misidentification Background

To examine background from a π misidentified as a μ (or e) I did the following:

- For D^+ generated 1,000,000 $D^+ \to \pi^+\pi^-\pi^+$ Monte Carlo events. There was 1 misidentified event seen for each of the following modes, out of the 25704 $D^+ \to \pi^+\pi^-\pi^+$ events that passed the other cuts. These modes are: $D^+ \to \pi^+\mu^+\mu^-$, $D^+ \to \pi^+e^+e^-$, $D^+ \to \pi^+\mu^\pm e^\mp$, and $D^+ \to \pi^-e^+e^+$.
- For D_s^+ generated 250,000 $D_S^+ \to K^+\pi^-\pi^+$ Monte Carlo events. There were 0 misidentified events seen for 2335 $D_S^+ \to K^+\pi^-\pi^+$ events that passed the other cuts.
- For D^0 generated 250,000 $D^0 \to \pi^+\pi^-$ Monte Carlo events. There were 0 misidentified events seen for 9157 $D^0 \to \pi^+\pi^-$ events that passed the other cuts.

I also planned to use 1,000,000 previously generated $D^+ \to K^-\pi^+\pi^+$ Monte Carlo events to test for a pion misidentified as a muon (or electron) in the $D^+ \to K^-\ell^+\ell^+$ decay modes. Since there were 0 misidentified events seen for 2581 $D^+ \to K^-\pi^+\pi^+$ events that passed the other cuts. However, it was requested at the September meeting that I use data to check the misidentification rate. Since this will involve a chance that real decay modes would be observed, I will wait to do this until after the box is opened. At the December meeting it was suggested that I try to include the misidentified pion background into the fit of the flat background.

Since the number of events in the flat background, after the reflection cuts, is small a shape for this fit must be determined. The first step is to model the shape using Monte Carlo events. Therefore, I produced Ntuples from Monte Carlo events where I deliberately misidentified pions as leptons. For example I filled the momentum four-vector for $D^+ \to \pi^+\pi^-\pi^+$ as $D^+ \to \pi^+\mu^-\mu^+$, $D^+ \to \pi^+e^-e^+$ and $D^+ \to \pi^+\mu^-e^+$ to create the Ntuples for this mock data. I then applied all the kinematics cuts and plotted the histograms. I used events from the most likely Monte Carlo generated pion sources. These were: for $D^+ \to \pi\ell\ell$ events the $D^+ \to \pi^+\pi^-\pi^+$ reflections, for $D^+ \to K\ell\ell$ the $D^+ \to K^-\pi^+\pi^+$ reflections, for $D_s^+ \to K\ell\ell$ I used only the $D_s^+ \to K^+\pi^+\pi^-$ reflections, and for $D^0 \to \ell^+\ell^-$ the $D^0 \to \pi^+\pi^-$ reflections. The resulting shapes are Gaussians with a center shifted from the expected mass. Unfortunately most or all of these Gaussians are within the "boxes". These plots are shown in Figure 29 and Figure 30 for D^+, Figure 31 for D_s^+, and Figure 32 for D^0. The next step is to determine the normalization for these shapes and thus the misidentification rate. Looking at the $D^+ \to K^-\ell^+\ell^+$ modes is the best way to do this.

The resulting misidentification rate will be included in the background for the 90% CL calculations. These modes, with the exception of $D^+ \to K^-\pi^+\pi^+$, are Cabibbo suppressed and thus reduced by a factor of ~30 from the normalization branching ratios. Therefore we decided to use the $D^+ \to K^-\ell^+\ell^+$ modes to set a conservative misidentification rate for the other modes. The rate was determined first by counting the number of $D^+ \to K^-\ell^+\ell^+$ events within the "box" (See Figure 33), then subtracting the flat background calculated from the background events outside of the "box" and finally by dividing the results by the number of $D^+ \to K^-\pi^+\pi^+$ normalization events. This gave the misidentification rate of 13/17730 for $\pi\pi \to \mu\mu$, 6/17730 for $\pi\pi \to ee$, and 5.2/17730 for $\pi\pi \to \mu e$. The number of fitted events from the specific misidentification sources then multiplied this rate. The fitted numbers are 1334 for $D^+ \to \pi^+\pi^-\pi^+$, 888 for $D_s^+ \to K^+\pi^+\pi^-$, 1232 for $D_s^+ \to \pi^+\pi^+\pi^-$, and 853 for $D^0 \to \pi^+\pi^-$. For the doubly Cabibbo suppressed $D^+ \to K^+\pi^-\pi^+$ mode, I used the branching ratios from the PDG, the rates from above and assumed 17730 $D^+ \to K^-\pi^+\pi^+$ events. For example the rate for $D^+ \to K^+\mu^-\mu^+$ is $13 \cdot BR_{K^+\pi^-\pi^+}/BR_{K^-\pi^+\pi^+}$. For the cases of $D^+ \to \pi^+\ell^-\ell^+$, $D^+ \to K^+\ell^-\ell^+$, $D_s^+ \to K^+\ell^+\ell^-$, and $D_s^+ \to \pi^+\ell^+\ell^-$ the rate was doubled since there are two ways of getting then from $D^+ \to \pi^+\pi^-\pi^+$, $D^+ \to K^+\pi^-\pi^+$, $D_s^+ \to K^+\pi^+\pi^-$, and $D_s^+ \to \pi^+\pi^+\pi^-$ respectively. However, not all events from the misidentified modes are within the boxes; the $\pi\pi \to \mu e$ and $\pi\pi \to ee$ modes are all within the boxes but

the $\pi\pi \to \mu\mu$ modes are not necessarily within the boxes. There are only 75% of the $D^+ \to \pi^+\pi^-\pi^+$ events, 60% of the $D_s^+ \to K^+\pi^+\pi^-$ events and 40% of the $D_s^+ \to \pi^+\pi^+\pi^-$ that are within the box, but all the $D^0 \to \pi^+\pi^-$ are within the appropriate $\mu\mu$ boxes. Also we have to include the $D^+ \to \pi^+\pi^-\pi^+$ mode that is not removed as a reflection cut, as described below, from the $D_s^+ \to K\ell\ell$ modes. I did this by taking the $D^+ \to \pi^+\pi^-\pi^+$ MC rate from the $D^+ \to \pi^+\pi^-\pi^+$ modes (cut #1) in Table 12 and multiplied that by the number of misidentified events from the appropriate $D^+ \to \pi\ell\ell$ modes in Table 13 and then was added to the normal misidentification background in Table 13. The number of misidentification background events from these calculations is given in Table 13.

Table 13: Number of Misidentification Background Events

Mode	**# mis-ID**	**Mode**	**# mis-ID**	**Mode**	**# mis-ID**
$D^+ \to \pi^+\mu^+\mu^-$	1.47	$D_s^+ \to K^+\mu^+\mu^-$	1.33	$D^0 \to \mu^+\mu^-$	0.63
$D^+ \to \pi^+e^+e^-$	0.90	$D_s^+ \to K^+e^+e^-$	0.85	$D^0 \to e^+e^-$	0.29
$D^+ \to \pi^+\mu^\pm e^\mp$	0.78	$D_s^+ \to K^+\mu^\pm e^\mp$	0.70	$D^0 \to \mu^\pm e^\mp$	0.25
$D^+ \to \pi^-\mu^+\mu^+$	0.73	$D_s^+ \to K^-\mu^+\mu^+$	0.64		
$D^+ \to \pi^-e^+e^+$	0.45	$D_s^+ \to K^-e^+e^+$	0.39		
$D^+ \to \pi^-\mu^+e^+$	0.39	$D_s^+ \to K^-\mu^+e^+$	0.35		
$D^+ \to K^+\mu^+\mu^-$	0.20	$D_s^+ \to \pi^+\mu^+\mu^-$	0.72		
$D^+ \to K^+e^+e^-$	0.09	$D_s^+ \to \pi^+e^+e^-$	0.83		
$D^+ \to K^+\mu^\pm e^\mp$	0.08	$D_s^+ \to \pi^+\mu^\pm e^\mp$	0.72		
		$D_s^+ \to \pi^-\mu^+\mu^+$	0.36		
		$D_s^+ \to \pi^-e^+e^+$	0.42		
		$D_s^+ \to \pi^-\mu^+e^+$	0.36		

Results

General Method

$$BR_X = \frac{N_X/\varepsilon_X}{N_{\text{norm.}}/\varepsilon_{\text{norm.}}} \cdot BR_{\text{norm.}} = \frac{N_X}{N_{\text{norm.}}} \cdot \frac{\varepsilon_{\text{norm.}}}{\varepsilon_X} \cdot BR_{\text{norm.}} \quad (1)$$

Where $\frac{\varepsilon_{\text{norm.}}}{\varepsilon_X} = \frac{N^{MC}_{\text{norm.}}}{N^{MC}_X}$ (2)

Example for $D^+ \to \pi^+ e^+ e^-$

For $D^+ \to \pi^+ e^+ e^-$: $\frac{\varepsilon_{K\pi\pi}}{\varepsilon_{\pi^+e^+e^-}} = \frac{N^{MC}_{K\pi\pi}}{N^{MC}_{\pi^+e^+e^-}} = \frac{2653}{816} = 3.251.$

For a 90% CL Upper Limit one observes the number of events in the box, takes predicted background level and using the 90% CL table[8], $\frac{N_{\pi^+e^+e^-}}{N_{K\pi\pi}} < \frac{N_{90\%\text{ CL.}}}{24010} = \frac{3.46}{24010}$ therefore $BR_{\pi^+e^+e^-} < 4.69\times10^{-4} \cdot BR_{K\pi\pi}$ (90% CL). Thus:

$BR_{\pi^+e^+e^-} < 4.22\times10^{-5}$ (90% CL) as compared with our previous result of 6.6×10^{-5} (90% CL)[2].

Systematic Errors

The value N_x in Equation (1) must be corrected for systematic errors. To do this we use the method described in Cousins and Highland[9] (Eqn. 20). In this equation $N_x = U_x + \Delta U_x$ where U_x is the uncorrected value of N_x that is calculated from the table using the method of Feldman and Cousins[8]. And

$$\Delta U_x = \frac{U_x + B - n}{U_x + B} \cdot \frac{U_x^2 \sigma_r^2}{2} \quad (3)$$

where *B* is the predicted background and σ_r is the total systematic errors.

The sources of the systematic errors are given, as a fraction, in Table 15 as follows:

1) Normalization fit. This is the error from paw fits, i.e. ±165.6/24010 from figure 36.
2) Normalization Branching Ratio from the PDG.
3) Monte Carlo statistics of the normalization mode. Simply $1/\sqrt{N}$ from the column labeled "# Passed Cuts" in Table 10.
4) Monte Carlo statistics of the decay mode. Simply $1/\sqrt{N}$ as in (3).
5) Misidentification background. This includes statistical errors in the fit as in (1) above of the Cabibbo suppressed modes such as $D^+ \to \pi^+\pi^-\pi^+$ and in the number of $D^+ \to K^-\pi^+\pi^+$ used in the calculation of the misidentification rate. It also includes differences between a flat fit and exponential fit of the combinatorial background and errors in the determination of the number of events in the $D^+ \to K^-\ell^+\ell^+$ modes shown in Figure 33.
6) Monte Carlo Particle ID, including Muon Y-wall (±1%) and X-wall (±3%) efficiency corrections and SLIC wall acceptance corrections (±1% from Nick's memo[10]). The Muon Y-wall and X-wall efficiency were set to 100% in the Monte Carlo but were really 99±1% and 69±3% efficient respectively. The X-wall efficiency was corrected at the Ntuple level. The Monte Carlo assumed an

efficiency of 100% for both the X and Y planes. To correct for this I reduced the number of events from muon categories where a miss in the X-plane, due to poor hodoscope efficiency, would have become a category that we were not using. Hence, *mucat*=9 or *mucat*=8 (or 7) becomes *mucat*=7 if the X-plane is not hit, so since we keep *mucat*=7 events we can ignore this; however, we would loose *mucat*=6 or *mucat* =3 events if the X-wall was missed due to poor hodoscope efficiency. Therefore, I have only taken 69% of the *mucat*=6 or *mucat* =3 Monte Carlo events. Thus the error is ±3%*fraction of mucat=6 or 3 Monte Carlo events and not ±31%*fraction of *mucat*=6 or *mucat*=3 Monte Carlo events.

7) Deviations from a relative tagging efficiency. This is the difference in the ratio of yields between "Minimum Tagging" and the "Standard Tagging" in Table 10 for each decay mode from the average yield ratio for each parent particle (D^+, D_s^+ or D^0). This represents the errors due to differences in the kinematics between the dilepton modes and the normalization modes.

8) Particle ID efficiency, including hodoscope efficiencies – Muon Y-wall (±1%) and X-wall (±3%) and ±5% for electron identification[6, 10.]

9) Tails. This is calculated as 25% of the fraction, ε_X, of Monte Carlo events that remain outside of the "box", divided by the fraction, 1-ε_X, that remains within the "box". Where ε_X is the difference in the number of events between the shaded regions and the full plot, divided by the number of events in the full plot for each plot in Figure 17, Figure 20, Figure 21, and Figure 25.

10) Čerenkov ID efficiency. We tried to use a normalization mode with the same kinematics as the decay mode; however, most of the modes had a different number of kaons in the normalization mode than in the decay mode. In fact the only one with the same number was the $D^+ \to K^+\ell^\pm\ell^\mp$ modes. To tag a particle as a kaon candidate we used the cut *K*-Čerenkov Prob. >0.10. Thus, even when we made no explicit cut on the *K*-Čerenkov probability there still was a cut of >0.10. The different cuts are given in the following list:

D^+	*K*-Čerenkov Prob. >0.10	($D^+ \to K^-\pi^+\pi^+$ for $D^+ \to \pi\ell\ell$ modes)
	K-Čerenkov Prob. >0.13	($D^+ \to K^-\pi^+\pi^+$ for $D^+ \to K^+\ell^\pm\ell^\mp$ modes)
D_s^+	*K*-Čerenkov Prob. >0.18 on K^+ from $D_s^+ \to \phi\pi^+$, $\phi \to K^+K^-$	and for $D_s^+ \to K^+\ell^+\ell^-$
	K-Čerenkov Prob. >0.18 on K^- from $D_s^+ \to \phi\pi^+$, $\phi \to K^+K^-$	and for $D_s^+ \to K^-\ell^+\ell^+$
	K-Čerenkov Prob. >0.10	($D_s^+ \to \phi\pi^+$ for $D_s^+ \to \pi\ell\ell$ modes)
D^0	*K*-Čerenkov Prob. >0.13	($D^0 \to K^-\pi^+$ for all $D^0 \to \ell^+\ell^-$)

The efficiency of the *K*-Čerenkov probability cuts should be calculated using the fraction of $D^+ \to K^-\pi^+\pi^+$ events surviving the *K*-Čerenkov probability cut and all other kinematics cuts divided by a "100%" sample. The 100% sample was $D^+ \to K^-\pi^+\pi^+$ events where only the charge of the track identified the kaon. The errors in the fraction was calculated using a binomial distribution such that $\Delta\varepsilon = \sqrt{\varepsilon(1-\varepsilon)/N}$ where ε is the fraction and N is the number of events in the sample. The results are given in Table 14. The Monte Carlo sample was the complete $D^+ \to K^-\pi^+\pi^+$ sample but the data sample came from one (out of 33) tape. Since there is a difference between data and Monte Carlo it was decided to correct the number of Monte Carlo normalization events by the relative efficiency factor of Data/MC for the modes with a different number of kaons in the normalization mode than in the decay mode. (This is every mode except for the $D^+ \to K^+\ell^\pm\ell^\mp$ modes.) The value of the efficiency used in the factor for the data is an average of my efficiency for that cut and the efficiency

from Milind's study[7] (see Table 14). For example the correction was: 91/75.7 for $D^+ \to \pi^+\mu^+\mu^-$ and $D_s^+ \to K^+\mu^\pm e^\mp$, $(91/75.5)^2$ for $D_s^+ \to \pi^+\mu^+\mu^-$, and 66/63.1 for all D^0 modes. The systematic error for the uncertainty of the Čerenkov ID efficiency, for all applicable modes, was the greater of 2% or the difference between the kaon-ID efficiency for my data and the average kaon-ID efficiency. (See column **10** in Table 15).

Table 14: *K*-Čerenkov probability efficiency

Cut	ε - MC	Error: ε - MC	ε - Data	Error: ε - Data	ε - Avg. Data	Systematic Error
>0.10	75.7%	0.7%	91.2%	1.0%	91%	2%
>0.13	58.4%	0.8%	63.1%	1.7%	66%	3%
>0.18	53.2%	0.8%	57.9%	1.8%	64%	6%

It should be noted that sources 6-10 could be lumped together as "Tagging Errors".

Table 15: The systematic errors.

Mode	**1**	**2**	**3**	**4**	**5**	**6**	**7**	**8**	**9**	**10**	**Total**
$D^+ \to \pi^+\mu^+\mu^-$	0.007	0.067	0.019	0.019	0.051	0.019	0.023	0.014	0.022	0.020	0.099
$D^+ \to \pi^+e^+e^-$	0.007	0.067	0.019	0.035	0.069	0.010	0.015	0.050	0.036	0.020	0.124
$D^+ \to \pi^+\mu^\pm e^\mp$	0.007	0.067	0.019	0.028	0.065	0.015	0.024	0.037	0.020	0.020	0.113
$D^+ \to \pi^-\mu^+\mu^+$	0.007	0.067	0.019	0.022	0.025	0.019	0.027	0.014	0.013	0.020	0.089
$D^+ \to \pi^-e^+e^+$	0.007	0.067	0.019	0.038	0.034	0.010	0.054	0.050	0.035	0.020	0.121
$D^+ \to \pi^-\mu^+e^+$	0.007	0.067	0.019	0.032	0.032	0.015	0.062	0.037	0.019	0.020	0.114
$D^+ \to K^+\mu^+\mu^-$	0.008	0.067	0.022	0.029	0.001	0.019	0.004	0.014	0.016	0.000	0.082
$D^+ \to K^+e^+e^-$	0.008	0.067	0.022	0.047	0.000	0.010	0.023	0.050	0.025	0.000	0.105
$D^+ \to K^+\mu^\pm e^\mp$	0.008	0.067	0.022	0.039	0.000	0.015	0.022	0.037	0.011	0.000	0.093
$D_s^+ \to K^+\mu^+\mu^-$	0.038	0.250	0.029	0.039	0.034	0.019	0.025	0.014	0.032	0.020	0.265
$D_s^+ \to K^+e^+e^-$	0.038	0.250	0.029	0.064	0.046	0.010	0.008	0.050	0.098	0.020	0.289
$D_s^+ \to K^+\mu^\pm e^\mp$	0.038	0.250	0.029	0.051	0.043	0.015	0.027	0.037	0.037	0.020	0.271
$D_s^+ \to K^-\mu^+\mu^+$	0.040	0.250	0.029	0.038	0.017	0.019	0.029	0.014	0.023	0.020	0.263
$D_s^+ \to K^-e^+e^+$	0.040	0.250	0.029	0.062	0.023	0.010	0.013	0.050	0.084	0.020	0.282
$D_s^+ \to K^-\mu^+e^+$	0.040	0.250	0.029	0.051	0.022	0.015	0.054	0.037	0.045	0.020	0.274
$D_s^+ \to \pi^+\mu^+\mu^-$	0.036	0.250	0.026	0.024	0.047	0.019	0.005	0.014	0.061	0.028	0.269
$D_s^+ \to \pi^+e^+e^-$	0.036	0.250	0.026	0.042	0.063	0.010	0.007	0.050	0.107	0.028	0.292
$D_s^+ \to \pi^+\mu^\pm e^\mp$	0.036	0.250	0.026	0.035	0.060	0.015	0.125	0.037	0.067	0.028	0.303
$D_s^+ \to \pi^-\mu^+\mu^+$	0.036	0.250	0.026	0.025	0.023	0.019	0.045	0.014	0.050	0.028	0.267
$D_s^+ \to \pi^-e^+e^+$	0.036	0.250	0.026	0.044	0.032	0.010	0.007	0.050	0.116	0.028	0.290
$D_s^+ \to \pi^-\mu^+e^+$	0.036	0.250	0.026	0.033	0.030	0.015	0.068	0.037	0.062	0.028	0.278
$D^0 \to \mu^+\mu^-$	0.007	0.023	0.015	0.014	0.017	0.019	0.031	0.014	0.012	0.030	0.062
$D^0 \to e^+e^-$	0.007	0.023	0.015	0.025	0.022	0.010	0.036	0.050	0.030	0.030	0.087
$D^0 \to \mu^\pm e^\mp$	0.007	0.023	0.015	0.018	0.021	0.015	0.005	0.037	0.014	0.030	0.066

Data

The "boxes" for all of the decay modes have been opened. The results of opening these "boxes" are described in Table 16. The predicted background is a combination of the misidentification background from Table 13 and either a flat background if there were any events in the region above the "box" or zero if there were no events in the region above the "box". I then used the 90% CL upper limit table from Feldman and Cousins[8] to get the predicted number of events. I also corrected the predicted number of events from the table using Equation 3 for the systematic errors outlined in Table 15. The plots of the data for the decay and normalization modes are shown in Figure 34, Figure 36 and Figure 37 for D^+ decay modes, Figure 38, Figure 39, Figure 40, Figure 41, and Figure 42 for D_s^+ decay modes and, Figure 43 and Figure 44 for D^0 decay modes. The reflection cuts have been made along with the vertex $\chi^2 < 6.0$ cut.

Table 16: Open "box" Data

Mode	Predicted Background	Observed	90% CL Upper Limit[8]	90% CL SysErr Corr[9]
$D^+ \to \pi^+\mu^+\mu^-$	2.67	2	3.31	3.35
$D^+ \to \pi^+e^+e^-$	0.90	1	3.46	3.53
$D^+ \to \pi^+\mu^\pm e^\mp$	0.78	1	3.58	3.64
$D^+ \to \pi^-\mu^+\mu^+$	1.53	1	2.89	2.92
$D^+ \to \pi^-e^+e^+$	0.45	2	5.47	5.60
$D^+ \to \pi^-\mu^+e^+$	0.39	1	3.97	4.05
$D^+ \to K^+\mu^+\mu^-$	2.40	3	5.02	5.07
$D^+ \to K^+e^+e^-$	0.09	4	8.51	8.72
$D^+ \to K^+\mu^\pm e^\mp$	0.08	1	4.28	4.34
$D_s^+ \to K^+\mu^+\mu^-$	2.00	0	1.26	1.32
$D_s^+ \to K^+e^+e^-$	0.85	2	5.06	5.77
$D_s^+ \to K^+\mu^\pm e^\mp$	1.10	1	3.27	3.57
$D_s^+ \to K^-\mu^+\mu^+$	1.04	0	1.59	1.68
$D_s^+ \to K^-e^+e^+$	0.39	0	2.05	2.22
$D_s^+ \to K^-\mu^+e^+$	1.15	1	3.23	3.53
$D_s^+ \to \pi^+\mu^+\mu^-$	1.65	1	2.80	3.02
$D_s^+ \to \pi^+e^+e^-$	0.83	0	1.72	1.85
$D_s^+ \to \pi^+\mu^\pm e^\mp$	0.72	2	5.19	6.01
$D_s^+ \to \pi^-\mu^+\mu^+$	1.16	0	1.52	1.60
$D_s^+ \to \pi^-e^+e^+$	0.42	1	3.94	4.44
$D_s^+ \to \pi^-\mu^+e^+$	0.36	3	7.06	8.21
$D^0 \to \mu^+\mu^-$	2.46	2	3.49	3.51
$D^0 \to e^+e^-$	2.04	0	1.25	1.26
$D^0 \to \mu^\pm e^\mp$	2.88	2	3.08	3.09

I also have determined fitting functions for the signal region. I used a similar technique to that used in fitting the misidentification background plots but I am now fitting a Gaussian plus an Exponential for the modes with electron tails and a Gaussian for the dimuon modes. I used Monte Carlo events to get the shapes.

Final Results

For all modes I then used this 90% CL upper limit predicted number of events from Table 16 for N_X in Equation 1 above to calculate the Uncorrected 90% CL upper limit branching ratios. I also used the systematic error corrected value of N_X, using Equation 3 above, to calculate the Corrected 90% CL upper limit branching ratios. The final results for both the uncorrected and corrected branching ratios, along with the 1998 PDG values, are given in Table 17. (Also see Figure 45).

Table 17: 90% CL Upper Limit Branching Ratios

Mode	Uncorrected BR	Corrected BR	BR (1998 PDG)
$D^+ \to \pi^+\mu^+\mu^-$	1.46×10^{-5}	1.48×10^{-5}	1.8×10^{-5}
$D^+ \to \pi^+e^+e^-$	5.06×10^{-5}	5.17×10^{-5}	6.6×10^{-5}
$D^+ \to \pi^+\mu^\pm e^\mp$	3.37×10^{-5}	3.42×10^{-5}	1.2×10^{-4}
$D^+ \to \pi^-\mu^+\mu^+$	1.66×10^{-5}	1.67×10^{-5}	8.7×10^{-5}
$D^+ \to \pi^-e^+e^+$	9.31×10^{-5}	9.56×10^{-5}	1.1×10^{-4}
$D^+ \to \pi^-\mu^+e^+$	4.86×10^{-5}	4.96×10^{-5}	1.1×10^{-4}
$D^+ \to K^+\mu^+\mu^-$	4.33×10^{-5}	4.38×10^{-5}	9.7×10^{-5}
$D^+ \to K^+e^+e^-$	1.95×10^{-4}	2.00×10^{-4}	2.0×10^{-4}
$D^+ \to K^+\mu^\pm e^\mp$	6.71×10^{-5}	6.80×10^{-5}	1.3×10^{-4}
$D_s^+ \to K^+\mu^+\mu^-$	1.32×10^{-4}	1.38×10^{-4}	5.9×10^{-4}
$D_s^+ \to K^+e^+e^-$	1.42×10^{-3}	1.61×10^{-3}	
$D_s^+ \to K^+\mu^\pm e^\mp$	5.72×10^{-4}	6.25×10^{-4}	
$D_s^+ \to K^-\mu^+\mu^+$	1.70×10^{-4}	1.80×10^{-4}	5.9×10^{-4}
$D_s^+ \to K^-e^+e^+$	5.87×10^{-4}	6.34×10^{-4}	
$D_s^+ \to K^-\mu^+e^+$	6.23×10^{-4}	6.82×10^{-4}	
$D_s^+ \to \pi^+\mu^+\mu^-$	1.32×10^{-4}	1.43×10^{-4}	4.3×10^{-4}
$D_s^+ \to \pi^+e^+e^-$	2.48×10^{-4}	2.66×10^{-4}	
$D_s^+ \to \pi^+\mu^\pm e^\mp$	5.23×10^{-4}	6.05×10^{-4}	
$D_s^+ \to \pi^-\mu^+\mu^+$	7.80×10^{-5}	8.22×10^{-5}	4.3×10^{-4}
$D_s^+ \to \pi^-e^+e^+$	6.08×10^{-4}	6.86×10^{-4}	
$D_s^+ \to \pi^-\mu^+e^+$	6.31×10^{-4}	7.34×10^{-4}	
$D^0 \to \mu^+\mu^-$	5.16×10^{-6}	5.18×10^{-6}	4.1×10^{-6}
$D^0 \to e^+e^-$	6.20×10^{-6}	6.23×10^{-6}	1.3×10^{-5}
$D^0 \to \mu^\pm e^\mp$	8.08×10^{-6}	8.12×10^{-6}	1.9×10^{-5}

Discussion of Normalization Sample

Because of the apparent loss of significance of these results I studied the loss of events due to various cuts that were different between my $D^+ \to \pi^+\mu^+\mu^-$ results and Nick's previously published results[2]. I noticed that while the estimated number of observed results described above was similar the number of events from the normalizing mode was about half of what Nick used. One mistake I made was to exclusively tag the muon and electron tracks such that if they were possible muon or electron candidates then they could not be pion candidates. This amounted to a loss of about 20% of the $D^+ \to K^-\pi^+\pi^+$ events. Thus I went from 17140 to 20630 $D^+ \to K^-\pi^+\pi^+$ events. Removing the possible D_s^+ reflections is an additional loss of about 5% of the events. Both of these effects are only noticeable for the $D^+ \to K^-\pi^+\pi^+$ data events. The other two cuts that differ from Nick's analysis are the Čerenkov cut on the kaon in $D^+ \to K^-\pi^+\pi^+$ events and the removal of all category 3 tracks. The change in the number of data and Monte Carlo events and the net effect is shown in Table 18. There is also about a 10% difference between my estimated number of observed events (4.99) and Nick's estimated number of observed events (4.6), due to my estimating the background level. The new standard results are presented in Table 18.

Table 18: The effects on the significance due to different cuts

Cut	MC	Data	% Difference
Standard – Old (Version 2.1)	2361	17140±135	
Standard - New (Version 2.2)	2300	20630±153	23.5%
Standard without D_s^+ reflection subtraction	2483	21600±158	19.5%
Standard without D_s^+ reflection subtraction and No *K*-Čerenkov	3204	29270±191	25.8%
Standard without D_s^+ reflection subtraction, No *K*-Čerenkov, and allow category 3 tracks	3965	36560±213	27.1%

$$\%Diff. = \frac{BR(Old) - BR(Cut)}{BR(Cut)} \cdot 100\% \qquad (4)$$

To more correctly model the systematic effects the following modifications have been made to the D^+ and D_s^+ normalization's. For the $D^+ \to \pi\ell\ell$ modes the Čerenkov cut on the kaon in the $D^+ \to K^-\pi^+\pi^+$ normalization sample has been lowered to >0.10 from 0.13, but for the $D^+ \to K\ell\ell$ modes it remains >0.13. (See Figure 36 and Figure 37 for $D^+ \to \pi\ell\ell$ and $D^+ \to K\ell\ell$, respectively. Also see Figure 18 and Figure 19 for the Monte Carlo normalization.) For the $D_s^+ \to K^+\ell^\pm\ell^\mp$ modes the Čerenkov cut is made on the K^+ in the $D_s^+ \to \phi\pi^+$ normalization sample but for the $D_s^+ \to K^-\ell^+\ell^+$ modes the Čerenkov cut is made on the K^- in the $D_s^+ \to \phi\pi^+$ normalization sample. (See Figure 40 and Figure 41 for $D_s^+ \to K^+\ell^\pm\ell^\mp$ and $D_s^+ \to K^-\ell^+\ell^+$, respectively. Also see Figure 22 and Figure 23 for the Monte Carlo normalization.) For the $D_s^+ \to \pi\ell\ell$ modes the Čerenkov cut on the kaons in the $D_s^+ \to \phi\pi^+$ normalization sample has been lowered to >0.10 from 0.18. (See and Figure 24 for the Monte Carlo normalization.)

[1] J. Rasmunssen and A. Schwartz, *A Search for Rare and Forbidden D^0, D^+, and D_s Decays in FNAL E791*, (Offline_doc_234) September 10, 1997.

[2] E. M. Aitala, *et al*., *Search for the Flavor-Changing Neutral-Current Decays $D^+ \to \pi^+ \mu^+ \mu^-$ and $D^+ \to \pi^+ e^+ e^-$*, Phys. Rev. Lett. **76**, 364 (1996).

[3] C. Zhang, *Muon ID Study using $D^+ \to \overline{K}^{*0} \mu^+ \nu$ mode*, (Offline_doc_219) November 2, 1995

[4] L. Cremaldi, *Čerenkov ID Midplane Study*, (Offline_doc_317) August 1996.

[5] N. Witchey, N. W. Reay, and A. Nguyen, *Muon Wall Efficiencies*, (Offline_doc_113) November 4, 1994.

[6] P. Gagnon, P. Burchat and P. Kasper, *Electron Identification in the E791 Offline Reconstruction Code*, (Offline_doc_88) April 1993.

[7] H. S. Cavalho, *E791 Čerenkov kaon ID efficiency study*, (Offline_doc_223) April 1995.

[8] G. J. Feldman and R. D. Cousins, *A Unified Approach to the Classical Statistical Analysis of Small Signals*, Phys. Rev. **D57**, 3873-3889 (1998).

[9] R. D. Cousins and V. L. Highland, *Incorporating systematic uncertainties into an upper limit*, Nucl. Inst. Meth. **A320**, 331-335 (1992).

[10] R. Sidwell, N. Stanton and N. Witchey, *Concise Technical Memo to Supplement FCNC PRL Draft#8*, (Offline_doc_417) April 5, 1995.

Appendix

Subroutine MUQLT_DIST_DPAD

```
      subroutine muqlt_dist_dpad(track,muindex,xhit,yhit,nxsigma,
     1     nysigma,mu_x,mu_y,distm,mucat)
C
      implicit none
      save

      include '/usr/tools/e791/includes/param_trk.inc'
      include '/usr/tools/e791/includes/param_ttt.inc'
      include '/usr/tools/e791/includes/tracks.inc'
      include '/usr/tools/e791/includes/param_ntk.inc'
      include '/usr/tools/e791/includes/sierra.inc'
      include '/usr/tools/e791/includes/calsum.inc'
      include '/usr/tools/e791/includes/mutrks.inc'
      include '/usr/tools/e791/includes/dstvn.inc'
c
      include '/usr/tools/e791/includes/param_muon.inc'
      include '/usr/tools/e791/includes/geom_muon.inc'
      include '/usr/tools/e791/includes/runid.inc'

C
C Arun Tripathi Jan 28, 1994.
C Documentation offline_199.ps
C This subroutine takes as input a muon track from rel 6 muon reconstruction
C code ( only DST information ) and returns the following.
C 1. A flag is set if the hit paddle is the one on which the projected hit
C    lies, both for X and Y walls.
C 2. If the projected paddle was not the one that got hit, find the distance
C    between the hit paddle position and the projected track position.
C 3. Find out the MS radius, and number of sigma's the hit is away from
C    the projected position.
C Input: TRACK - The muon candidate track number
C Output: XHIT - The flag that is set to 1 if projected and hit x-paddle are
C              the same.
C       YHIT - The flag that is set to 1 if projected and hit Y-paddles are
C              the same.
C       DELX - Separation between the projected and real x-hit
C       DELY - Separation between the projected and real y-hit.
C       NXSIGMA - Number of sigma's the hit is away from the projected X
C                 paddle after subtracting the half paddle width.
C       NYSIGMA - Number of sigma's the hit is away from the projected Y
C                 paddle after subtracting the half paddle width.
C

c  May 1998 mu_y = no. of hit paddle in Y wall.
c  May 1998 mu_x = no. of hit paddle in X wall.
c
c  May 1998 added mucat, distm as output and muindex as input to replace
c  Arun and Daniel's "proj_mu_d" and  "muqlt_dpad"

C
```

```
C The Z-positions of the X and Y walls.
C
      real zxwall,zywall
      data zxwall /2243.0/
      data zywall /2419.0/

C
C The distance between the muon walls and the track intercept in Z:
      real z1,z2

C
C     Where the extrapolated track intercepts the muon wall
C
      real dcx1,dcy1,dcx2,dcy2,w,x_c

C
C The flag to signal if the hit paddle is the same as the projected one
C
      integer xhit,yhit

C
C Input track number
C
      integer track,mucat,mu_x,mu_y
C
C Other local variables
C

      integer i,muindex
      real xms,yms,delx,dely
      real xmux(15),ymux(15),xmuy(16),ymuy(16)
      real x3,y3,dxdz3,dydz3
      real tdc_b,tdc_m,distm

C
C Number of sigma's from the projected hit position:
C
      real nxsigma,nysigma
C
C Initialize the X and Y paddle coordinates
C First the X wall

      do i = 1,15
            xmux(i) = -1000.
            ymux(i) = -1000.
      enddo

C
C The Y wall
C
      do i = 1,16
            xmuy(i) = -1000.
            ymuy(i) = -1000.
```

```
        enddo

C
C Now get the co-ordinates of the center of the paddles
C First the Y - wall. It's simpler

        do i = 1,16
                ymuy(i) = ( i - 8 )*14.0 - 7.0 + 1.2
        enddo

C
C The X-wall. It is not uniform
C
        do i = 1,6
                xmux(i) = ( i - 6 )*40.64 - 50.8 - 4.9
        enddo

        xmux(7) = -4.9
        xmux(8) = -4.9
        xmux(9) = -4.9

        do i = 10,15
          xmux(i) = (i - 10)*40.64 + 50.8 - 4.9
        enddo

        xhit = -1
        yhit = -1
        mucat = 0

        nxsigma = 99.
        nysigma = 99.

C
C Nick's multiple scattering window:
C

        xms = 55.6245/( pp(track) - 1.29029 )
        yms = 98.55266/( pp(track) - 1.86859 )

C
C Extrapolate the track to the muon walls ( in DC coordinates ):
C

        z1 = zxwall - av(3,3,track)
        z2 = zywall - av(3,3,track)
c
        if ( idstvn .lt. 7 ) then

                dcx1 = z1*dxdz(3,track) + av(1,3,track)
                dcy1 = z1*dydz(3,track) + av(2,3,track)
                dcx2 = z2*dxdz(3,track) + av(1,3,track)
                dcy2 = z2*dydz(3,track) + av(2,3,track)

C In release 7, region 3 info is not stored on DST. Compute these from
```

```
C region 1 info.
C
        elseif ( idstvn .eq. 7 ) then

                call region23(track,x3,y3,dxdz3,dydz3)

                dcx1 = z1*dxdz3 + x3
                dcy1 = z1*dydz3 + y3
                dcx2 = z2*dxdz3 + x3
                dcy2 = z2*dydz3 + y3

        endif
c
c       Subtract muon wall offsets
c
        dcx1=dcx1-mux_xoff
        dcy1=dcy1-mux_yoff
        dcx2=dcx2-muy_xoff
        dcy2=dcy2-muy_yoff
c
c       calculate distm
c
c       tdc_b=9150.0
        tdc_b=9134.0
        tdc_m=-10.0
        if(run_number.lt.1000)then
                tdc_b=9011.2
                tdc_m=-9.8
        elseif(run_number.ge.1000.and.run_number.lt.1400)then
                tdc_b=9150.0
                tdc_m=-10.0
        elseif(run_number.ge.1400.and.run_number.lt.2000)then
                tdc_b=8971.8
                tdc_m=-9.8
        endif
c
c       distm=abs(tdc_b+tdc_m*mutdcy(muindex)-dcx2)/sqrt(1.+tdc_m**2)
        distm=(tdc_b+tdc_m*mutdcy(muindex)-dcx2)/sqrt(1.+tdc_m**2)
        call hfill(15,tdc_b+tdc_m*mutdcy(muindex),dcx2,1.)
C
C Find the separation between the projected hit position and the hit paddle
C center.
C First the X-wall

        mu_x = -1
        x_c = -1000.

        if ( mupadx(muindex) .gt. 0 ) then
                mu_x=mupadx(muindex)
                x_c = xmux(mupadx(muindex))
                delx = abs( dcx1 - xmux(mupadx(muindex)) )
C
C The center X-paddles are wider
```

```
C
                if ( (mupadx(muindex) .ge. 7) .and. (mupadx(muindex) .le. 9) ) then
C
C See if the projected paddle was hit
C
                        if ( delx .lt. 30.48 ) then
                                xhit = 1
                        endif
C
C Get the number of sigma's the hit is from the projected position. In doing
C this, keep in mind that half paddle width must be added to any sigma-cut.

                        nxsigma = int(abs(delx - 30.48)/xms)

                else

C
C Other paddles:
C

                        if ( delx .lt. 20.32 ) then
                                xhit = 1
                        endif
C
C Again find the number of sigma away from the hit, after subtracting half
C paddle width.

                        nxsigma = int(abs(delx - 20.32)/xms)

                endif
        endif

C
C The Y-wall
C
        mu_y = -1
        if ( mupady(muindex) .gt. 0 ) then
                mu_y=mupady(muindex)
                dely = abs( dcy2 - ymuy(mupady(muindex)) )
                call hf1(19,dcy2-ymuy(mupady(muindex)),1.)
                if( dely .lt. 7. ) then
                        yhit = 1
                        call hfill(13,dcx2,dcy2,1.)
                        call hfill(14,float(mutdcy(muindex)),dcx2,1.)
                endif
C
C Number of sigma the hit is away from the projected position, after
C subtracting the half paddle width

                nysigma = int(abs(dely - 7.0)/yms)
        endif

C
C Now compute a number called 'mucat' that describes the quality of the
```

C muon tag. Higher the number, better the quality.

```
c
c  fix the window at 1 sigma:
c
        w = 1.5

        if ( (xhit .gt. 0) .and. (yhit.gt.0) ) then
                mucat = 9
        elseif ( (yhit.gt.0) .and. (nxsigma.le.w) ) then
                mucat = 8
        elseif ( (xhit.gt.0) .and. (nysigma.le.w) ) then
                mucat = 6
        elseif ((nysigma.le.w).and.(nxsigma.le.w)) then
                mucat = 5
        elseif ( (yhit.gt.0) .and. (nxsigma.gt.w) ) then
                mucat = 7
        elseif ( (xhit.gt.0) .and. (nysigma.gt.w) ) then
                if(dcy2.gt.-111.0.and.dcy2.lt.113.0.and. dcx2.gt.-161.0.and.dcx2.lt.139.0) then
                        mucat = 2
                else
                        mucat = 3
                endif
        elseif ((nysigma.le.w).and.(nxsigma.gt.w)) then
                mucat = 4
        endif

        return
        end
```

Figures

Standard Model **Flavor Changing Neutral Current**

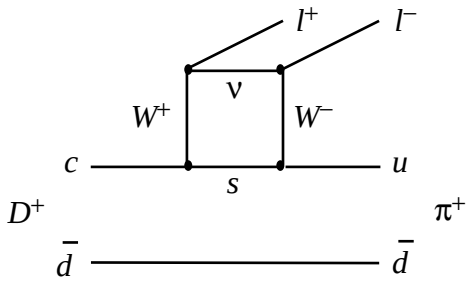

(a) $D^+ \to \pi^+ l^+ l^-$

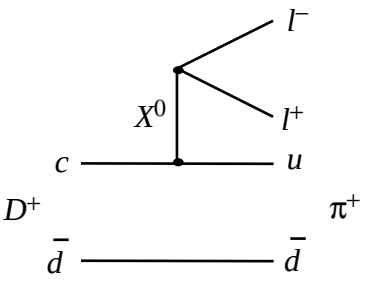

(d) $D^+ \to \pi^+ l^+ l^-$

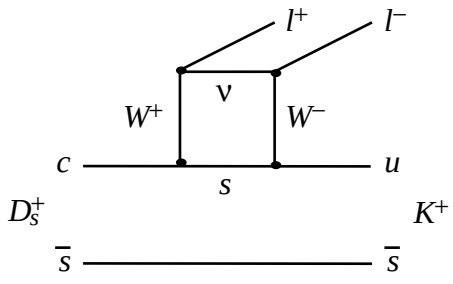

(b) $D_s^+ \to K^+ l^+ l^-$

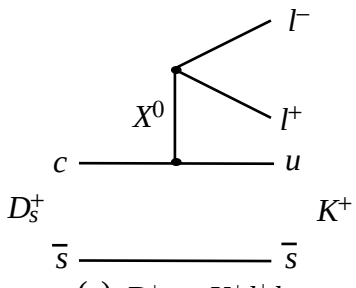

(e) $D_s^+ \to K^+ l^+ l^-$

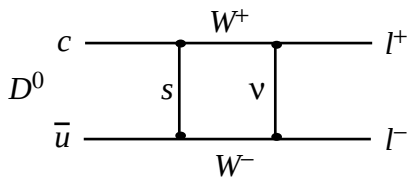

(c) $D^0 \to l^+ l^-$

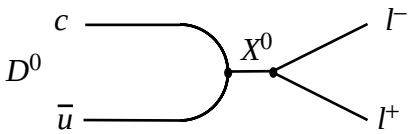

(f) $D^0 \to l^+ l^-$

Figure 1:
The Feynman diagrams for both the Standard Model (a-c) and FCNC (d-f) for D^+, D_s^+, and D^0 decay modes, where the *l*s are either both muons or both electrons.

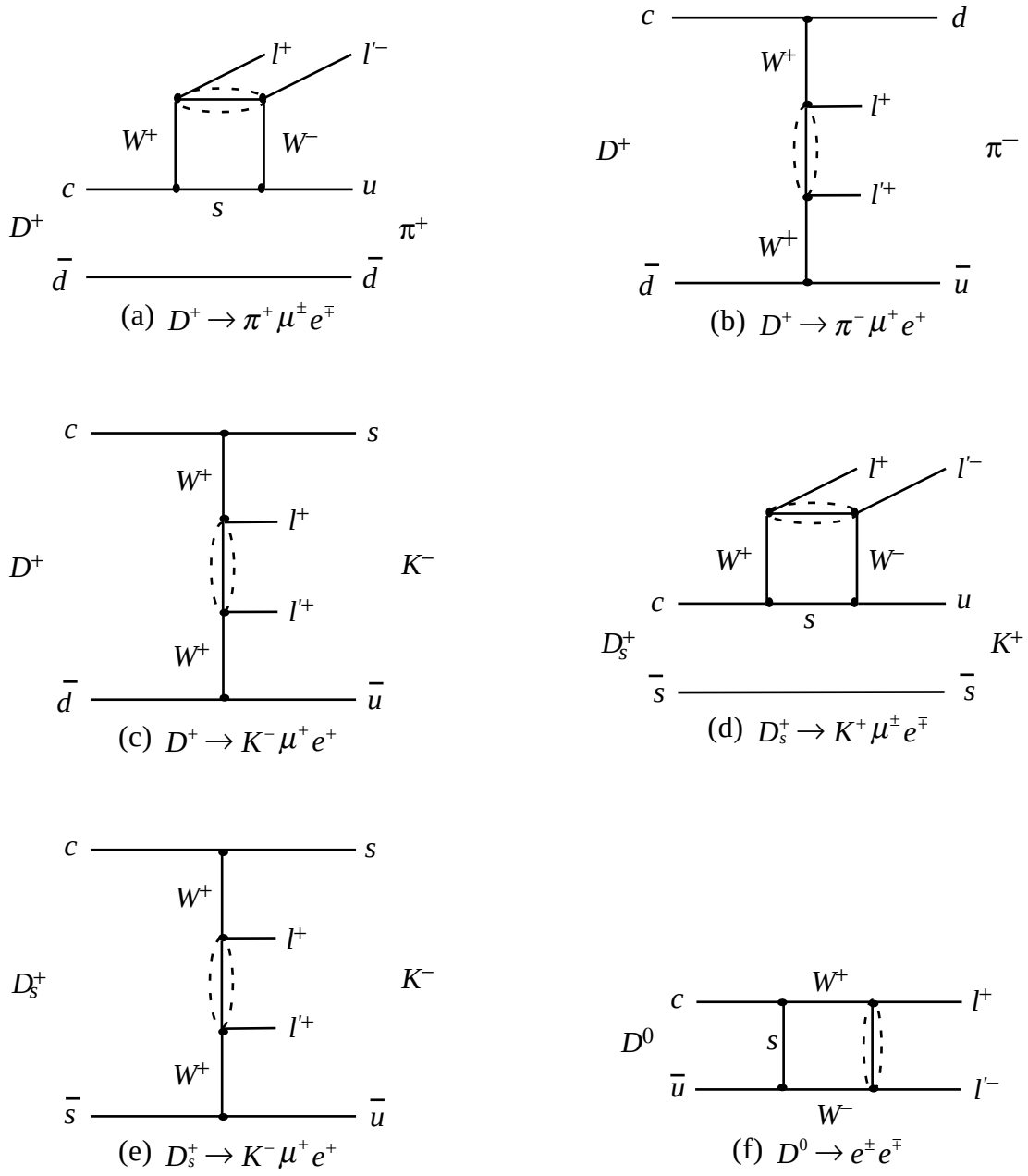

Figure 2:
The Feynman diagrams for the LFV modes D^+, D_s^+, and D^0 decays, where the *l*s are muons and the *l*'s are electrons or visa-versa as shown in the individual diagram titles. The simplest mechanism for these decay modes would be a neutrino oscillation, $\nu_\mu \leftrightarrow \nu_e$, in place of the neutrino exchange mechanism of the Standard Model in Figure 1.

Lepton Number Violating

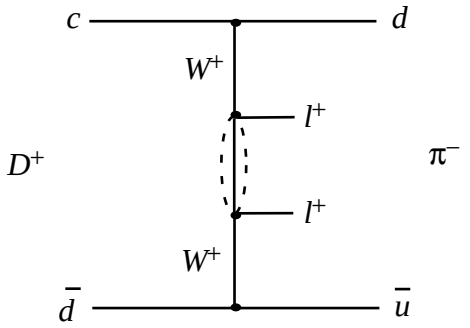

(a) $D^+ \to \pi^- l^+ l^+$

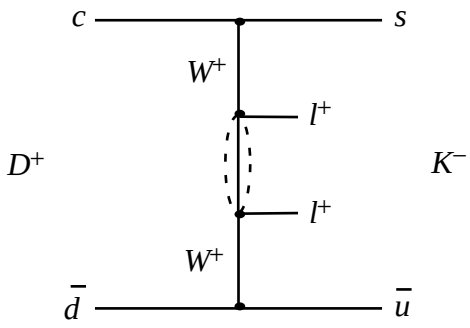

(b) $D^+ \to K^- l^+ l^+$

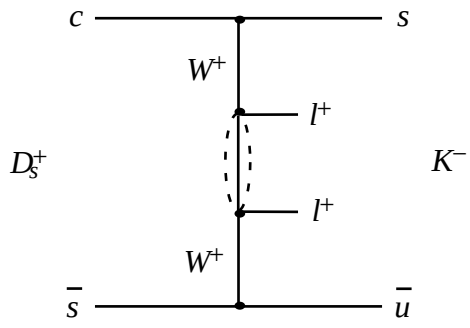

(c) $D_s^+ \to K^- l^+ l^+$

Figure 3:
The Feynman diagrams for the LNV modes for D^+, D_s^+, and D^0 decays, where the *l*s are either 2 muons or 2 electrons. One mechanism for these decay modes would be a neutrino-antineutrino oscillation, $\nu_\ell \leftrightarrow \overline{\nu}_\ell$, in place of the neutrino exchange mechanism of the Standard Model in Figure 1.

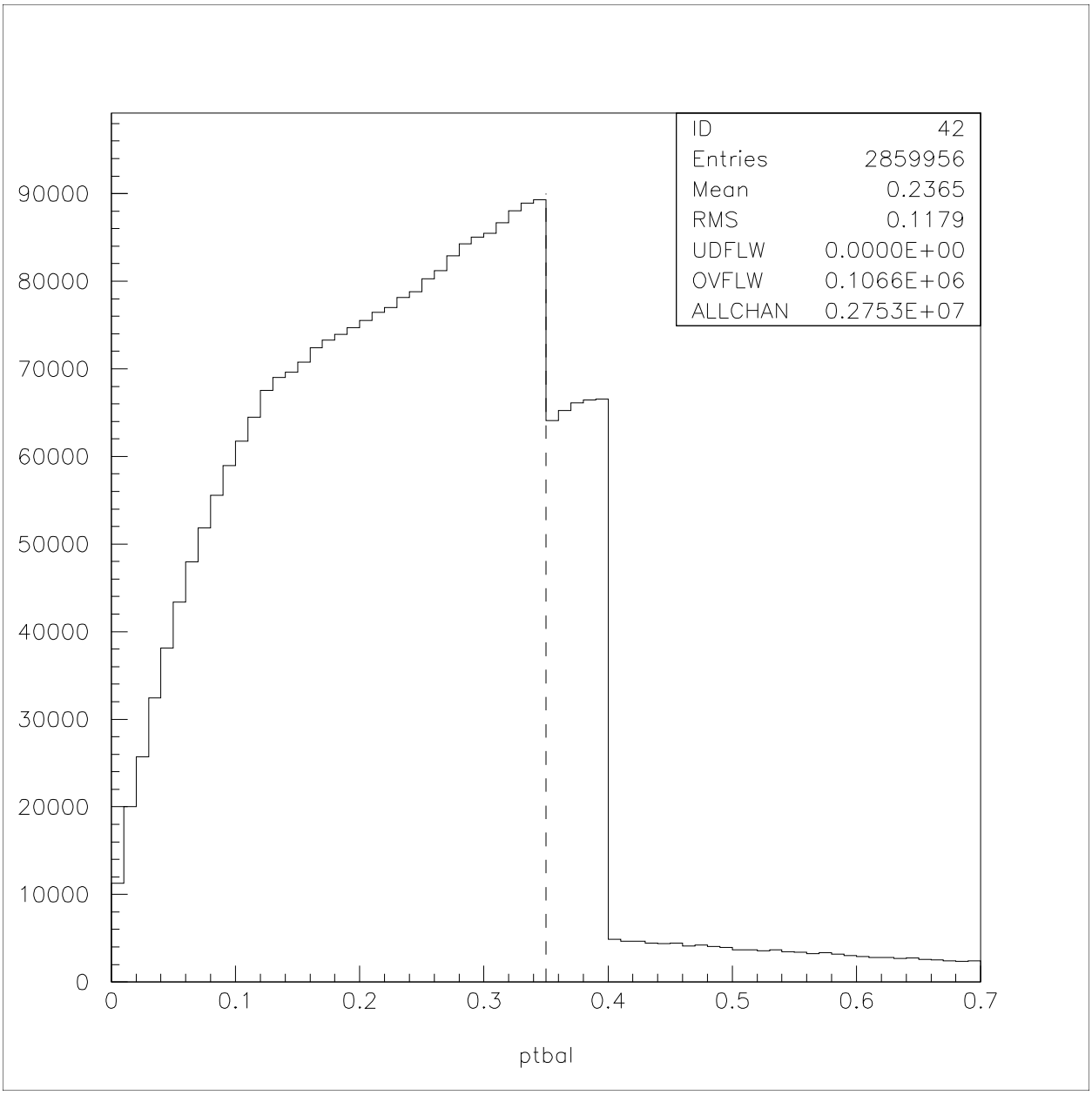

Figure 4:
The PTB from the data. The dashed line is 0.35 GeV/c.

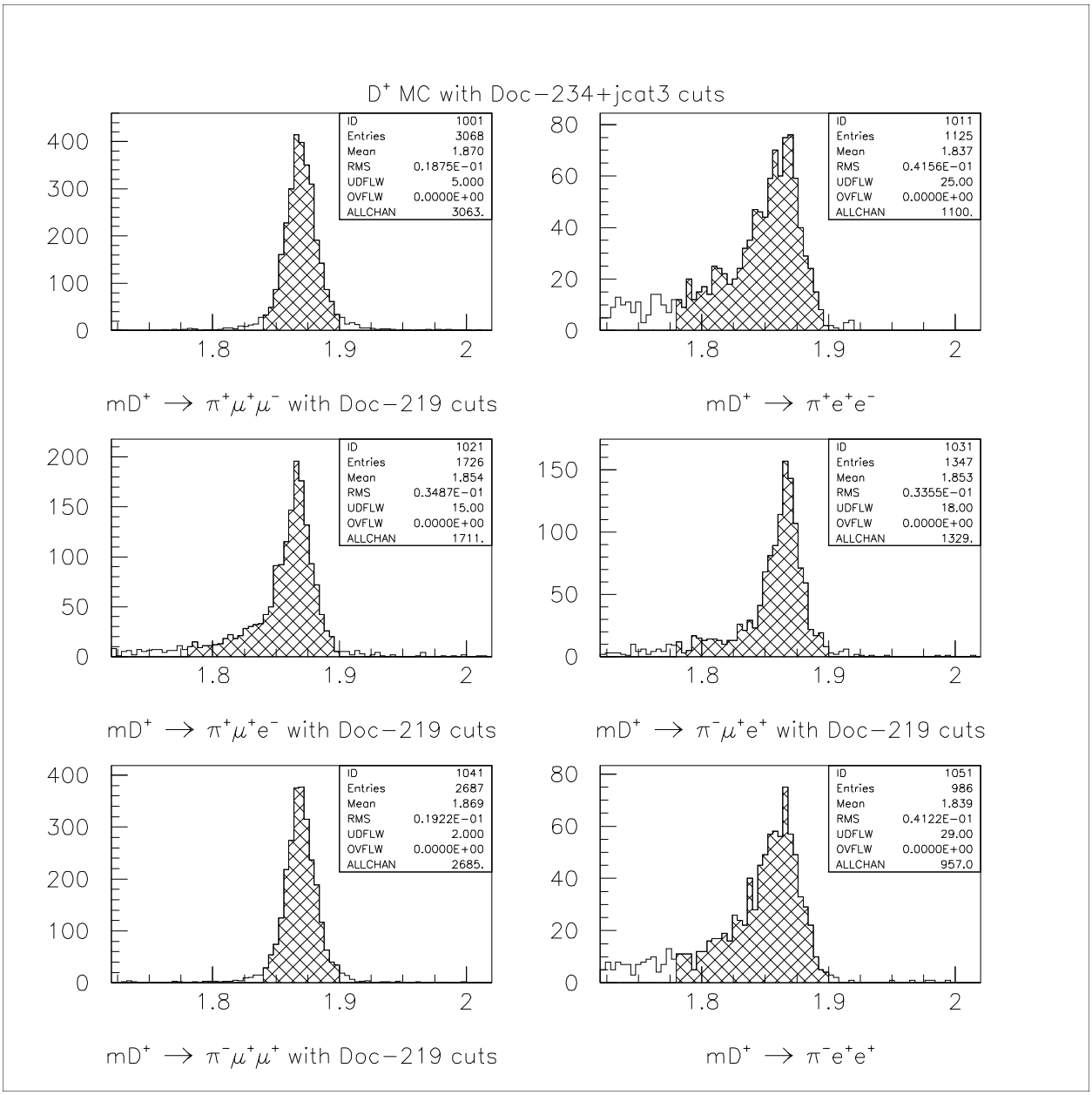

Figure 5:
Examples of the asymmetric mass cut and the bremsstrahlung tail in D^+ Monte Carlo events. The shaded region is the mass window.

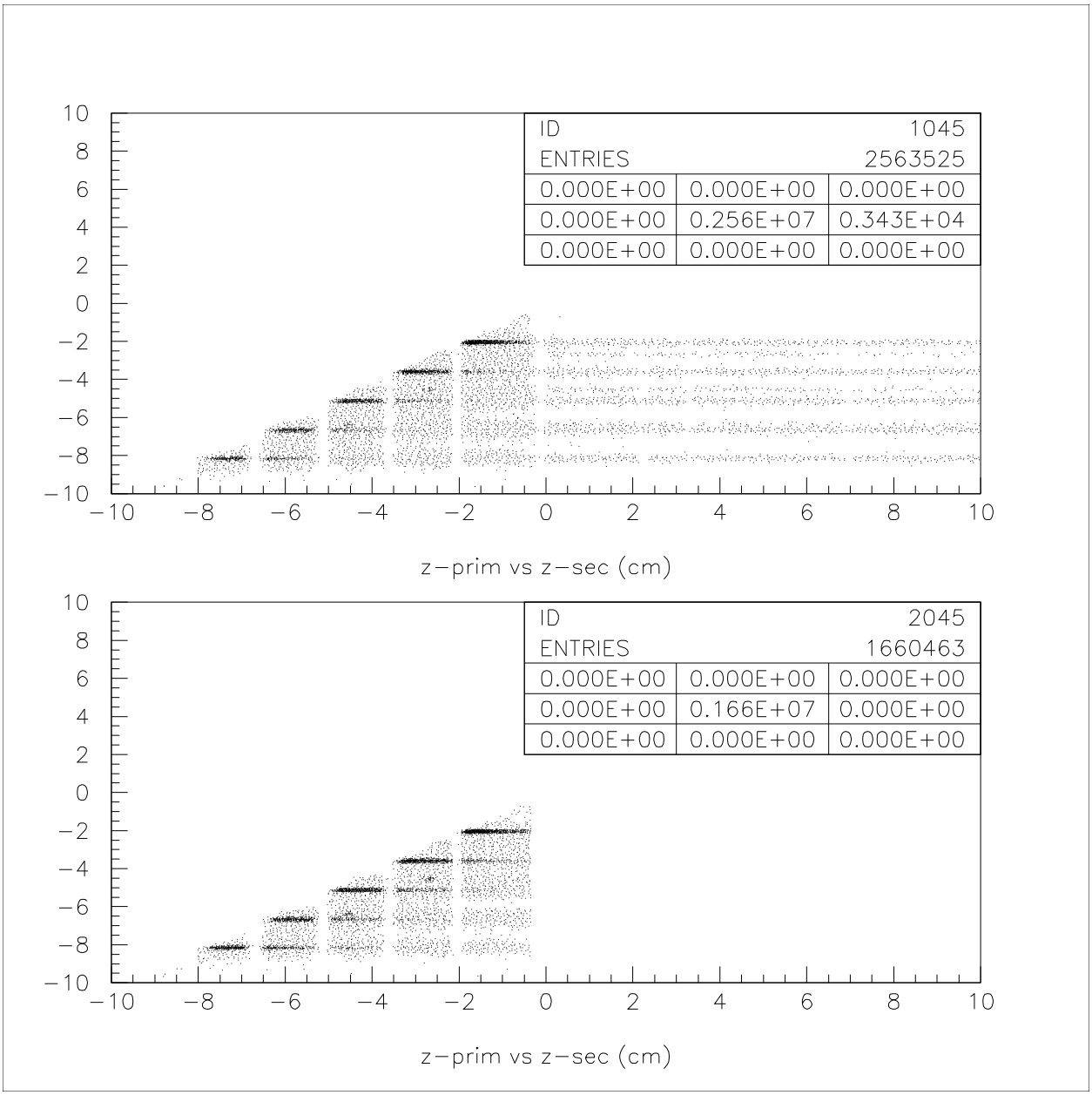

Figure 6:
z-primary vs. *z*-secondary for all events (Top) and for accepted events (Bottom).

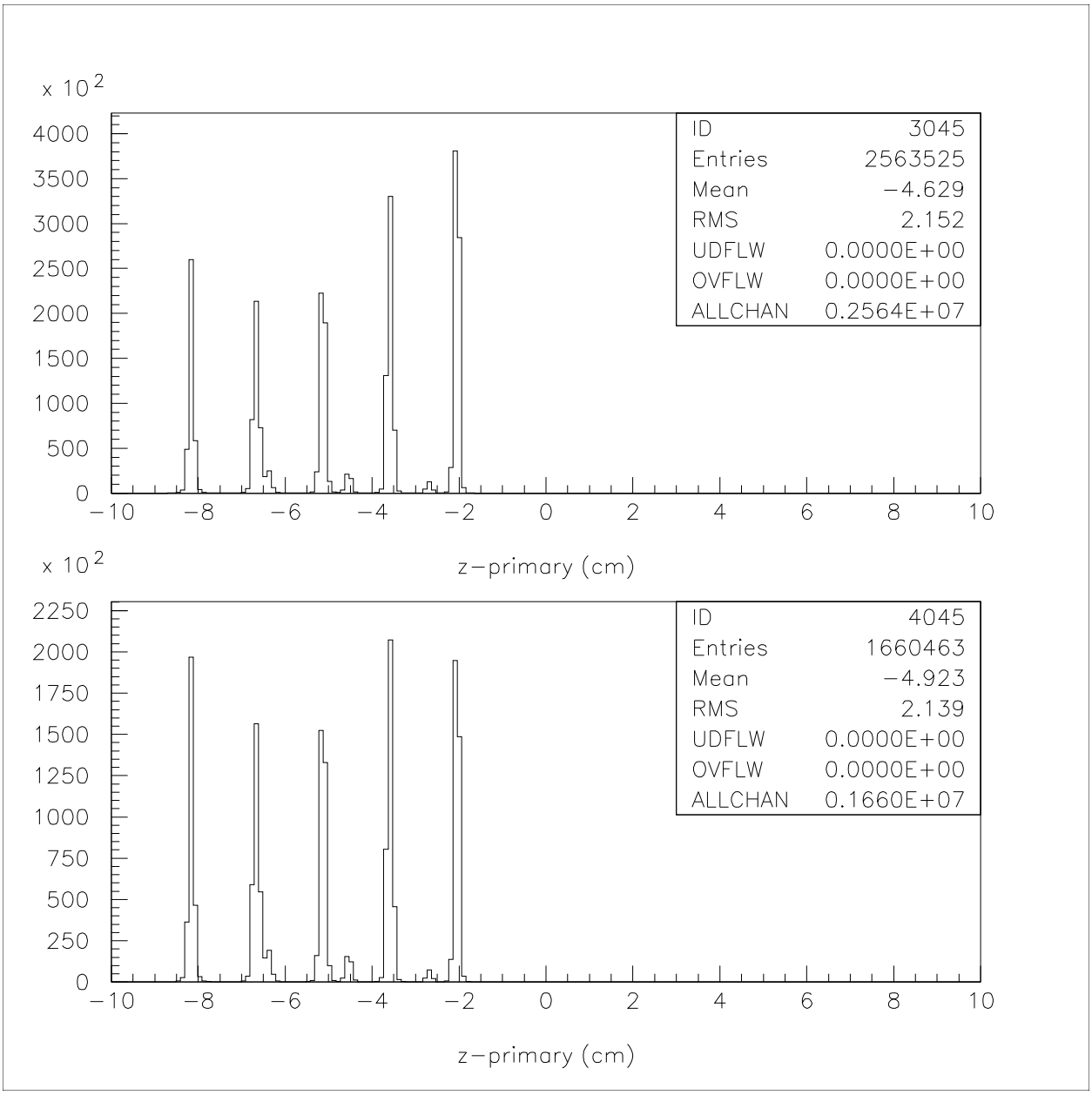

Figure 7:
z-primary for all events (Top) and for accepted events (Bottom).
The small bump located at the edge of the second target and between the third-and-fourth and fourth-and-fifth targets are the second, third and fourth targets, respectively, from the 4-target runs.

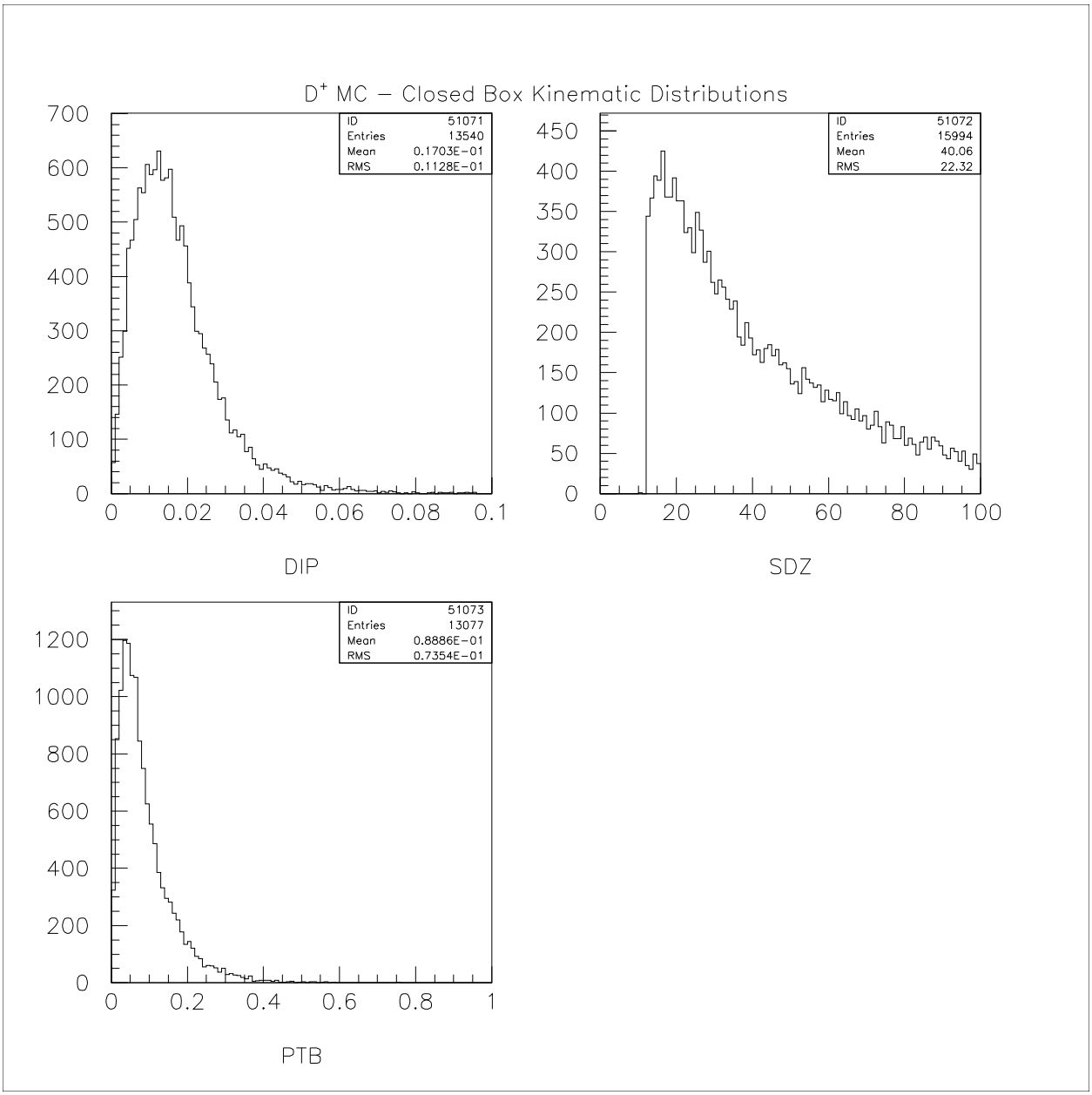

Figure 8:
D^+ Monte Carlo kinematics variables.

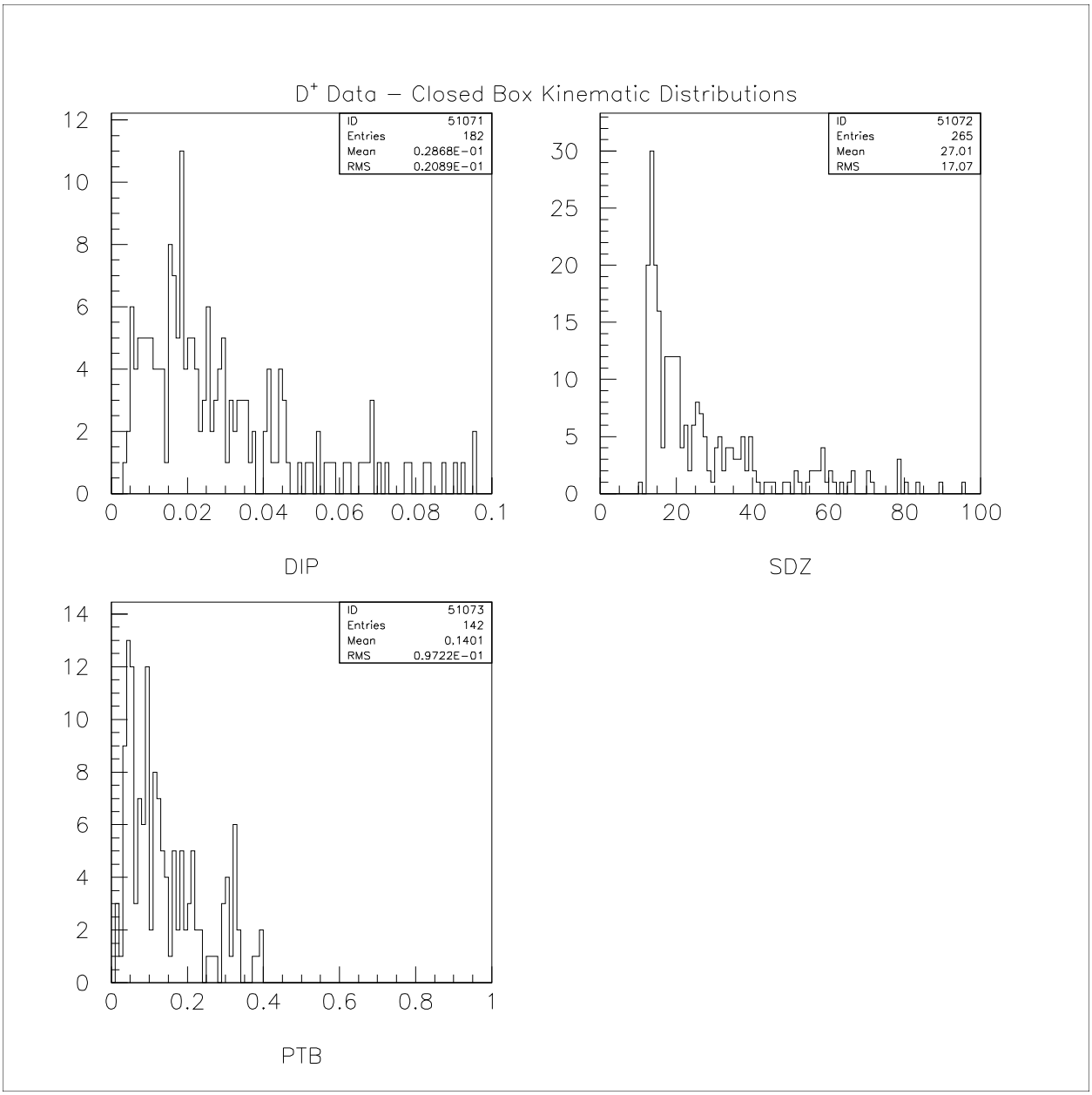

Figure 9:
D^+ closed "box" data kinematics variables.

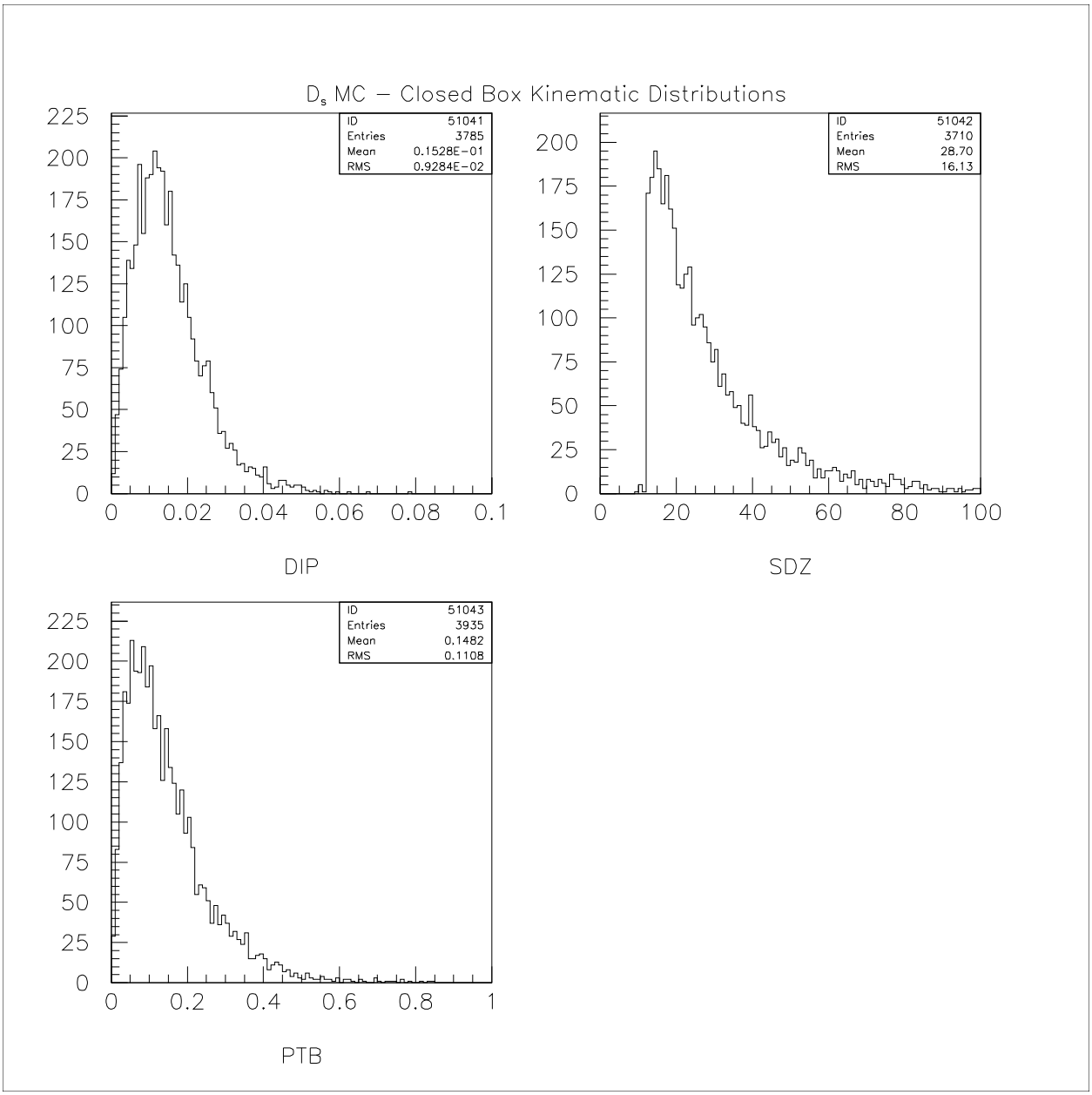

Figure 10:
D_s^+ Monte Carlo kinematics variables.

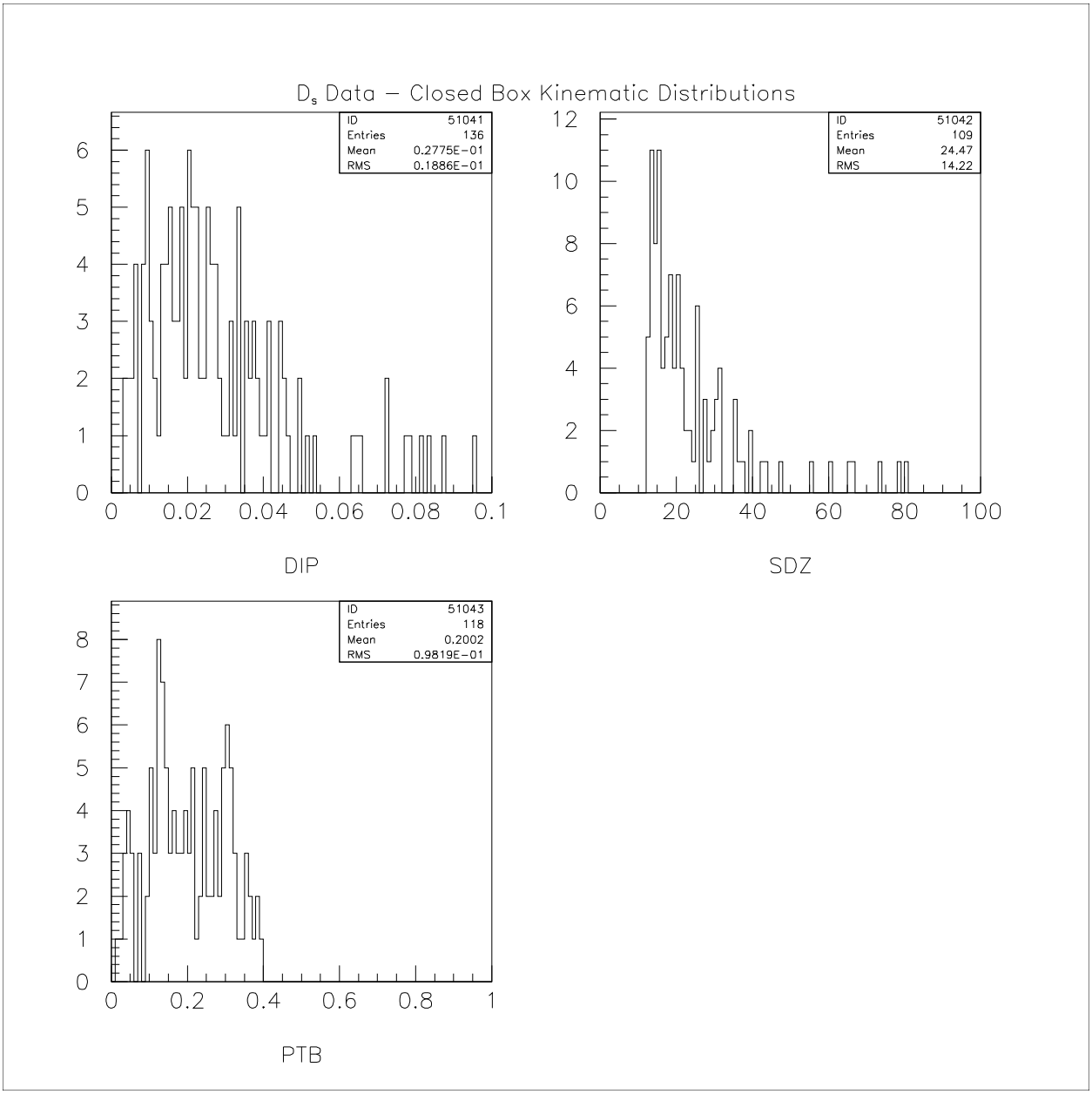

Figure 11:
D_s^+ closed "box" data kinematics variables.

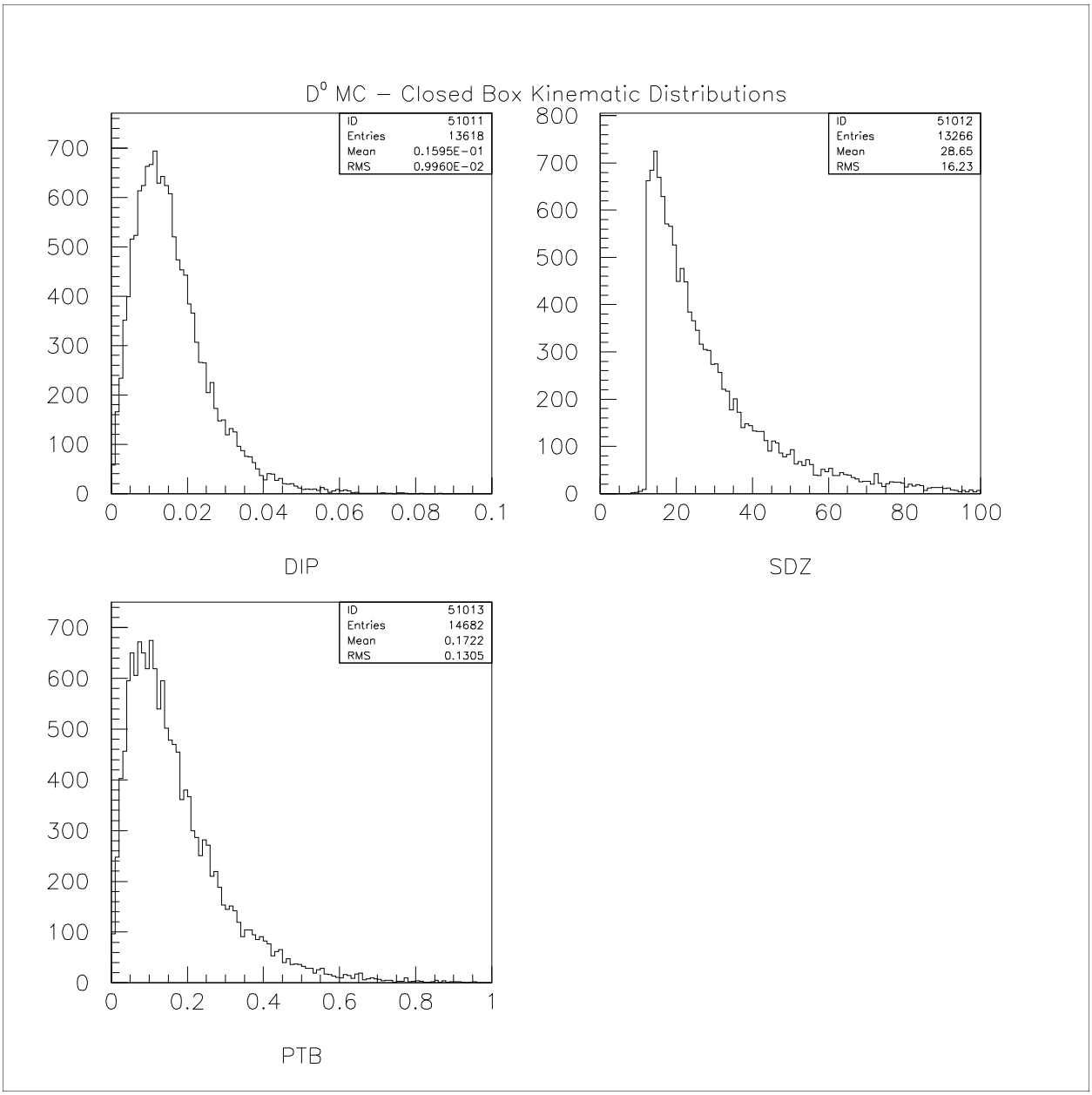

Figure 12:
D^0 Monte Carlo kinematics variables.

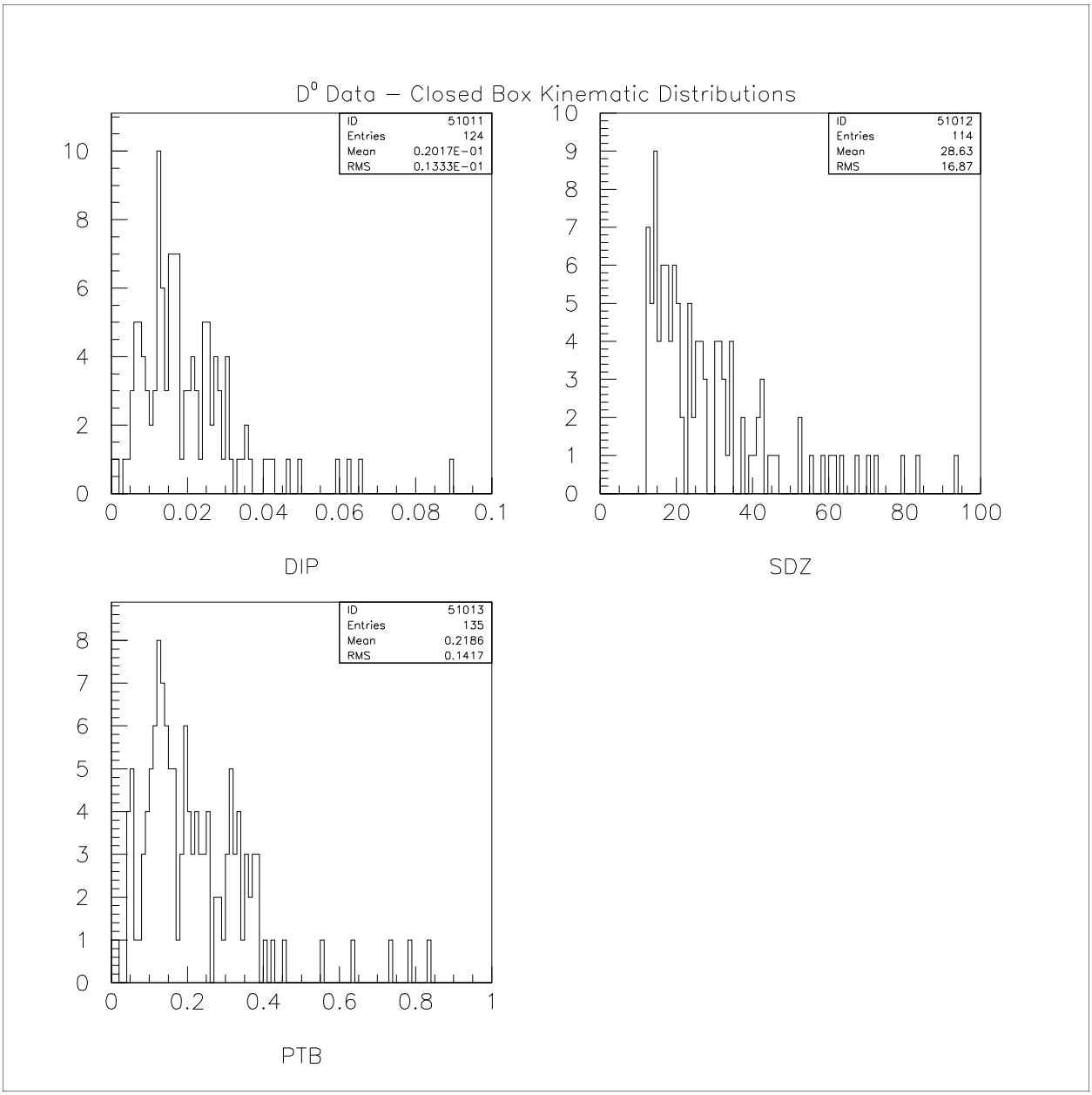

Figure 13:
D^0 closed "box" data kinematics variables.

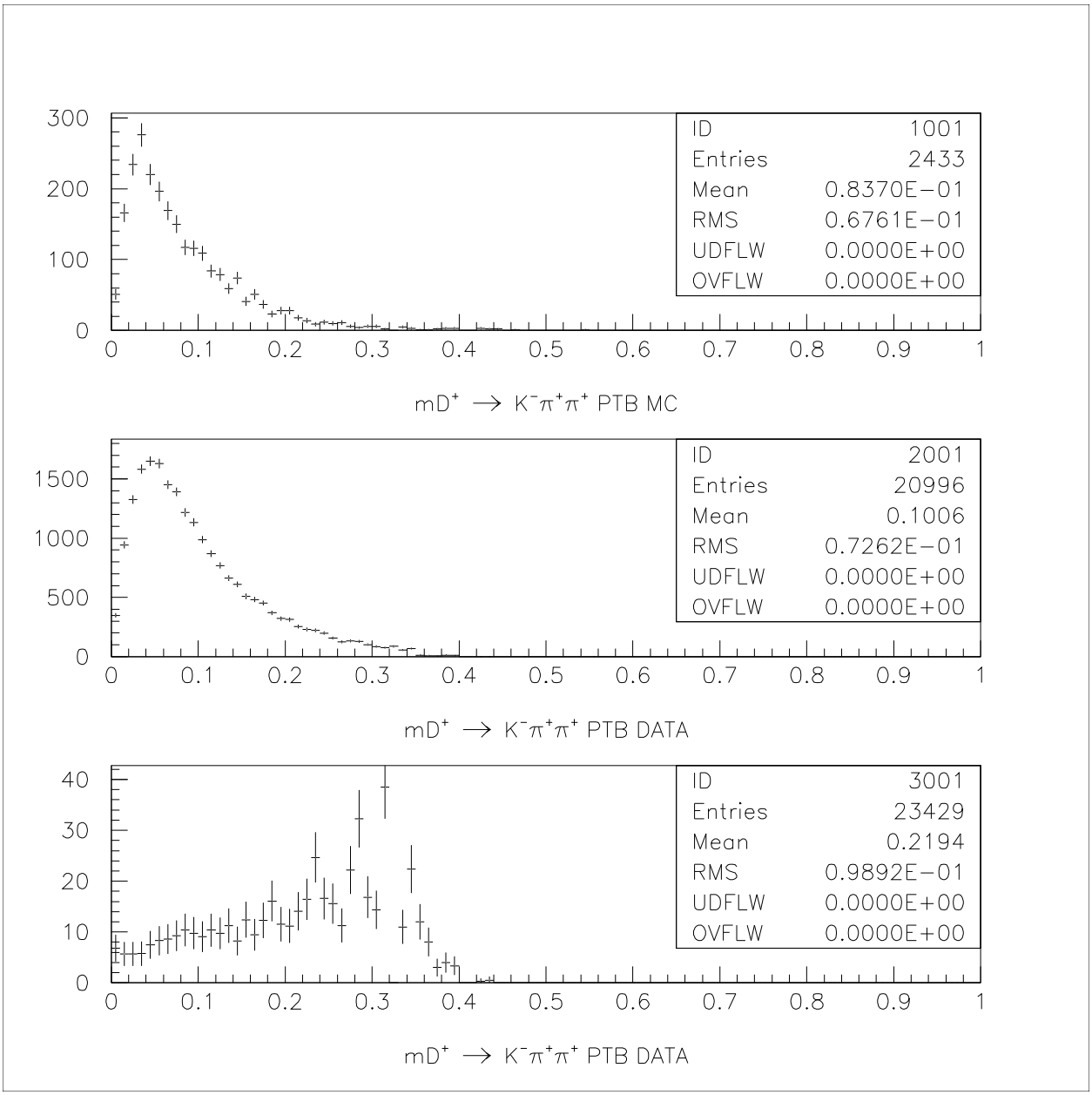

Figure 14:
PTB from $D^+ \to K^- \pi^+ \pi^+$ for Monte Carlo, data and data/MC.

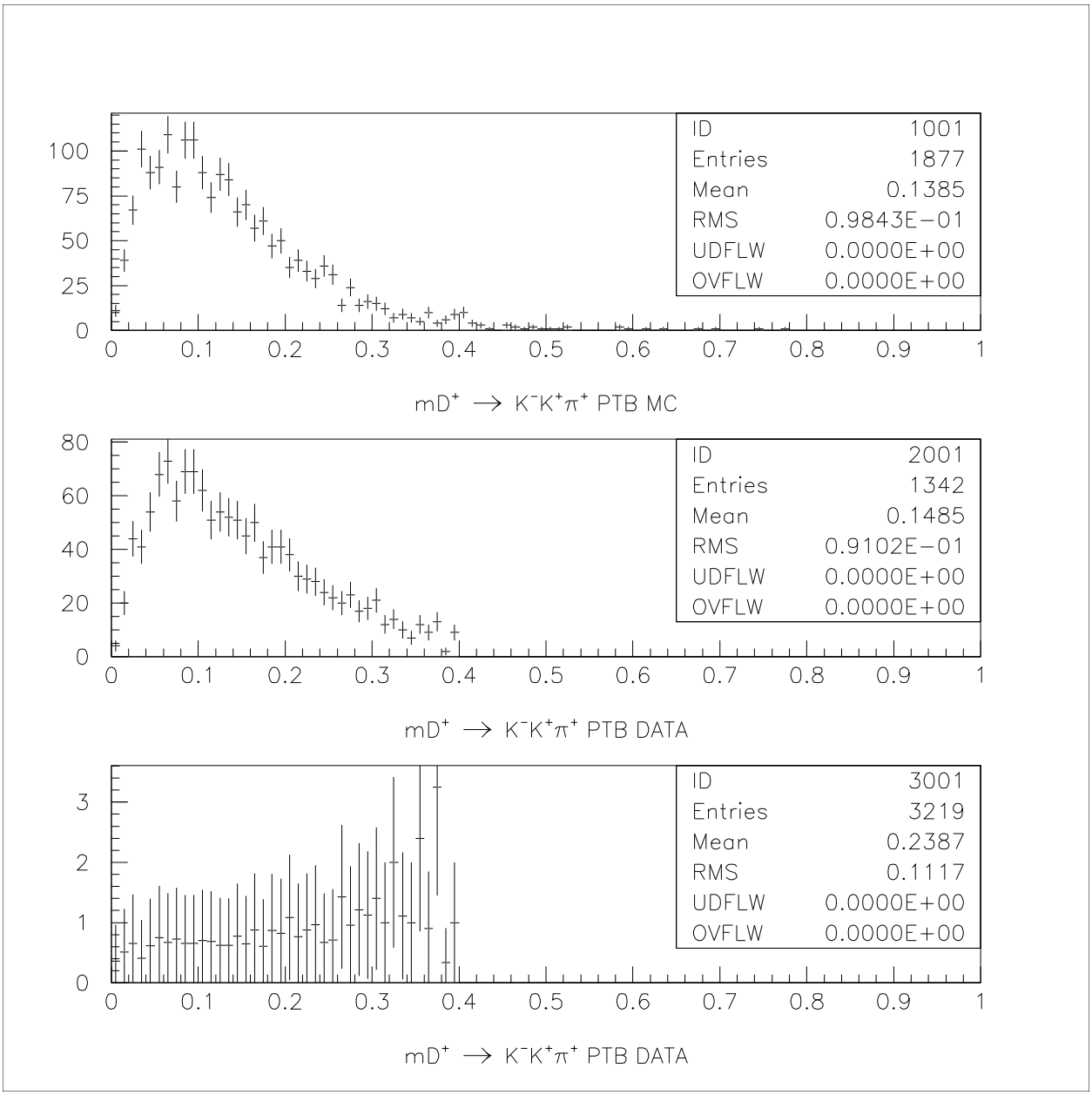

Figure 15:
PTB from $D_s^+ \to \phi\pi^+$ for Monte Carlo, data and data/MC.

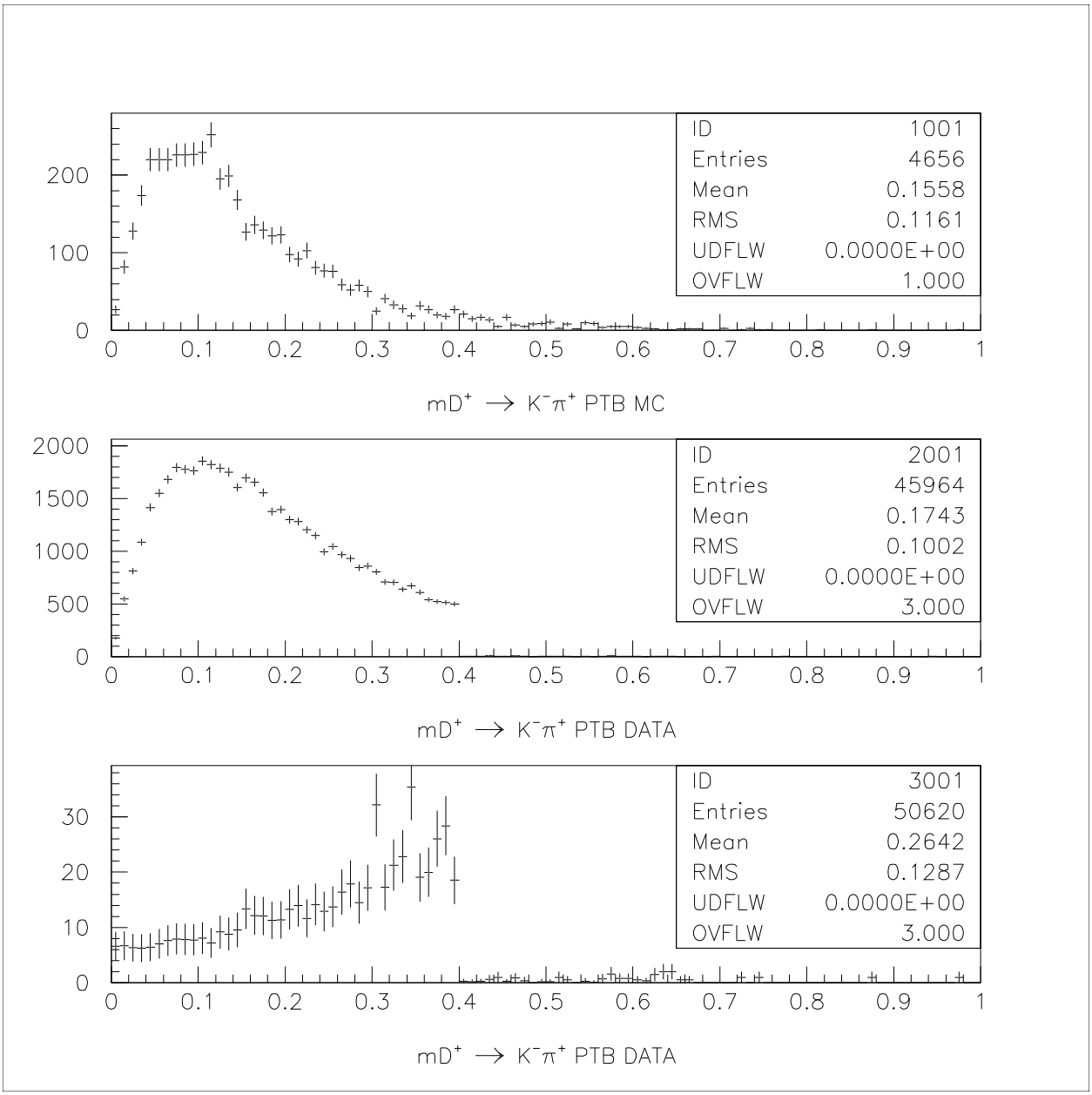

Figure 16:
PTB from $D^0 \to K^- \pi^+$ for Monte Carlo, data and data/MC.

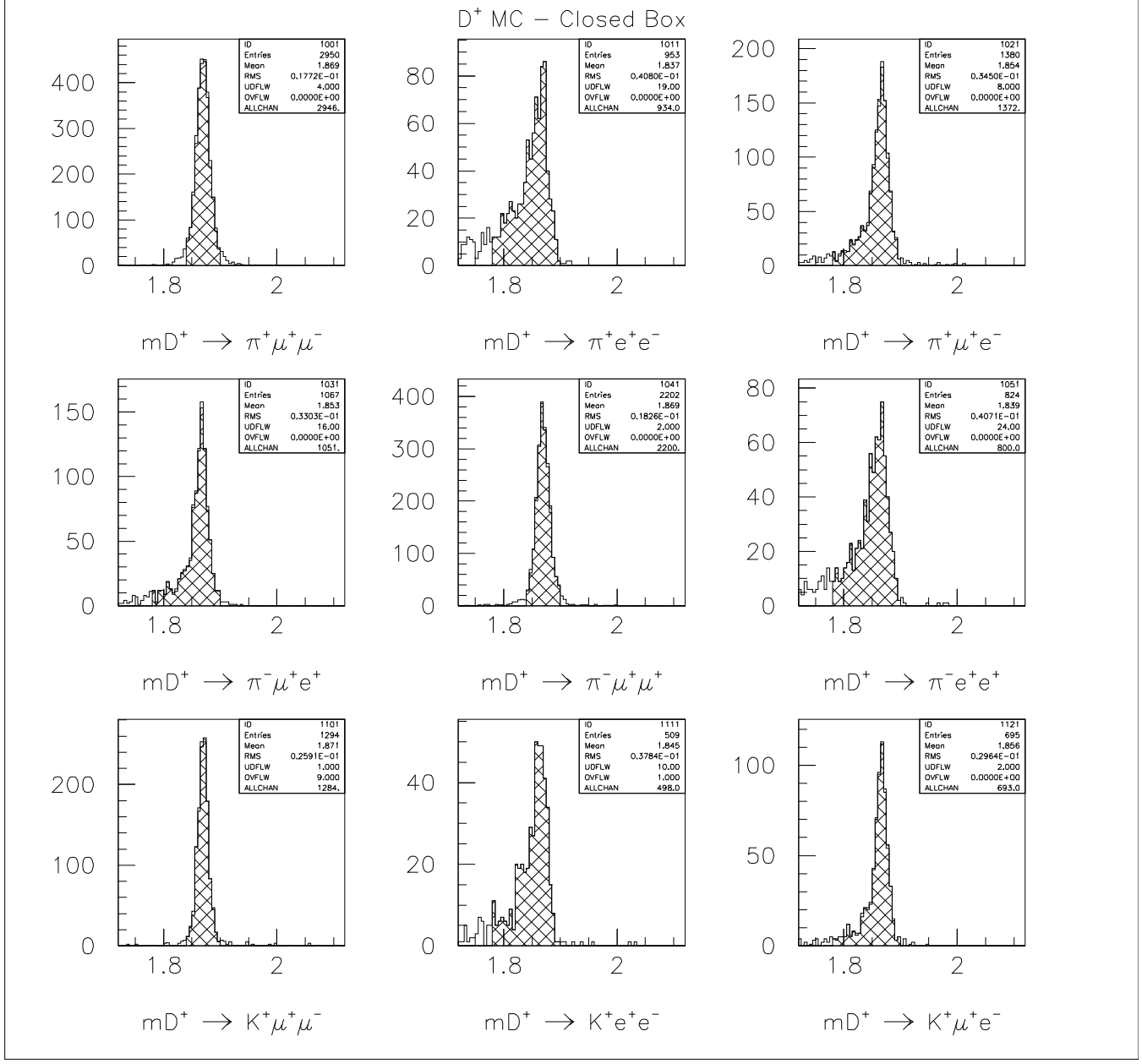

Figure 17:
D^+ Monte Carlo decay modes. Shaded region is "box". Bin width = 5 MeV/c^2.

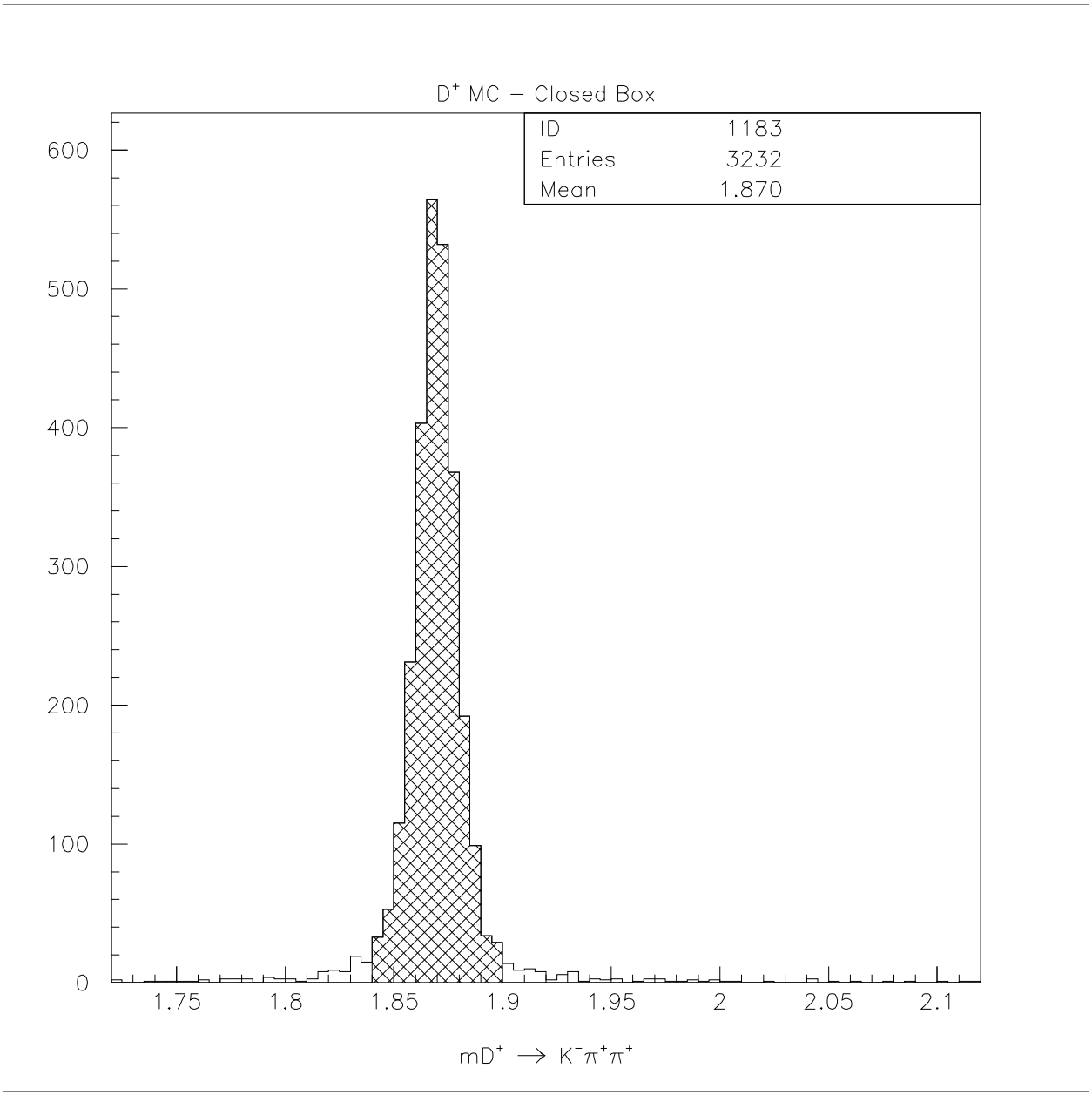

Figure 18:
Monte Carlo normalization - $D^+ \to K^-\pi^+\pi^+$ for the $D^+ \to \pi\ell\ell$ modes. Shaded region is "box". Bin width = 5 MeV/c^2.

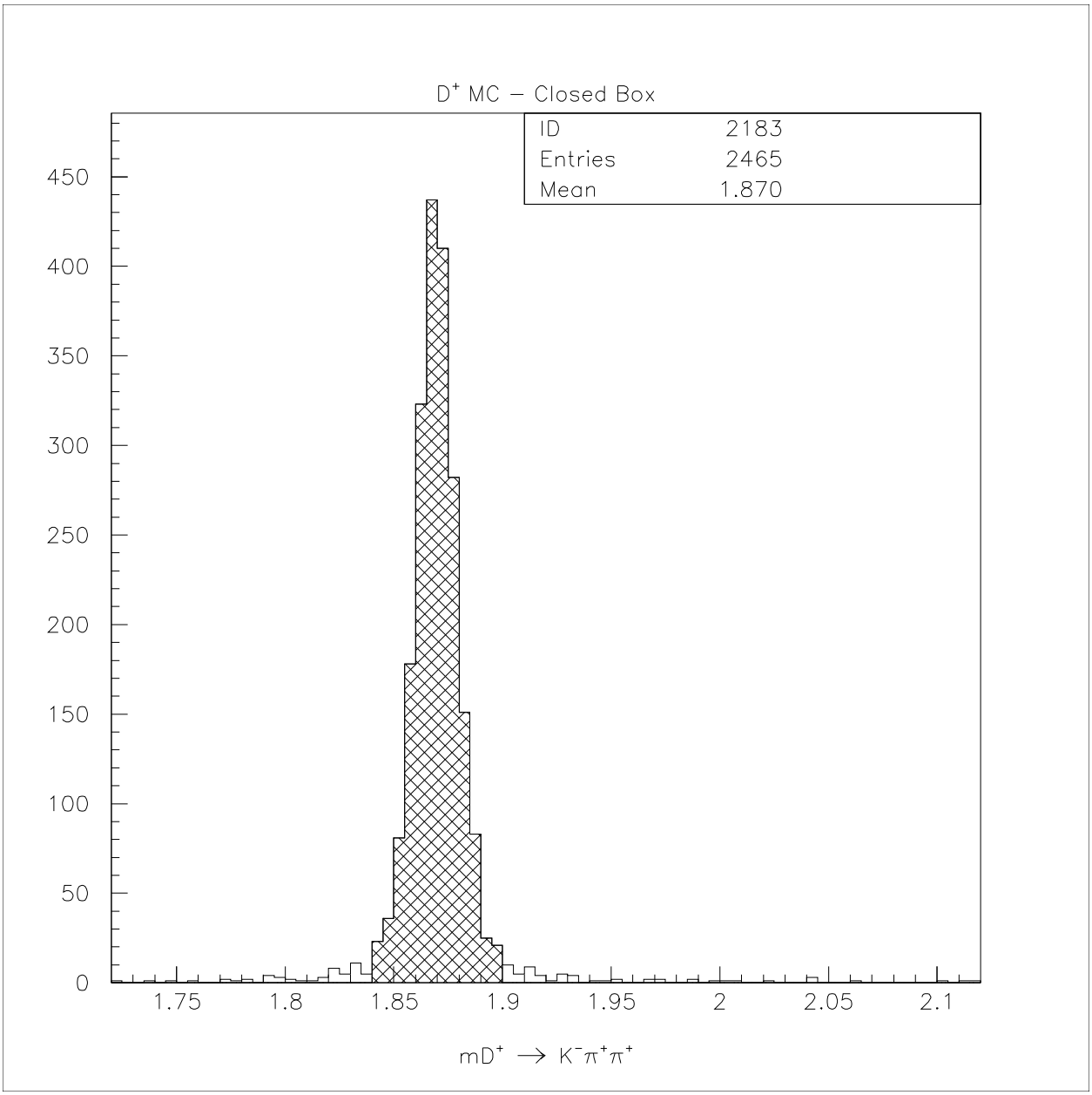

Figure 19:
Monte Carlo normalization - $D^+ \to K^-\pi^+\pi^+$ for the $D^+ \to K\ell\ell$ modes. Shaded region is "box". Bin width = 5 MeV/c^2.

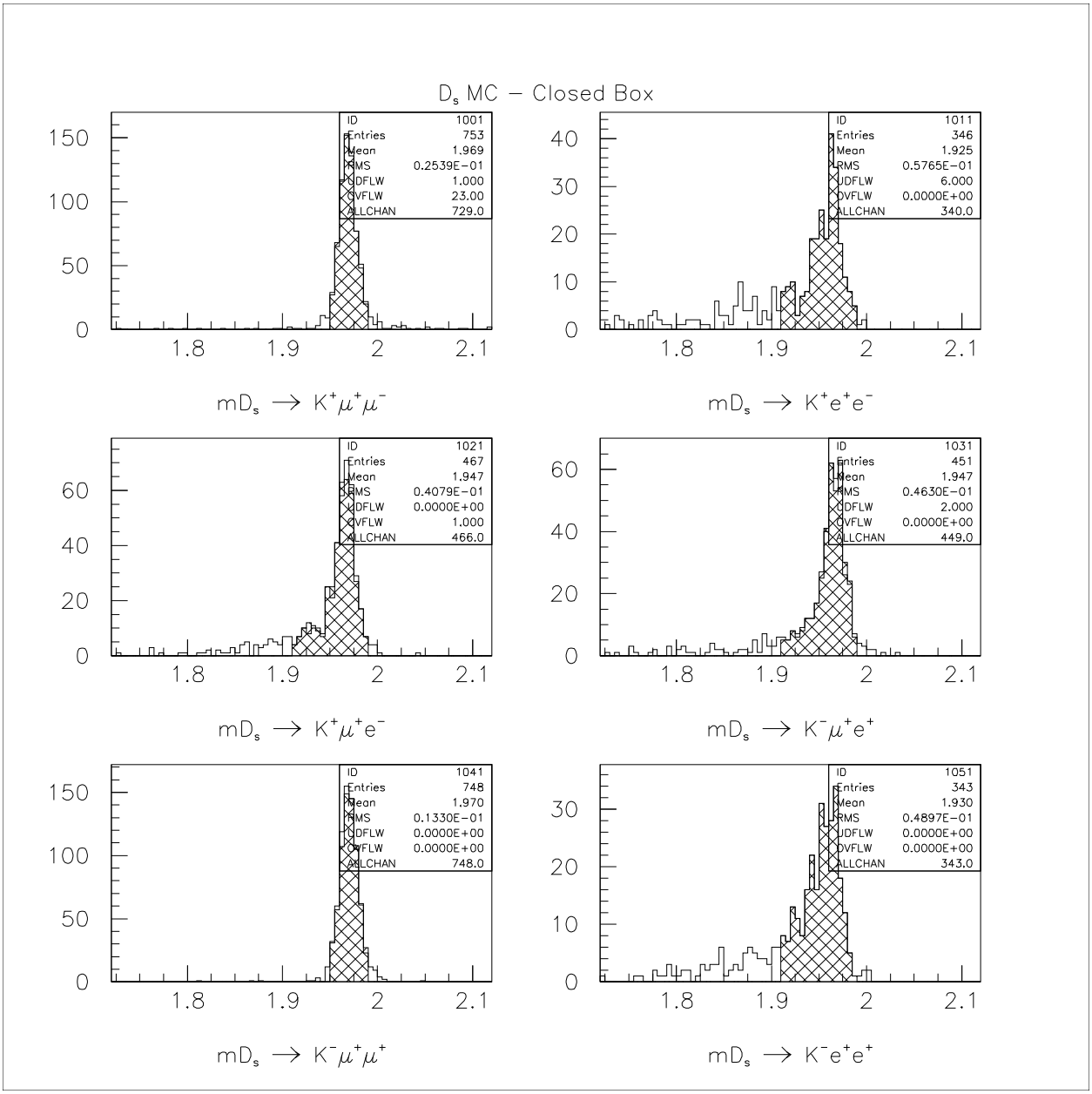

Figure 20:
$D_s \rightarrow K\ell\ell$ Monte Carlo decay modes. Shaded region is "box". Bin width = 5 MeV/c^2.

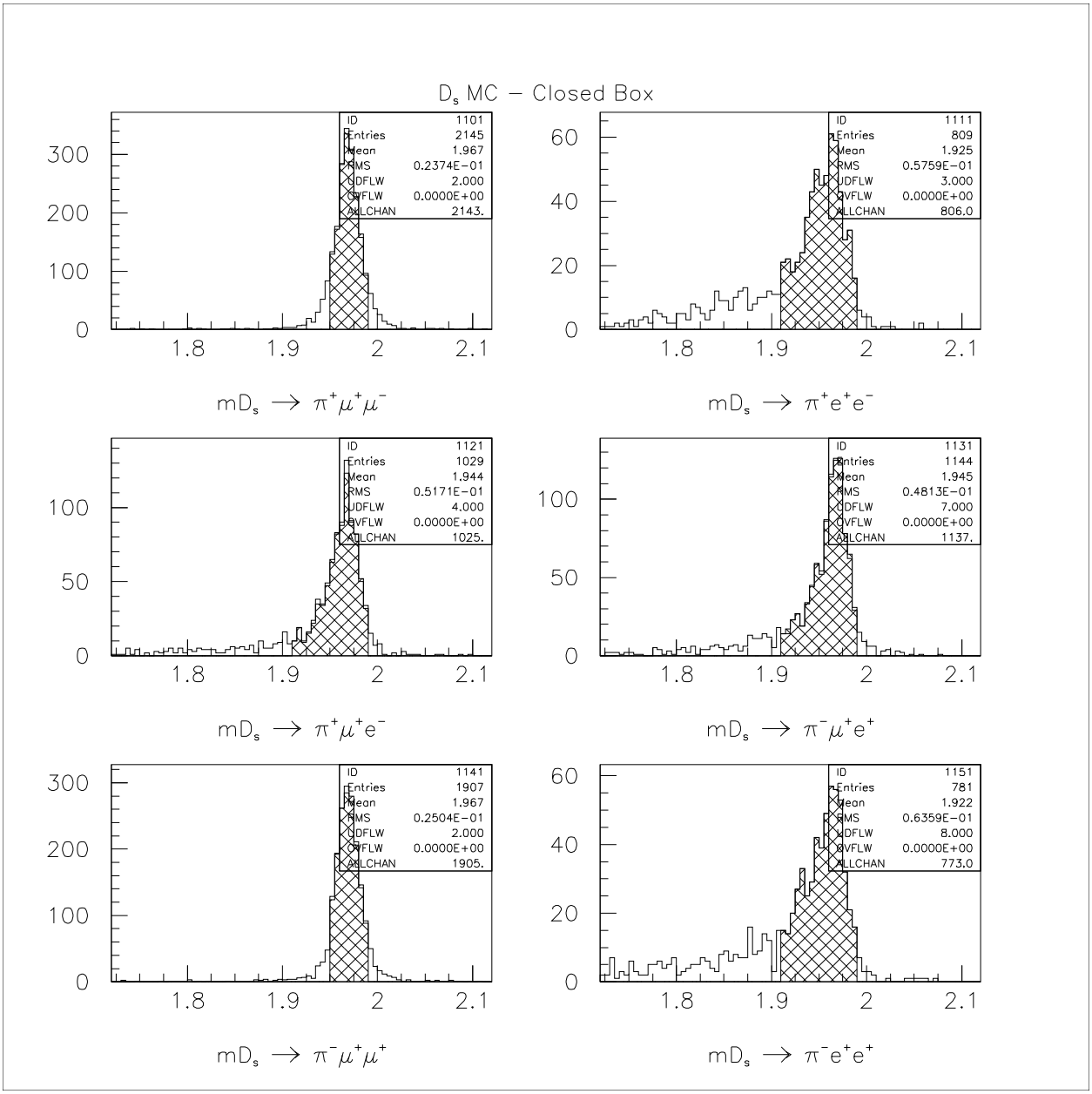

Figure 21:
$D_s \rightarrow \pi\ell\ell$ Monte Carlo decay modes. Shaded region is "box". Bin width = 5 MeV/c^2.

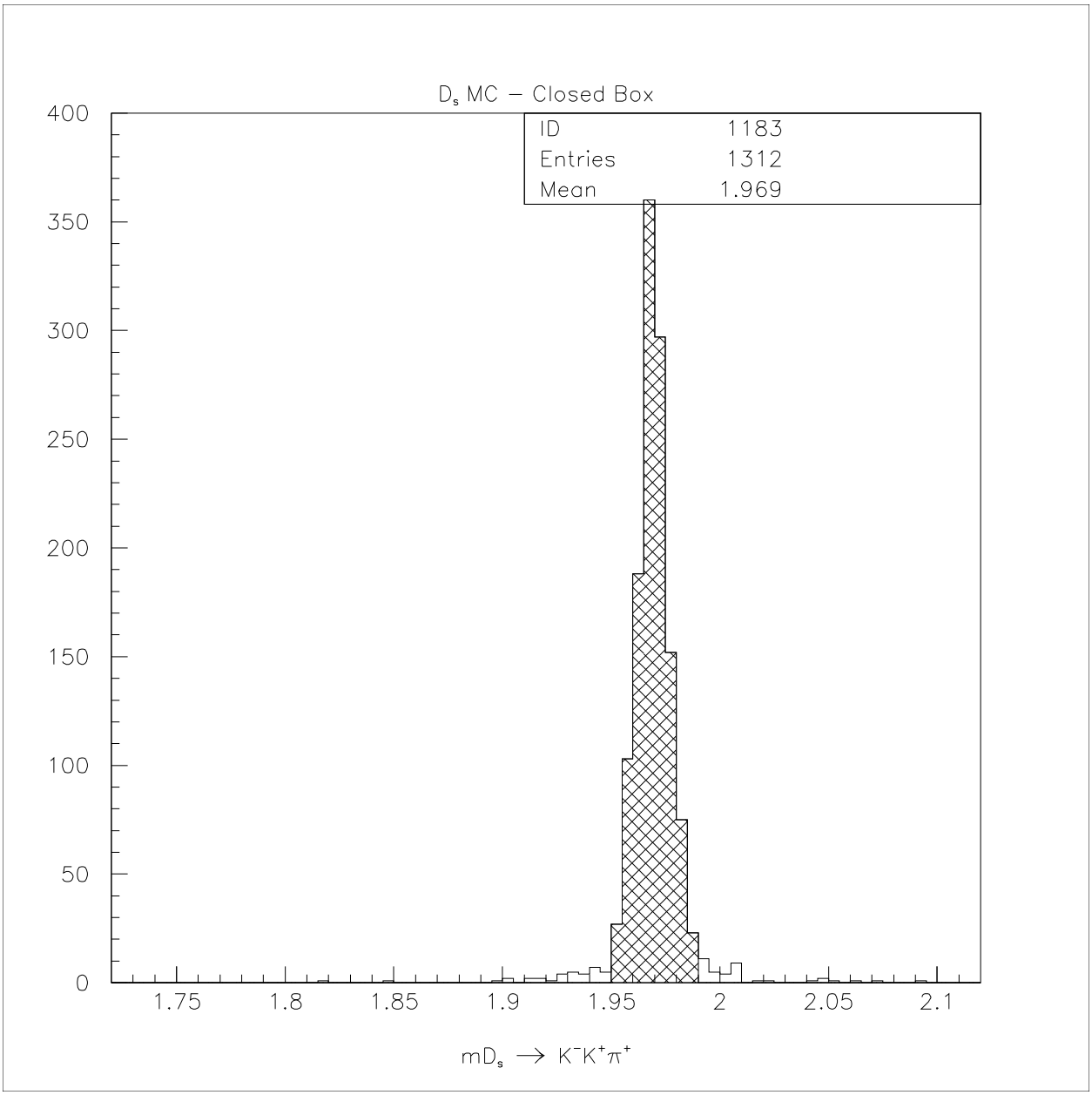

Figure 22:
Monte Carlo normalization - $D_s^+ \rightarrow \phi\pi^+$ for the $D_s^+ \rightarrow K^+\ell^\pm\ell^\mp$ modes. Shaded region is "box". Bin width = 5 MeV/c^2.

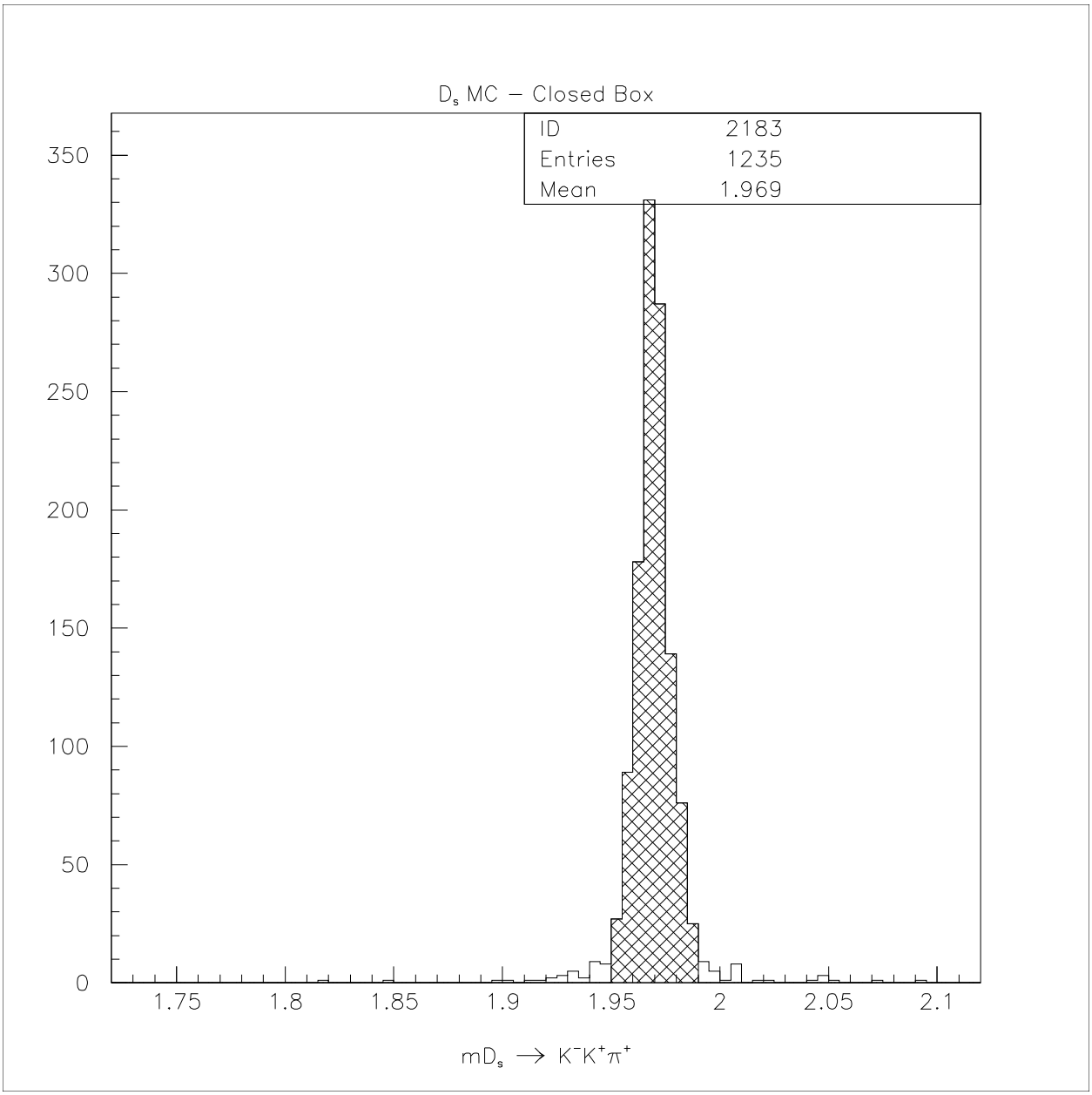

Figure 23:
Monte Carlo normalization - $D_s^+ \to \phi\pi^+$ for the $D_s^+ \to K^-\ell^+\ell^+$ modes. Shaded region is "box". Bin width = 5 MeV/c^2.

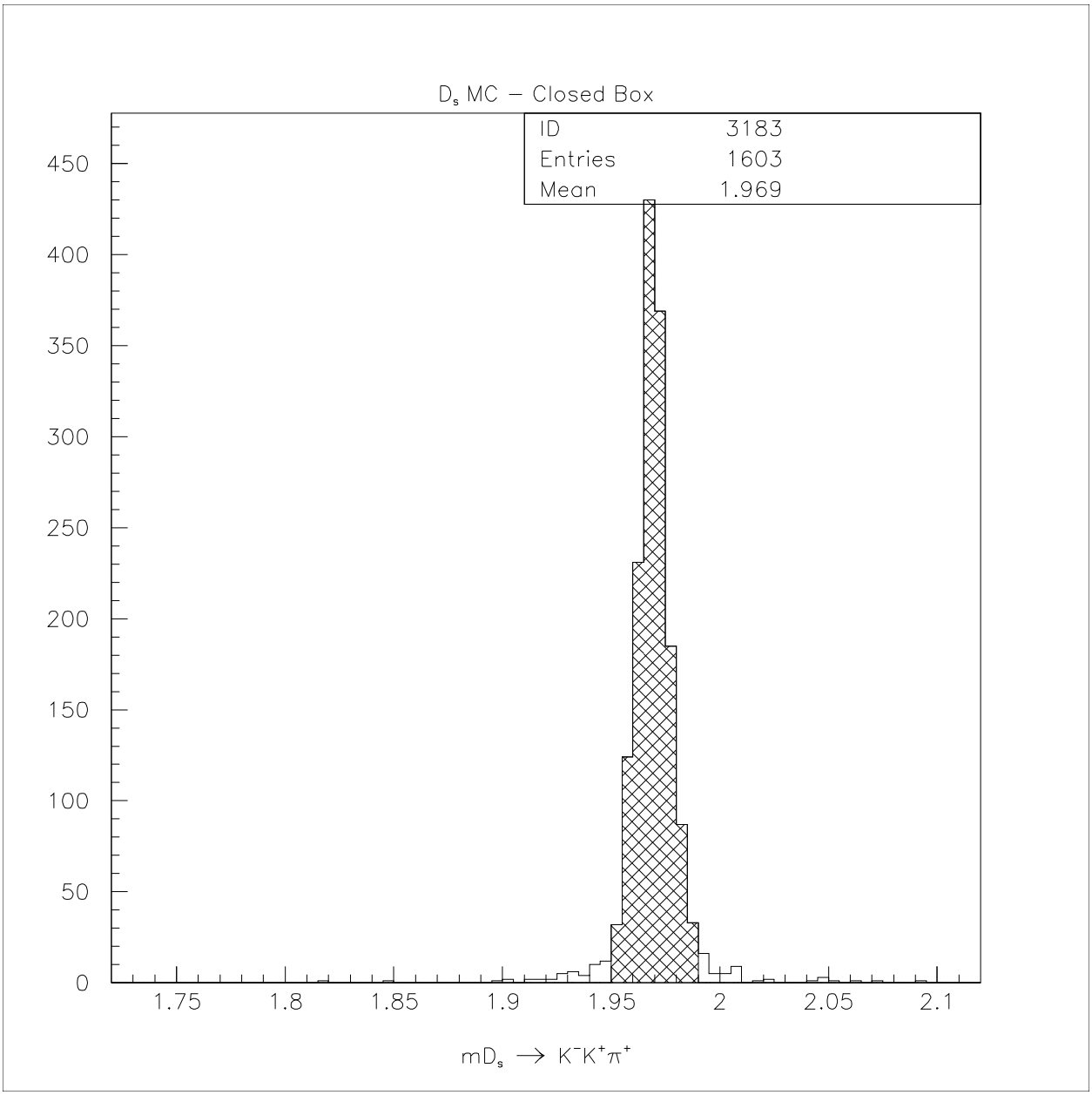

Figure 24:
Monte Carlo normalization - $D_s^+ \rightarrow \phi\pi^+$ for the $D_s \rightarrow \pi\ell\ell$ modes. Shaded region is "box". Bin width = 5 MeV/c^2.

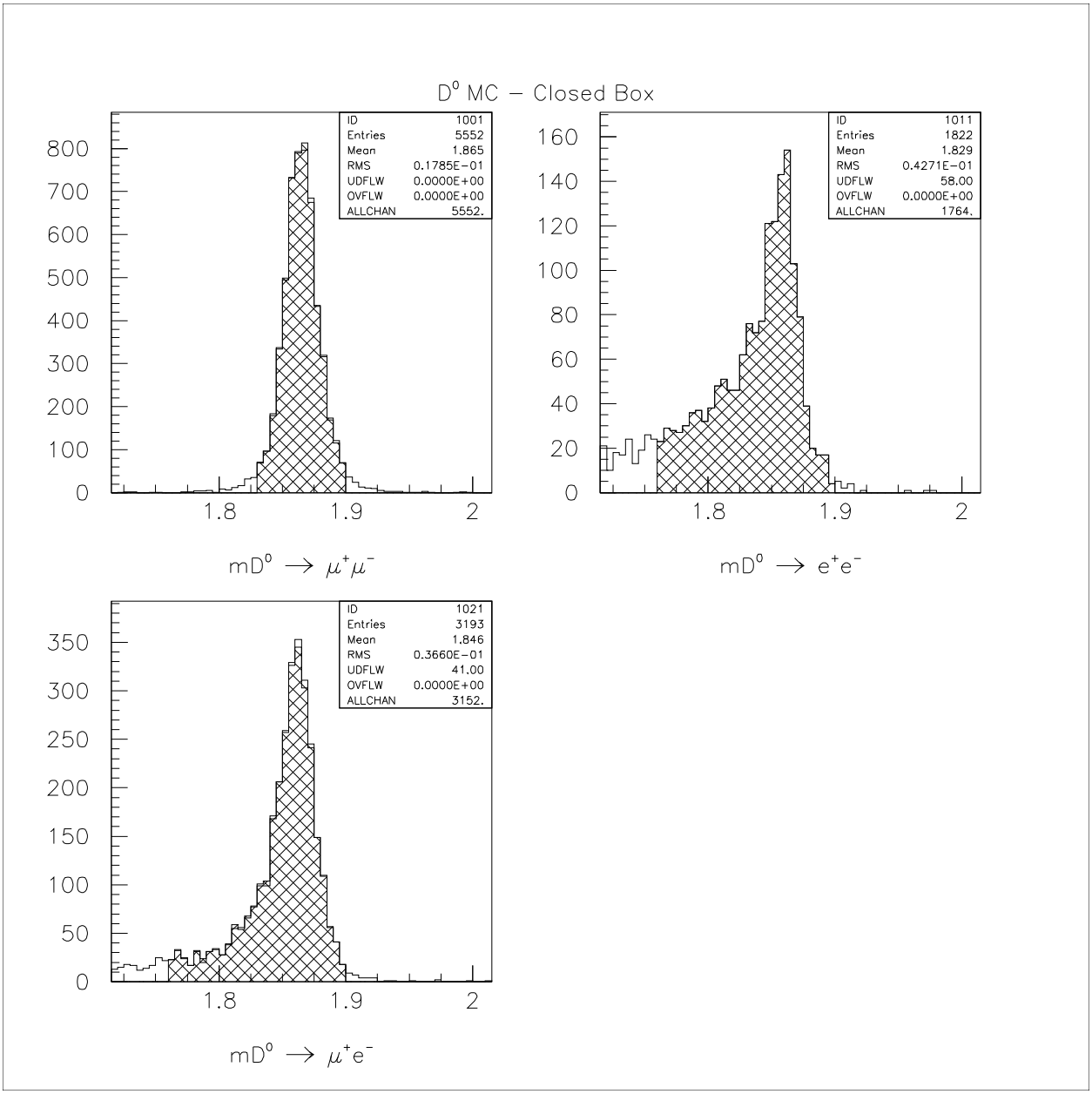

Figure 25.

D^0 Monte Carlo decay modes. Shaded region is "box". Bin width = 5 MeV/c^2.

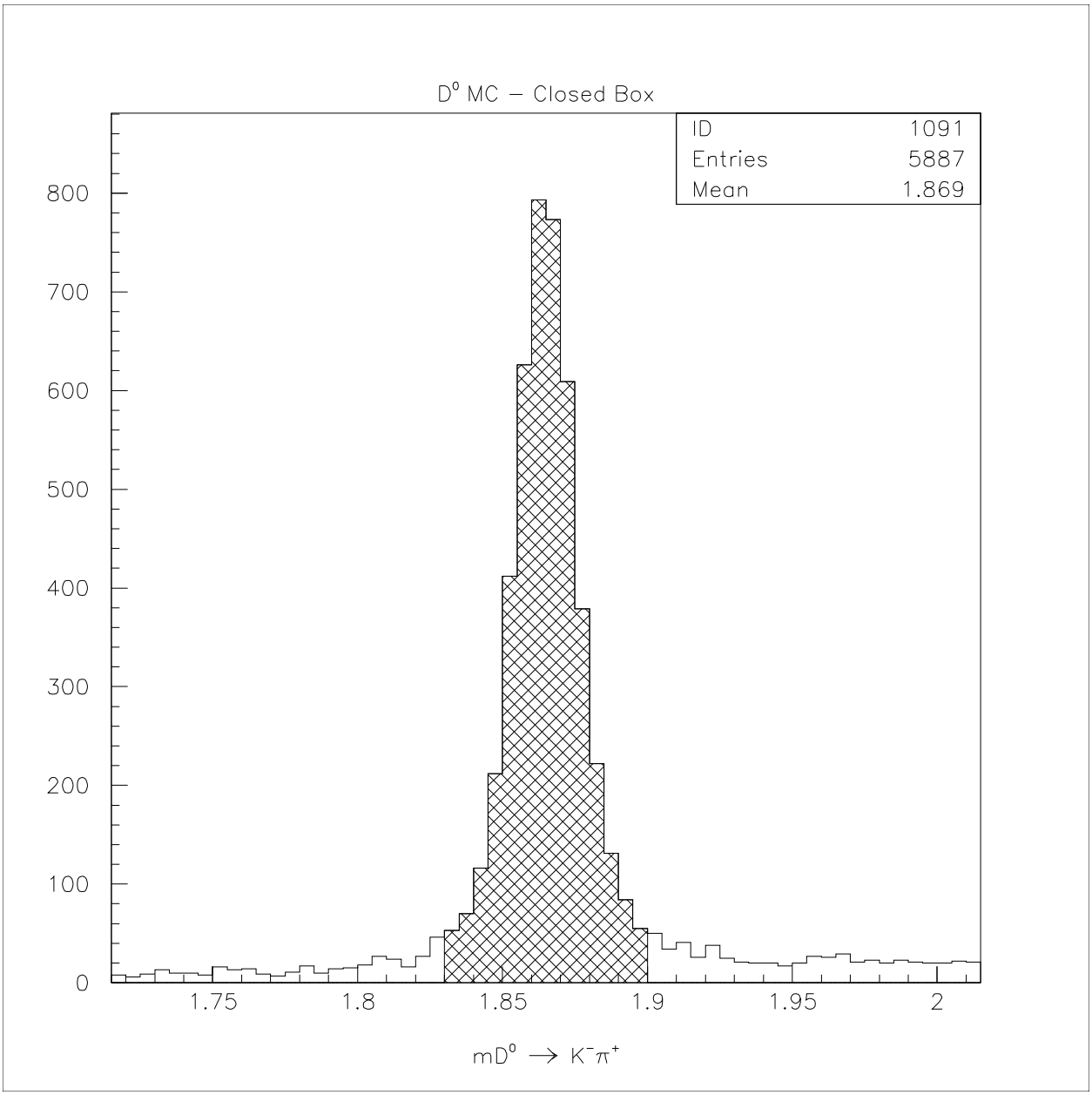

Figure 26:
Monte Carlo normalization - $D^0 \to K^- \pi^+$. Shaded region is "box". Bin width = 5 MeV/c^2.

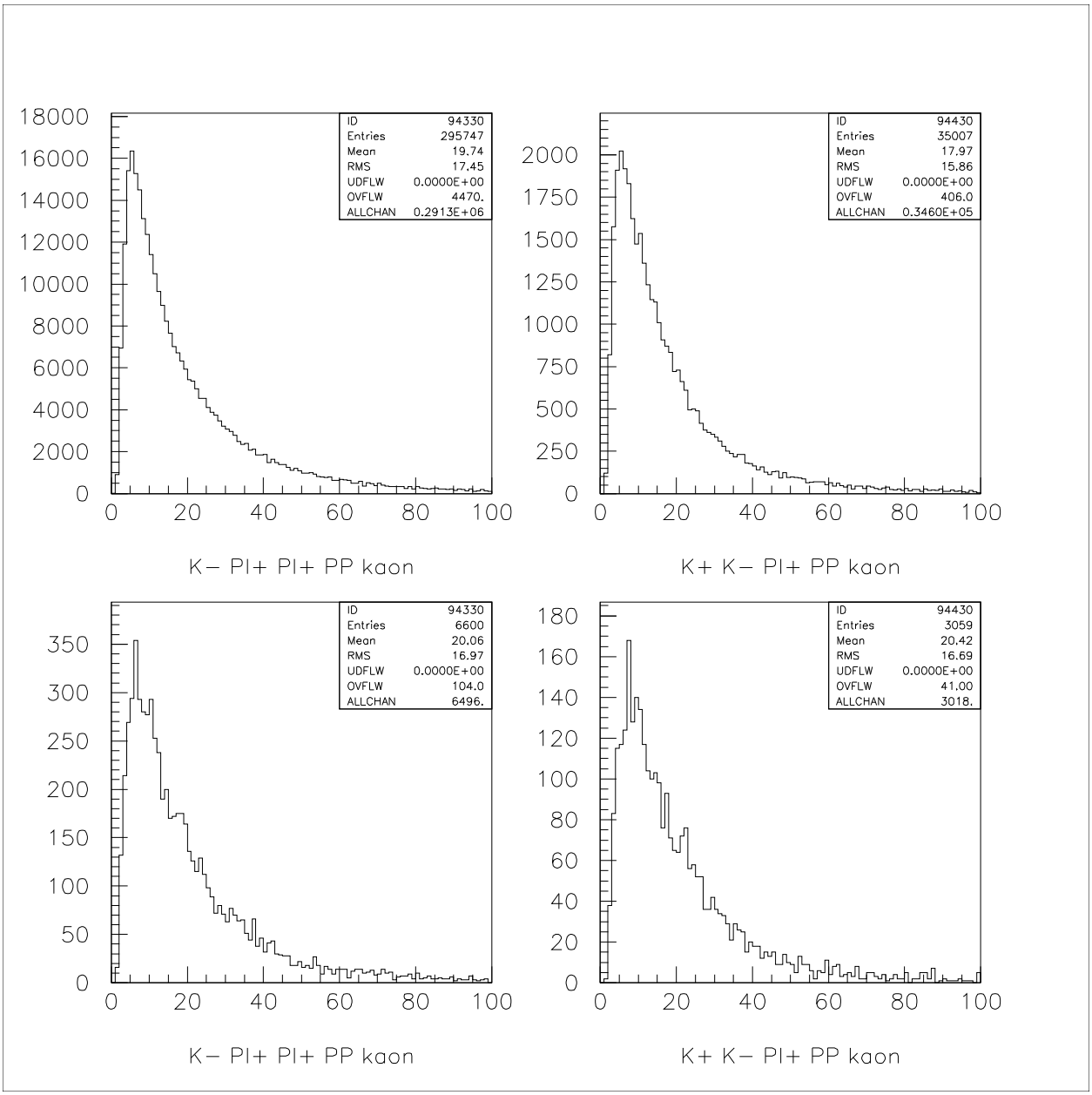

Figure 27:
A comparison between the kaon momentum from data (upper row) and Monte Carlo (lower row) for $D^+ \to K^- \pi^+ \pi^+$ (left column) and $D_s^+ \to \phi \pi^+$ (right column).

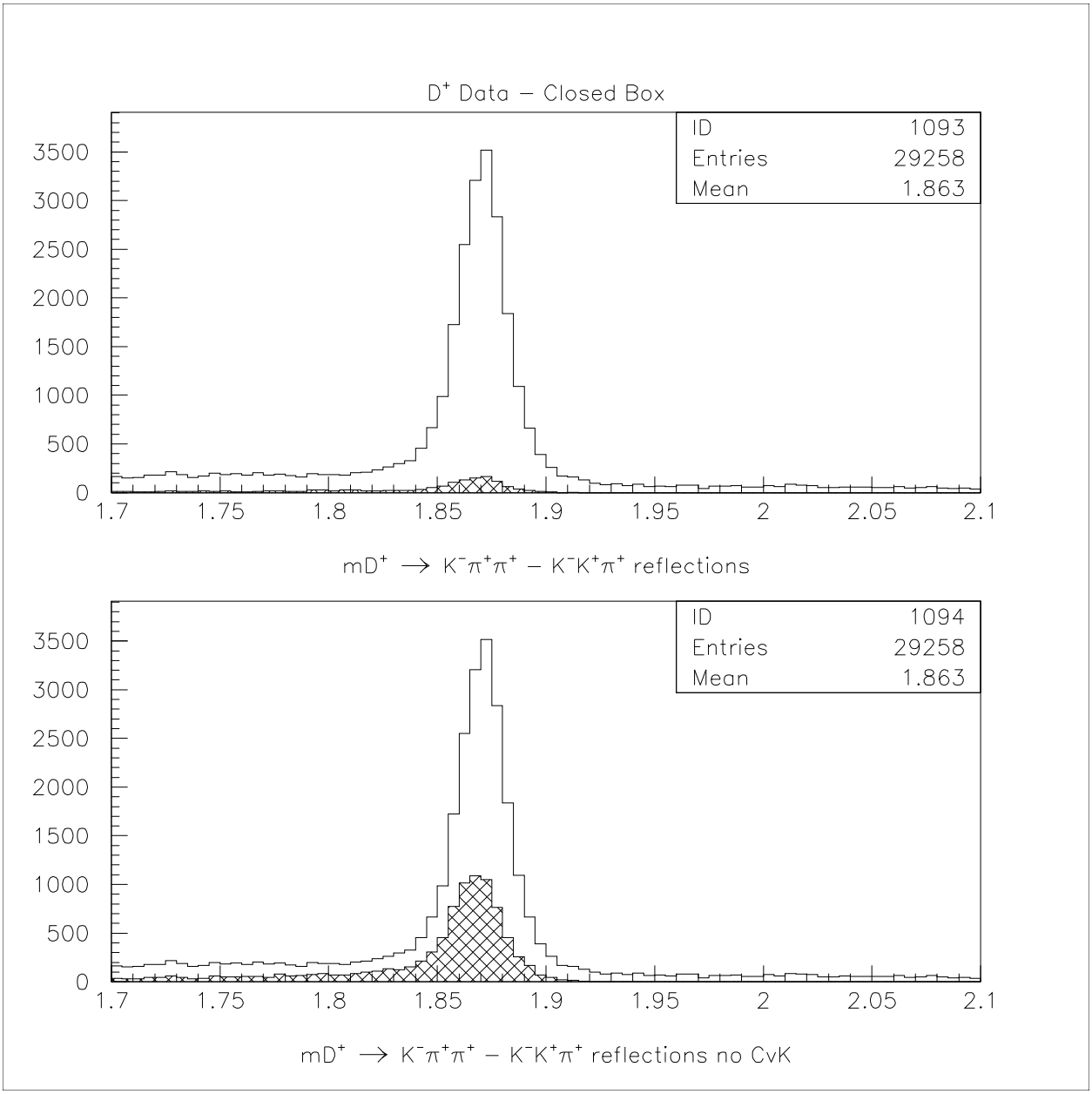

Figure 28:
Data normalization $D^+ \to K^-\pi^+\pi^+$ and the $D_S^+ \to K^-K^+\pi^+$ reflections (cross-hatched region), with the *K*-Čerenkov probability cut (top) and without the *K*-Čerenkov probability cut (bottom).
Bin width = 5 MeV/c^2.

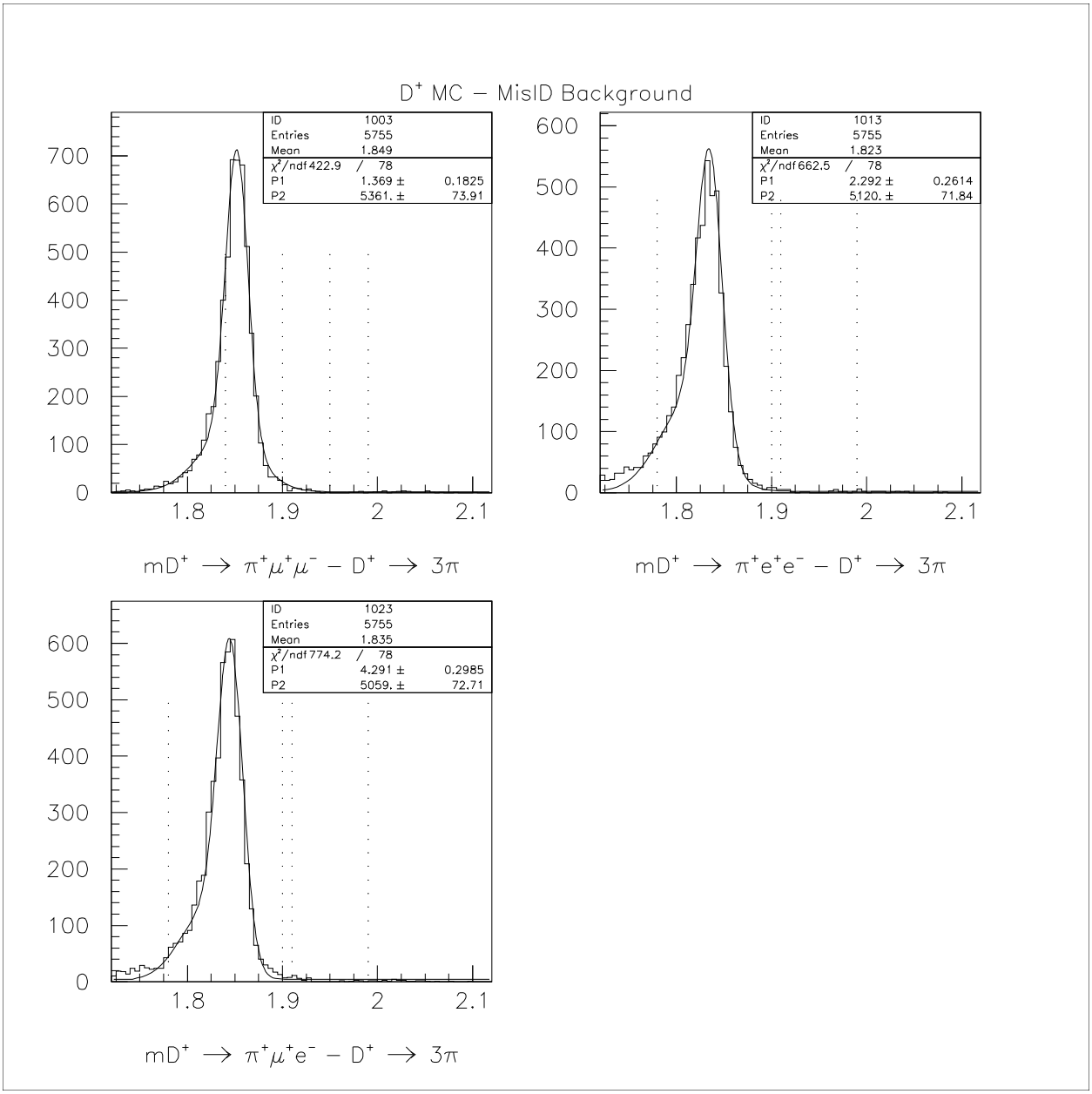

Figure 29:
Fits of the misidentified $D^+ \to \pi^+\pi^-\pi^+$ Monte Carlo for use in the background fitting of the $D^+ \to \pi\ell\ell$ modes.

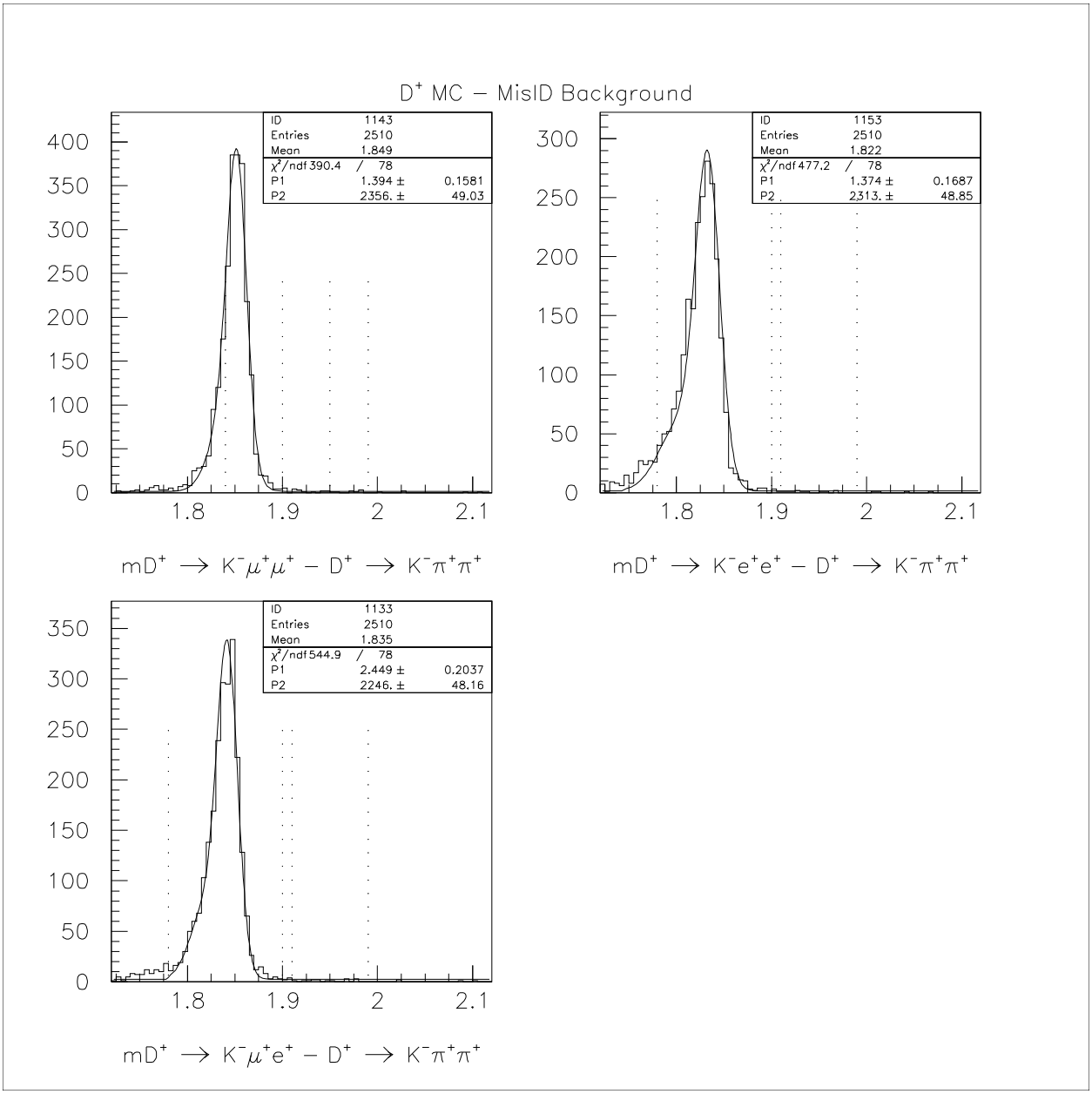

Figure 30:
Fits of the misidentified $D^+ \to K^-\pi^+\pi^+$ Monte Carlo for use in the background fitting of the $D^+ \to K^-\ell^+\ell^+$ modes.

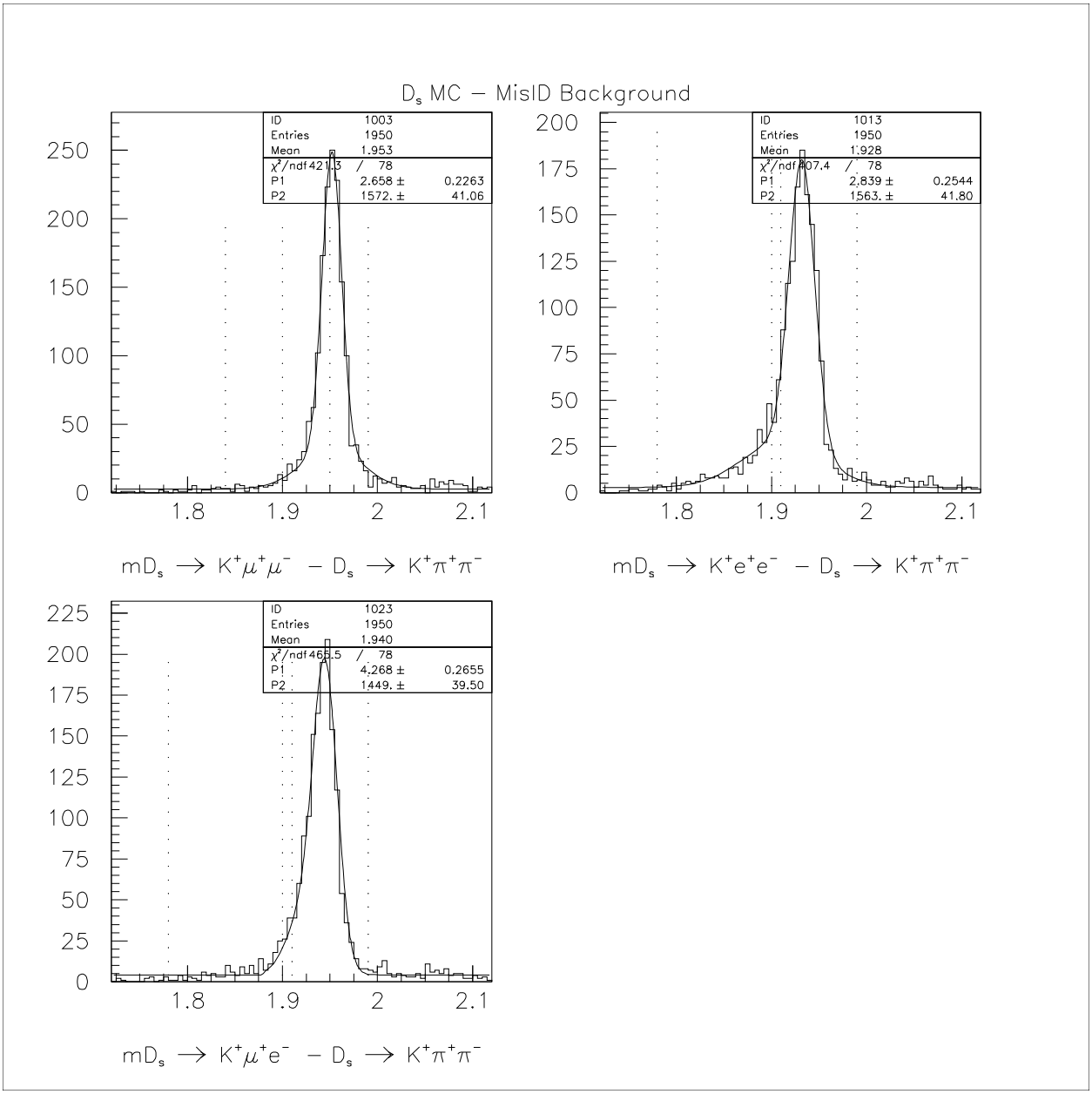

Figure 31:
Fits of the misidentified $D_s^+ \to K^+\pi^+\pi^-$ Monte Carlo for use in the background fitting.

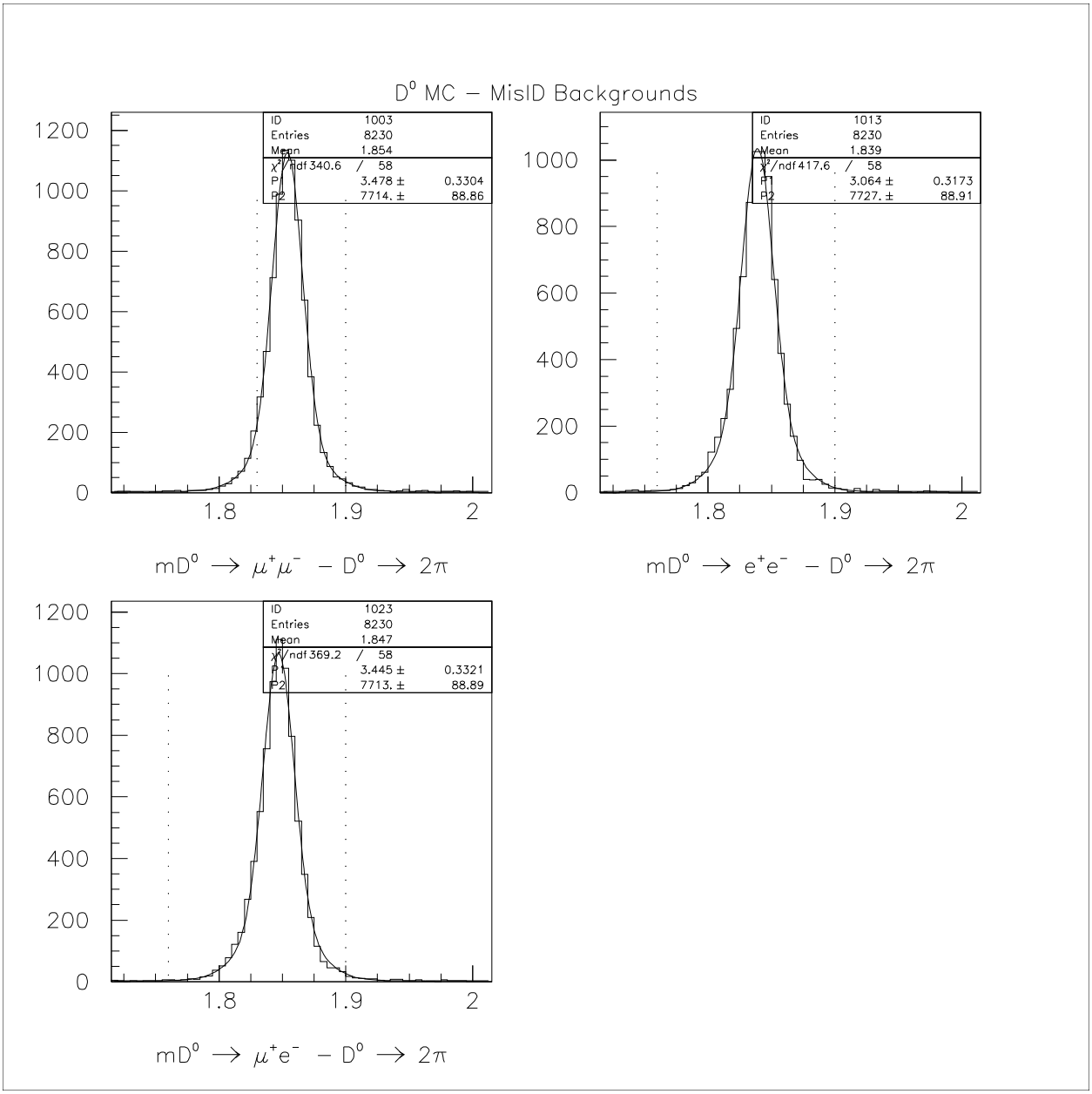

Figure 32:
Fits of the misidentified $D^0 \to \pi^+\pi^-$ Monte Carlo for use in the background fitting.

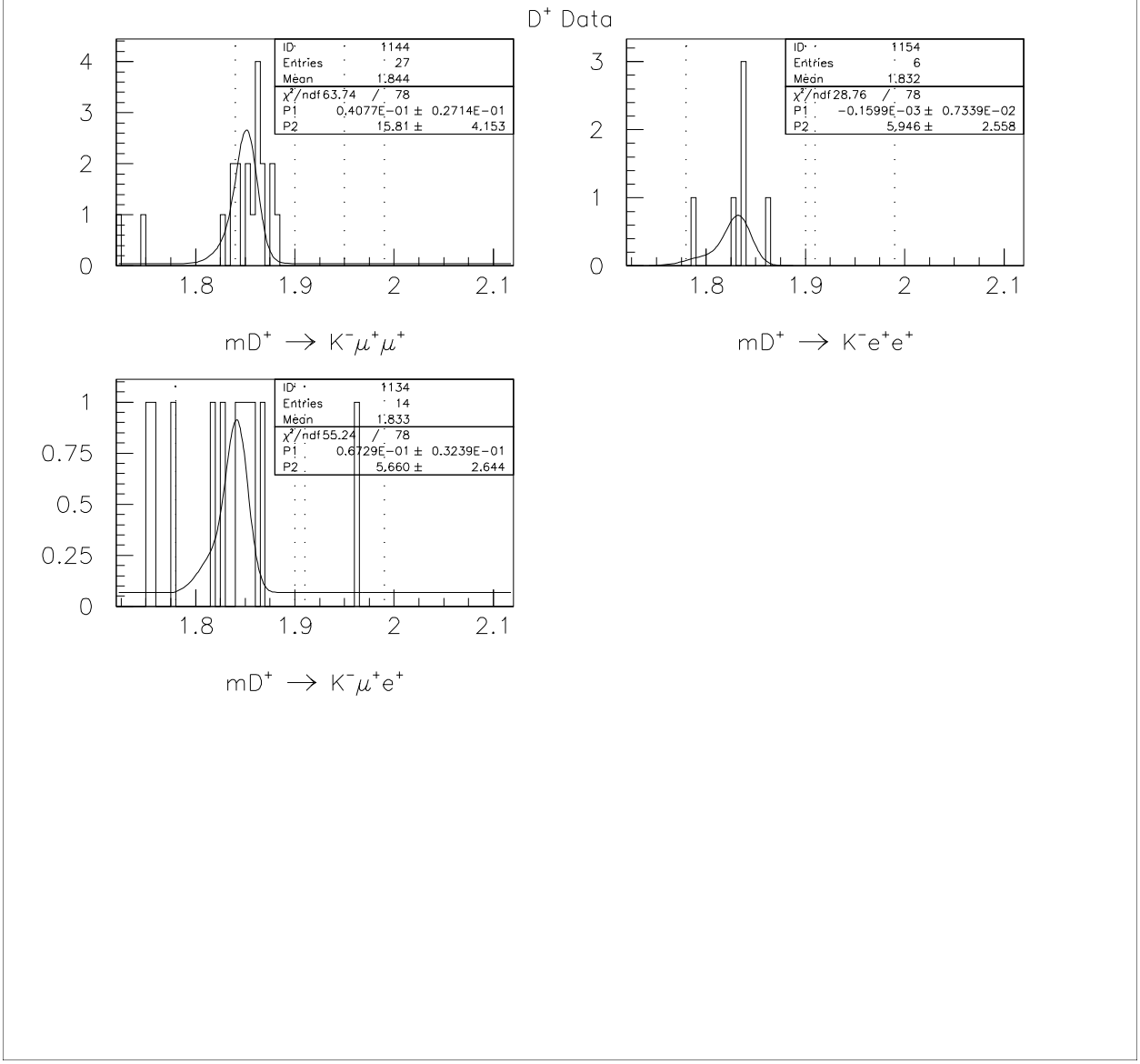

Figure 33:
The $D^+ \to K^- \ell^+ \ell^+$ modes used for determining the misidentification background rates.

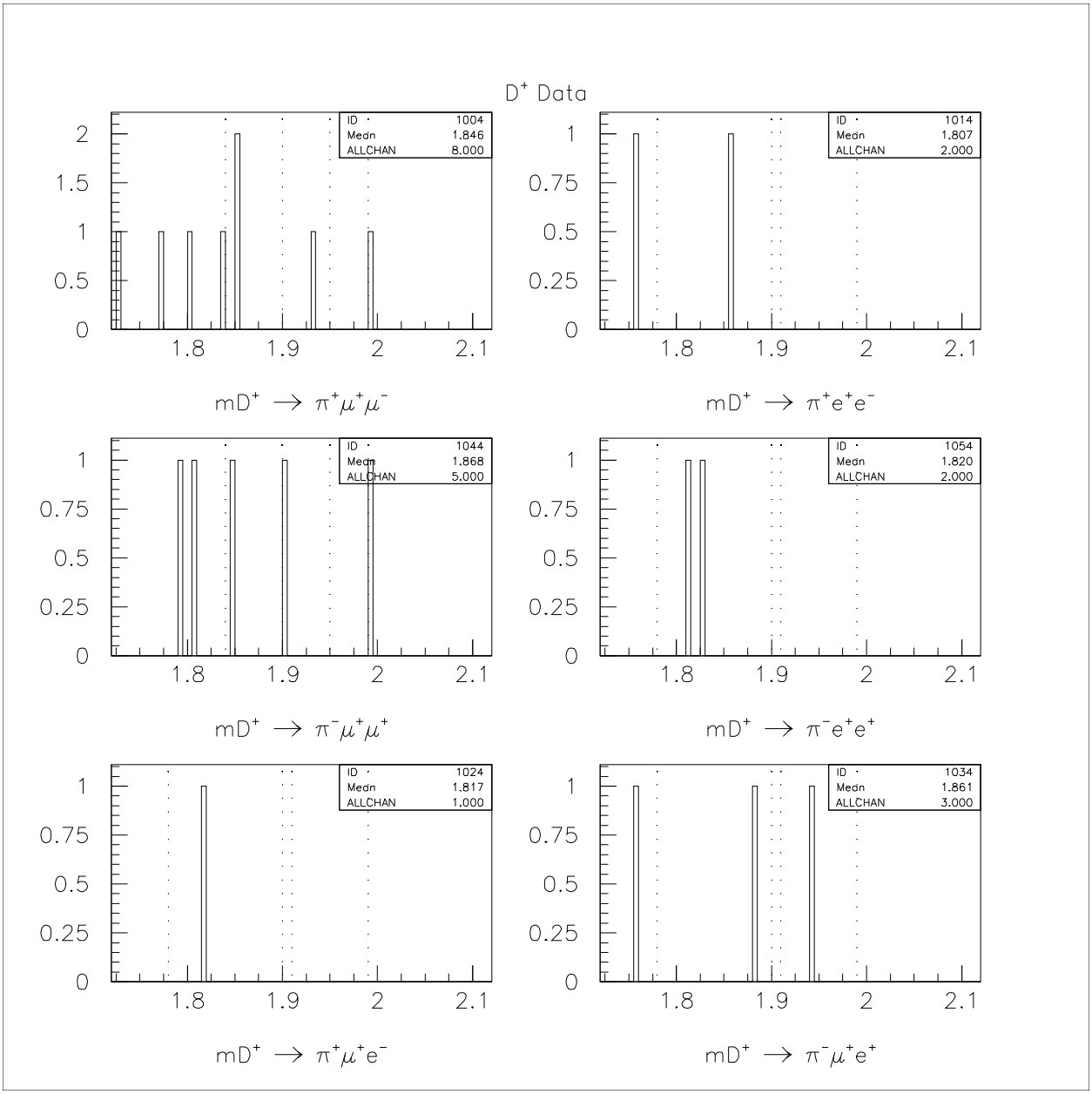

Figure 34:
$D^+ \to \pi\ell\ell$ data. Dotted lines are "box". Bin width = 5 MeV/c^2.

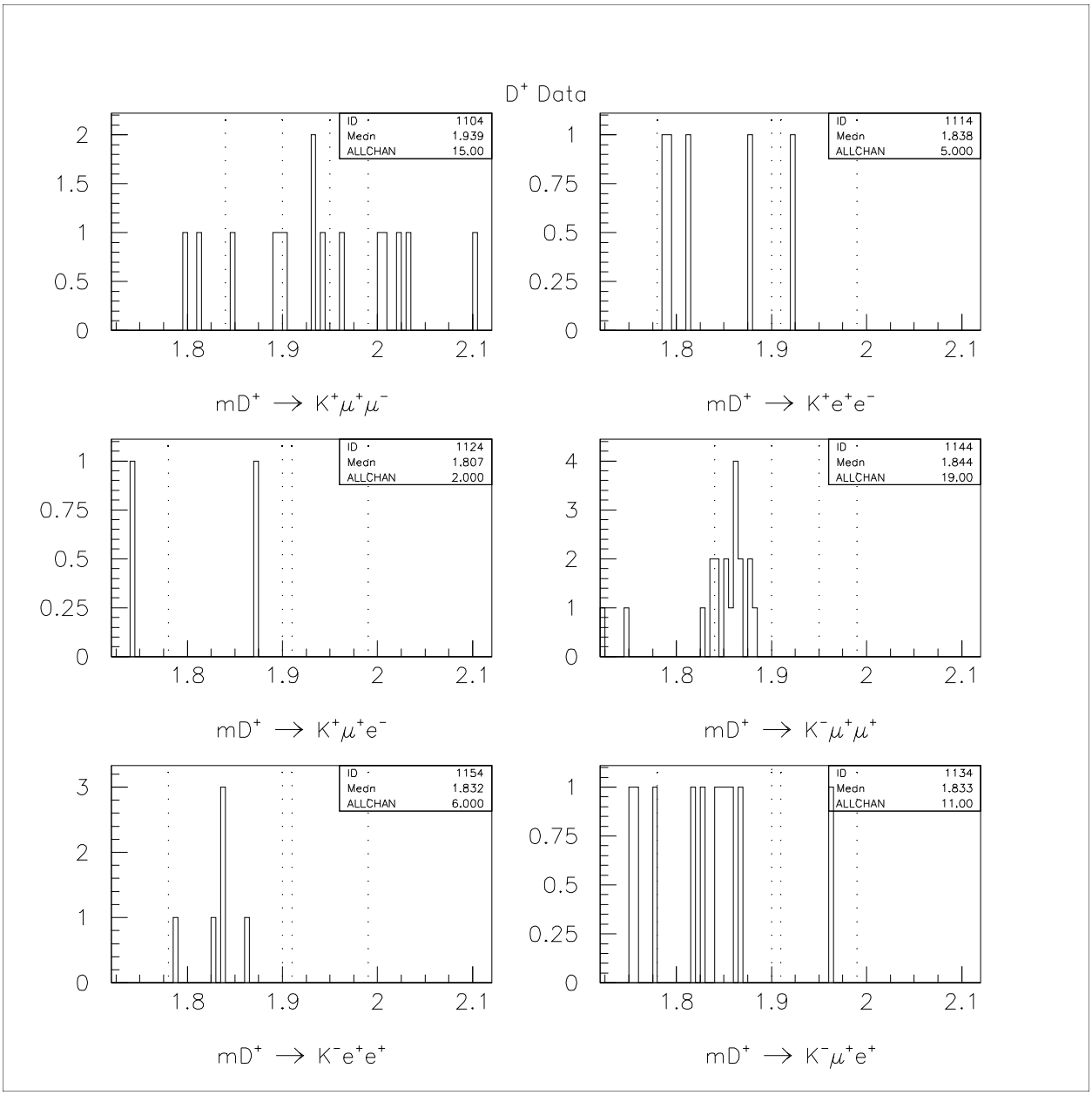

Figure 35:
D^+ data for all the $D^+ \to K\ell\ell$ modes with reflection background subtraction. Dotted lines are "box". Bin width = 5 MeV/c^2.

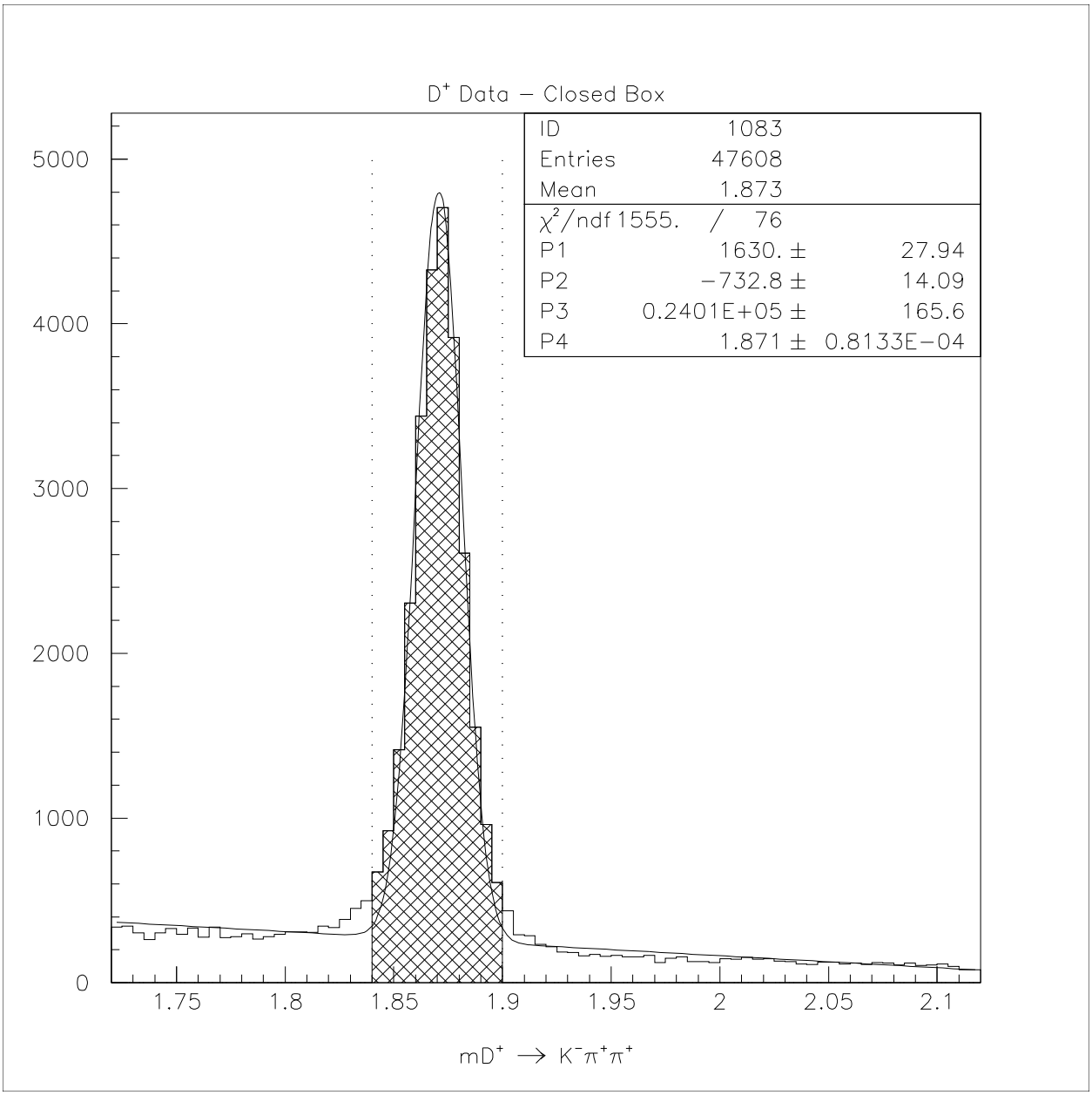

Figure 36:
Fitted data normalization $D^+ \to K^-\pi^+\pi^+$ for the $D^+ \to \pi\ell\ell$ modes. Width fixed at 10.5 MeV/c^2. Dotted lines are "box". Bin width = 5 MeV/c^2.

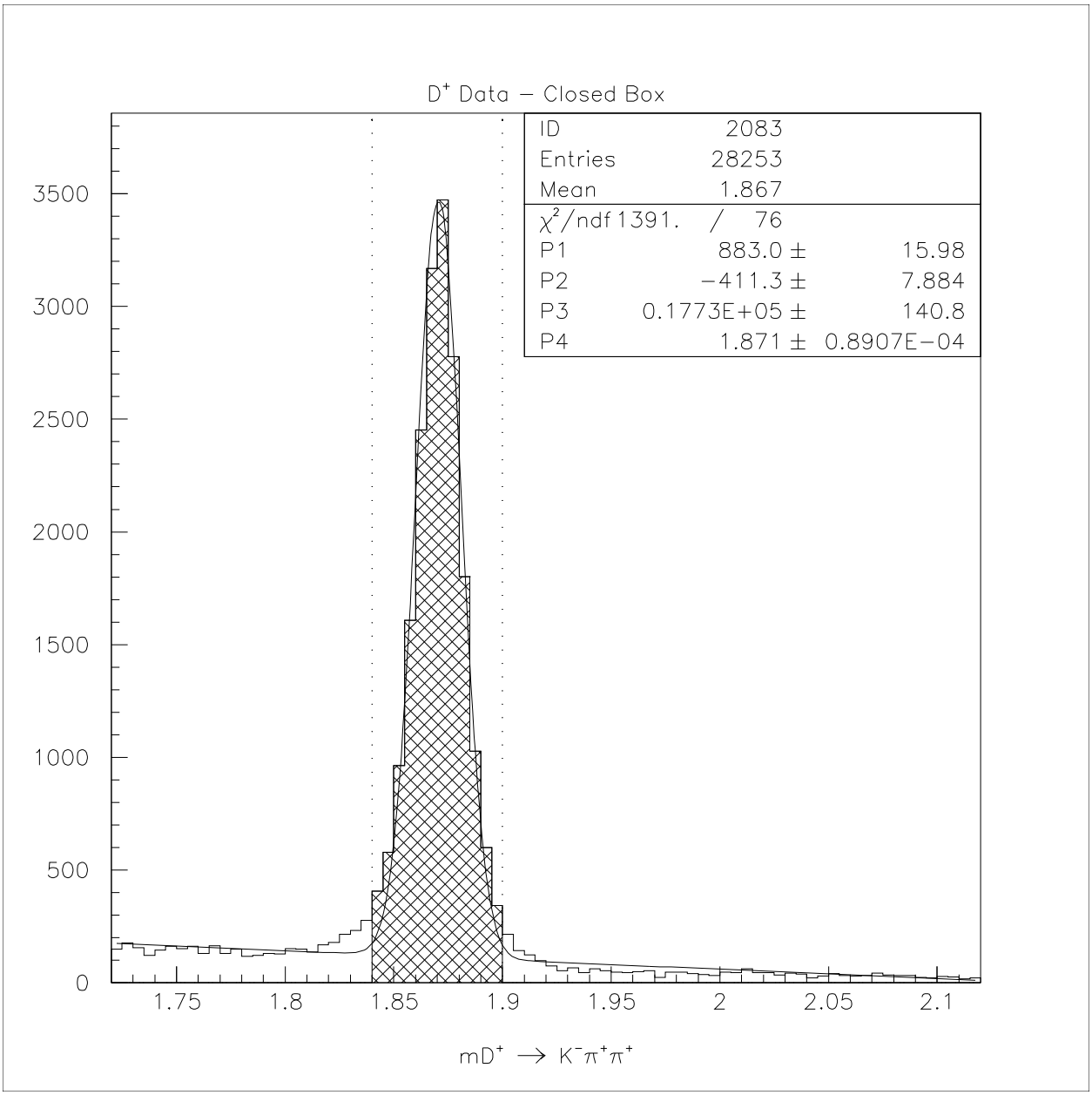

Figure 37:
Fitted data normalization $D^+ \to K^-\pi^+\pi^+$ for the $D^+ \to K\ell\ell$ modes. Width fixed at 10.5 MeV/c^2. Dotted lines are "box". Bin width = 5 MeV/c^2.

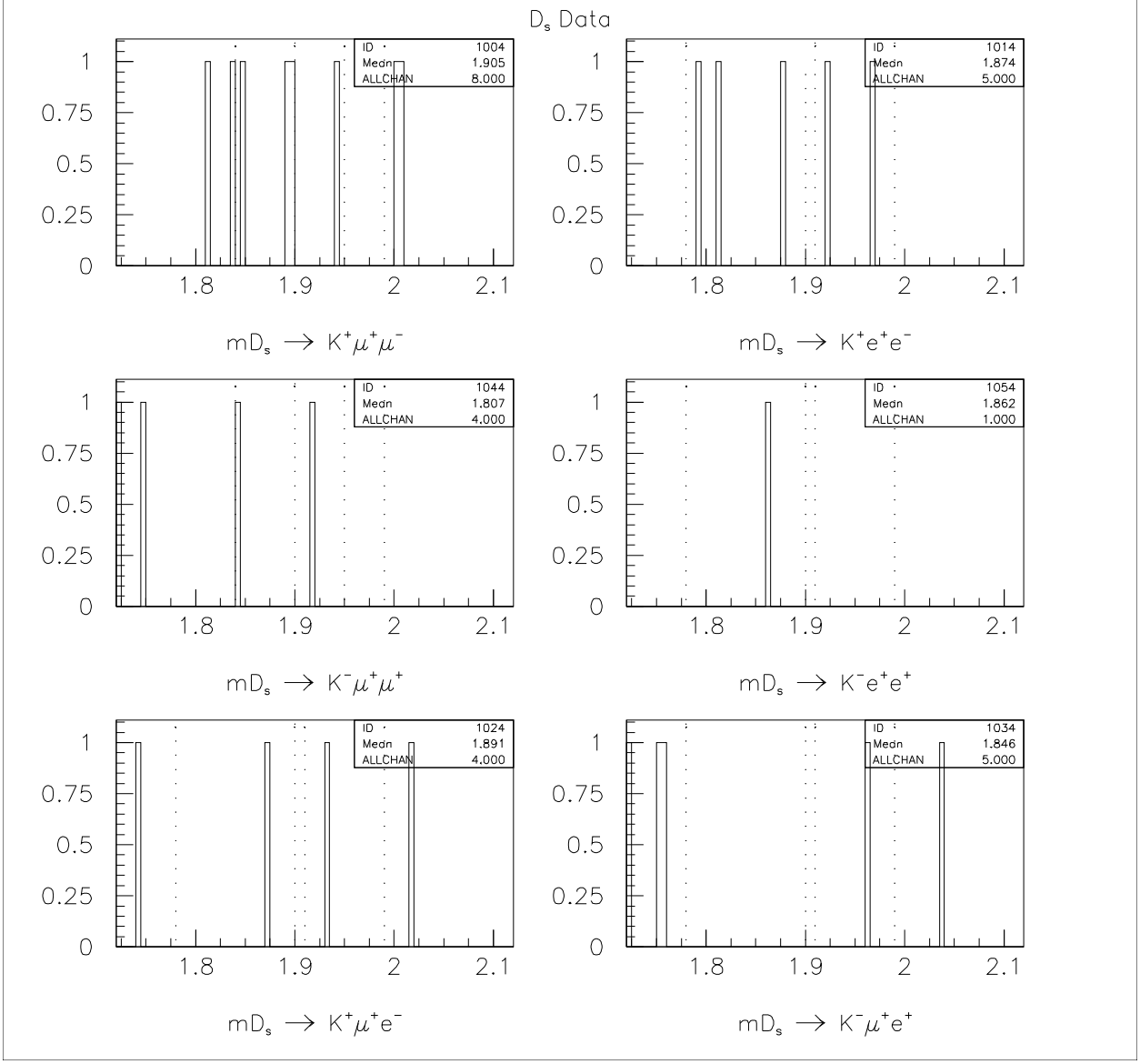

Figure 38:
$D_s^+ \to K\ell\ell$ data. Dotted lines are "box". Bin width = 5 MeV/c^2.

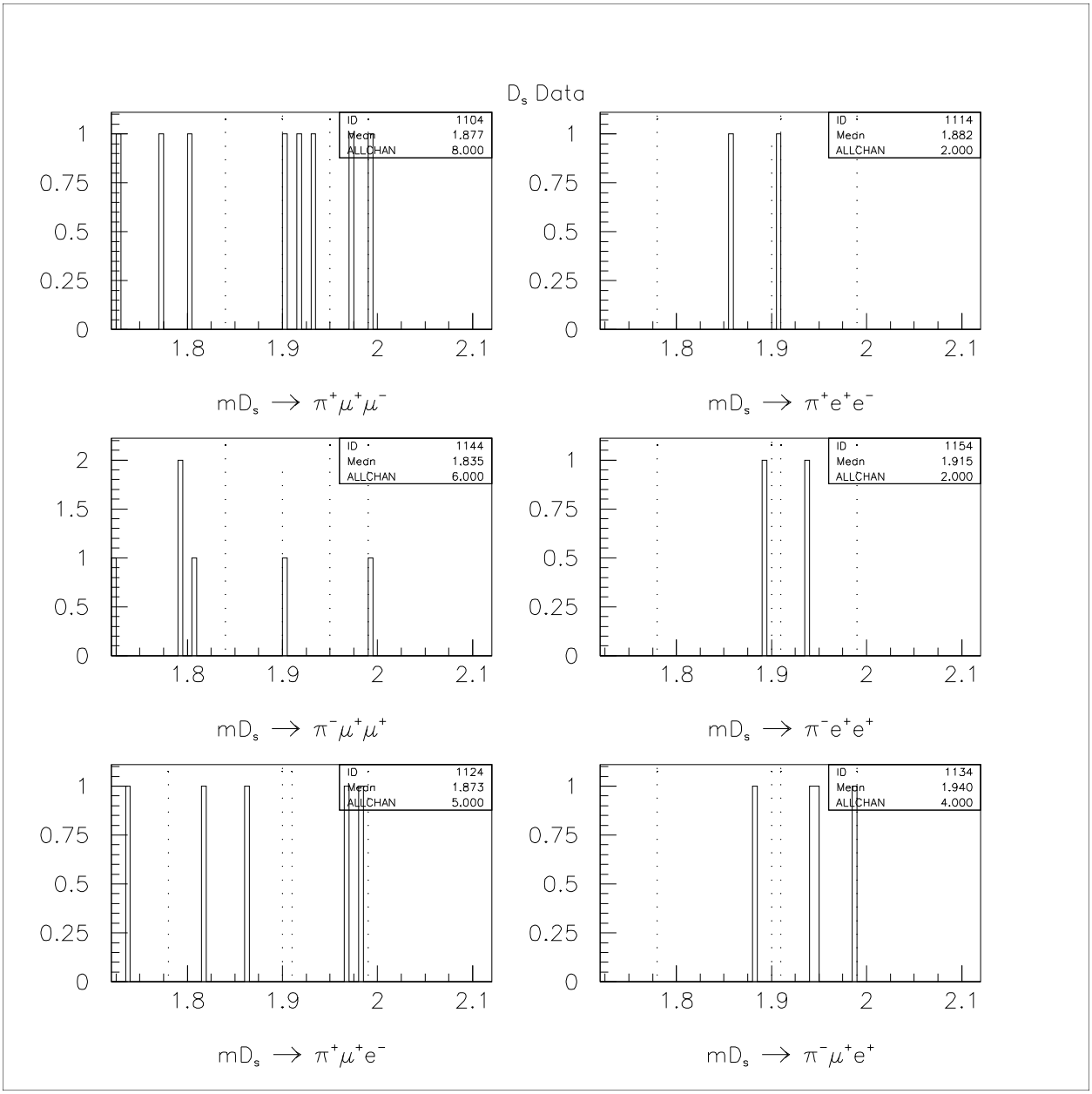

Figure 39:
$D_s^+ \to \pi\ell\ell$ data. Dotted lines are "box". Bin width = 5 MeV/c^2.

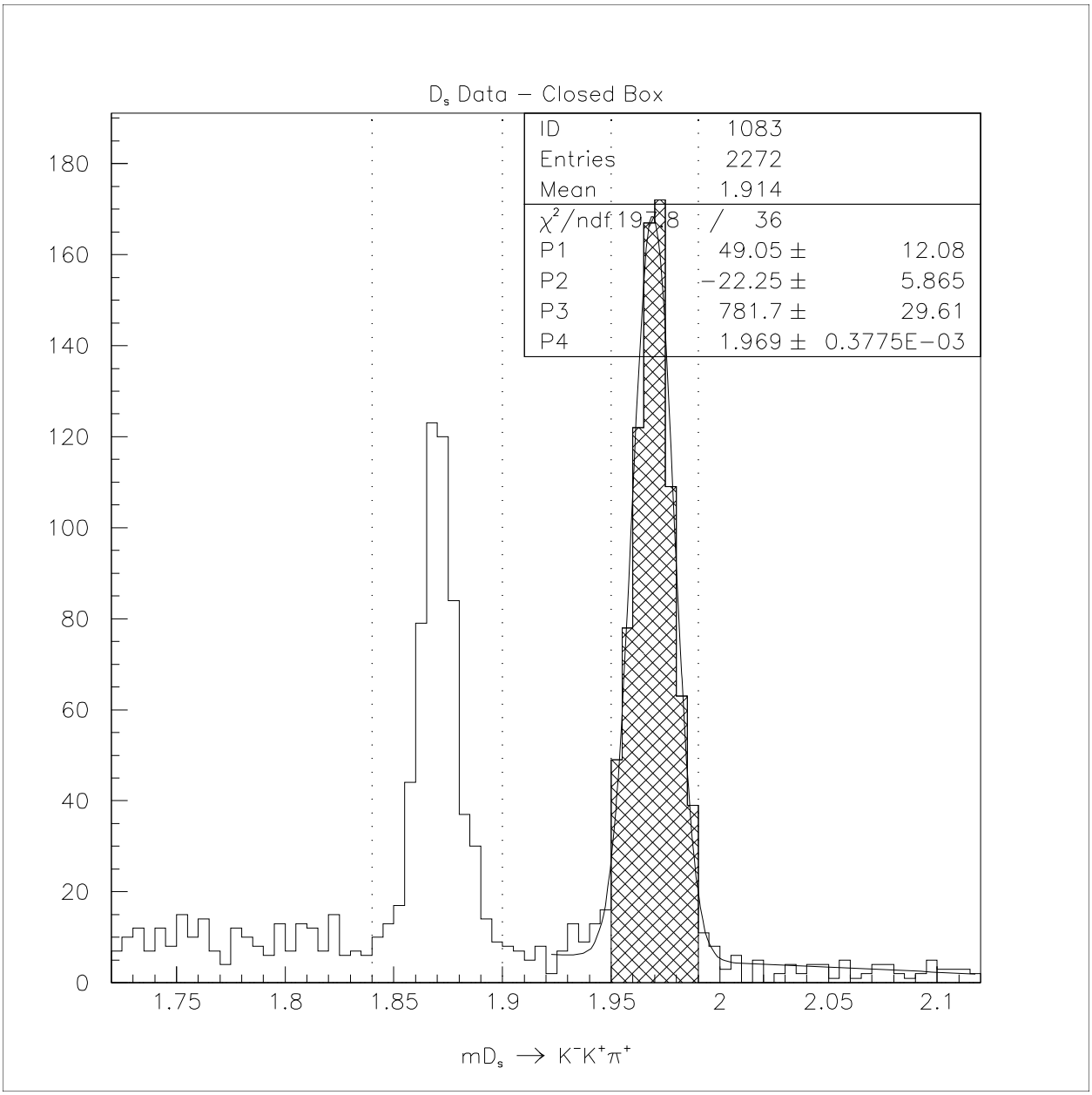

Figure 40:
Fitted data normalization $D_s^+ \to \phi\pi^+$ for the $D_s^+ \to K^+\ell^\pm\ell^\mp$ modes. Width fixed at 9.5 MeV/c^2. Dotted lines are "box". Bin width = 5 MeV/c^2.

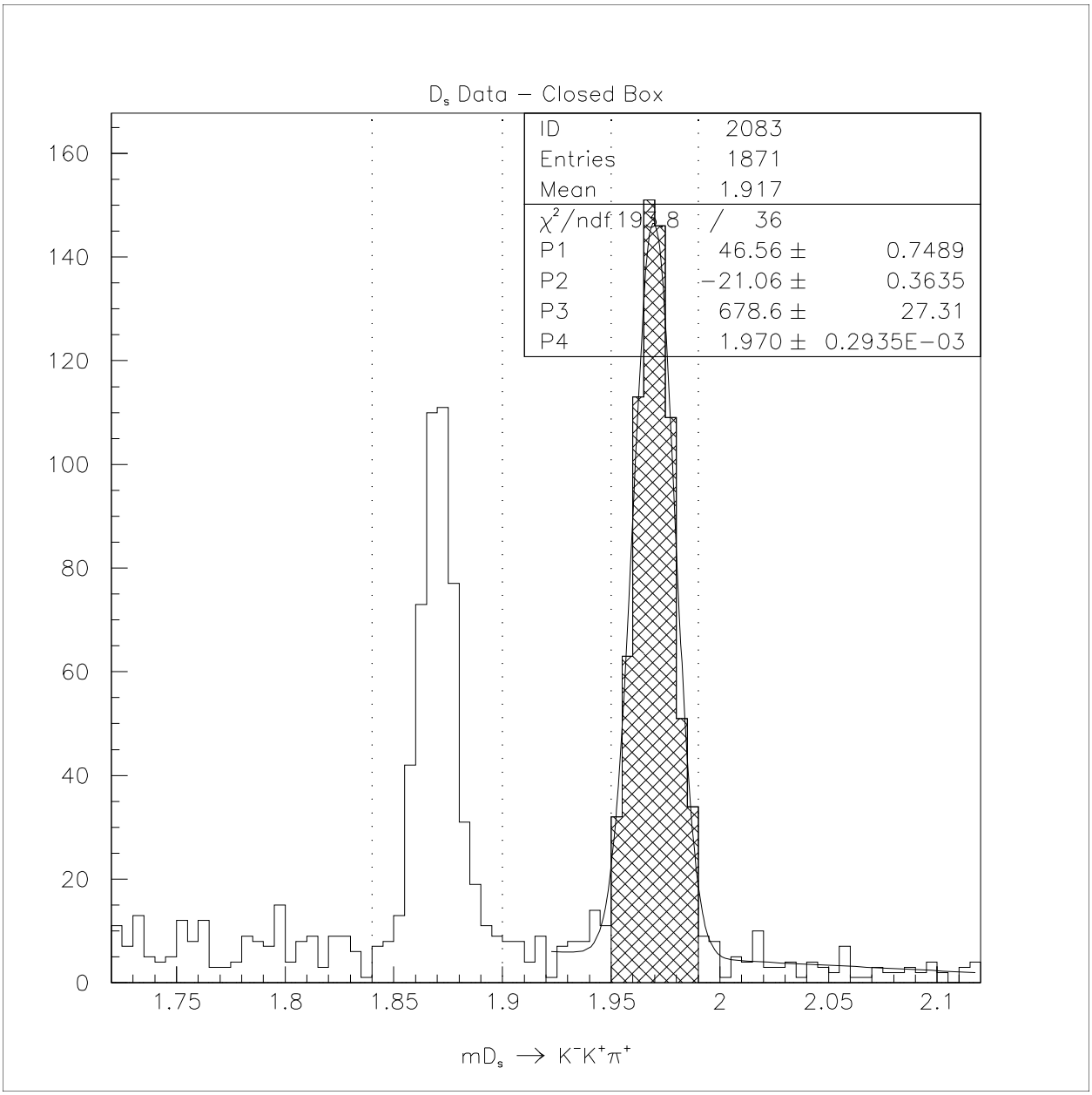

Figure 41:
Fitted data normalization $D_s^+ \rightarrow \phi\pi^+$ for the $D_s^+ \rightarrow K^-\ell^+\ell^+$ modes. Width fixed at 9.5 MeV/c^2. Dotted lines are "box". Bin width = 5 MeV/c^2.

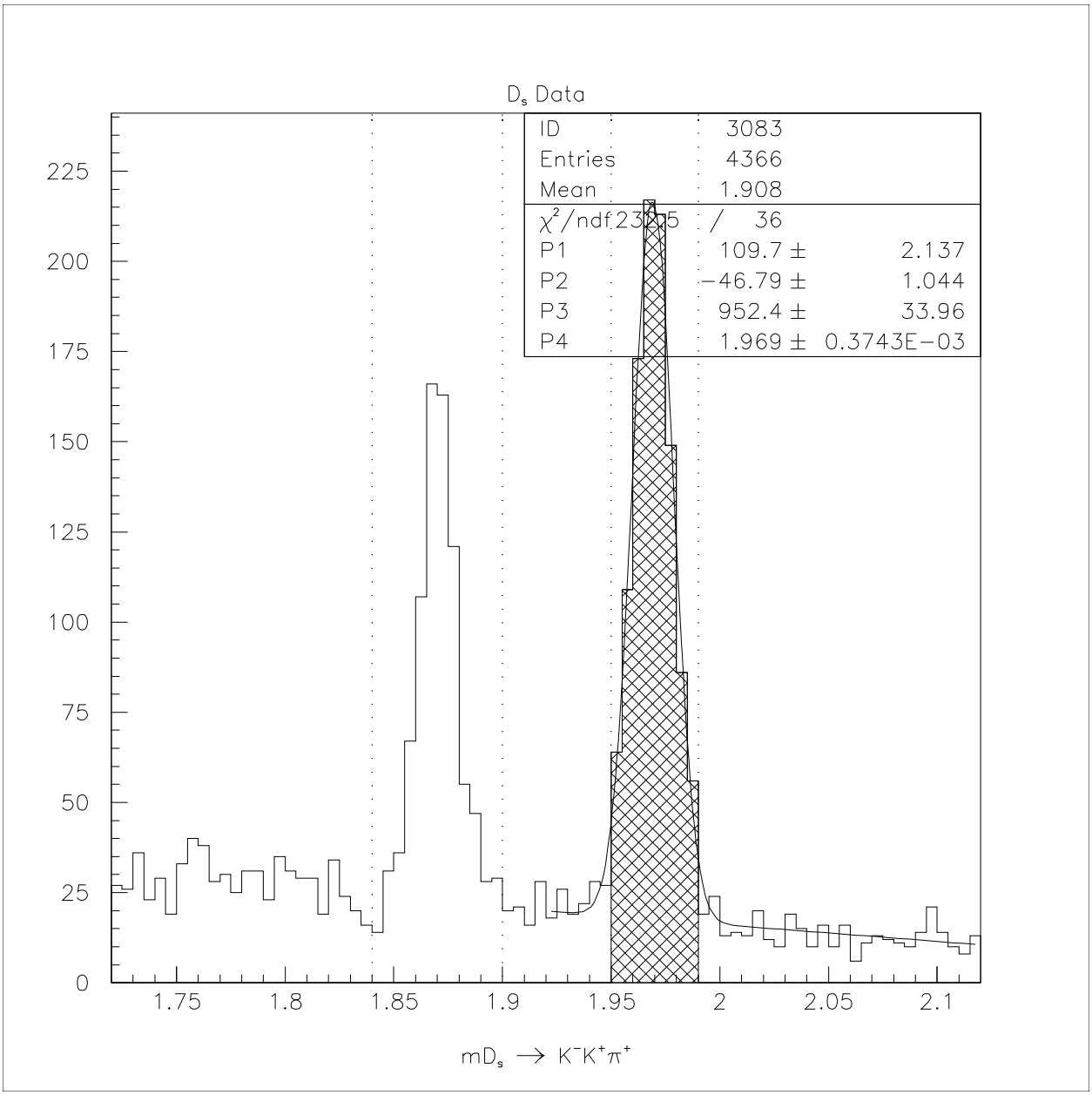

Figure 42:
Fitted data normalization $D_s^+ \to \phi\pi^+$ for the $D_s^+ \to \pi\ell\ell$ modes. Width fixed at 9.5 MeV/c^2.
Dotted lines are "box". Bin width = 5 MeV/c^2.

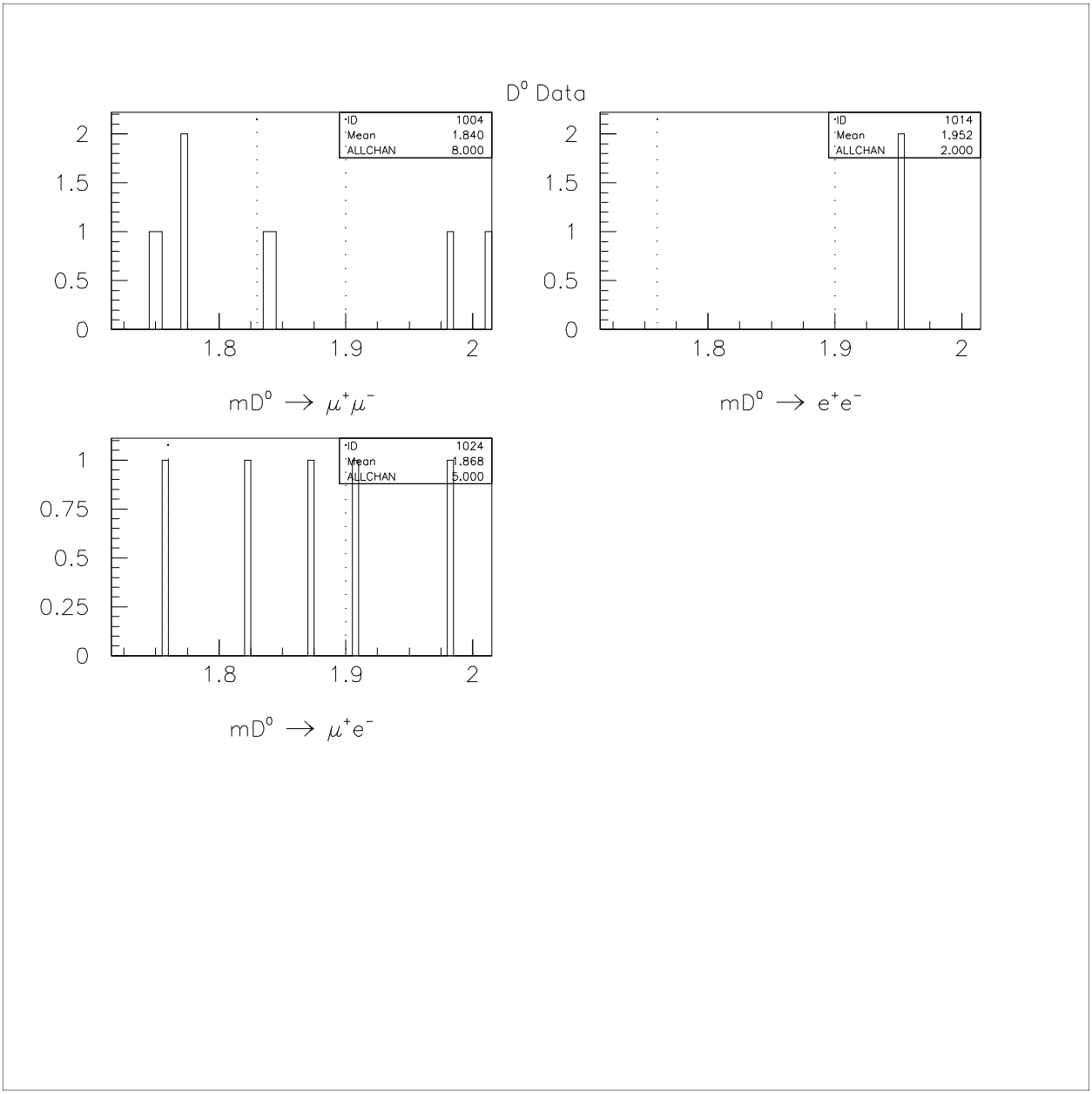

Figure 43:
D^0 data. Dotted lines are "box". Bin width = 5 MeV/c^2.

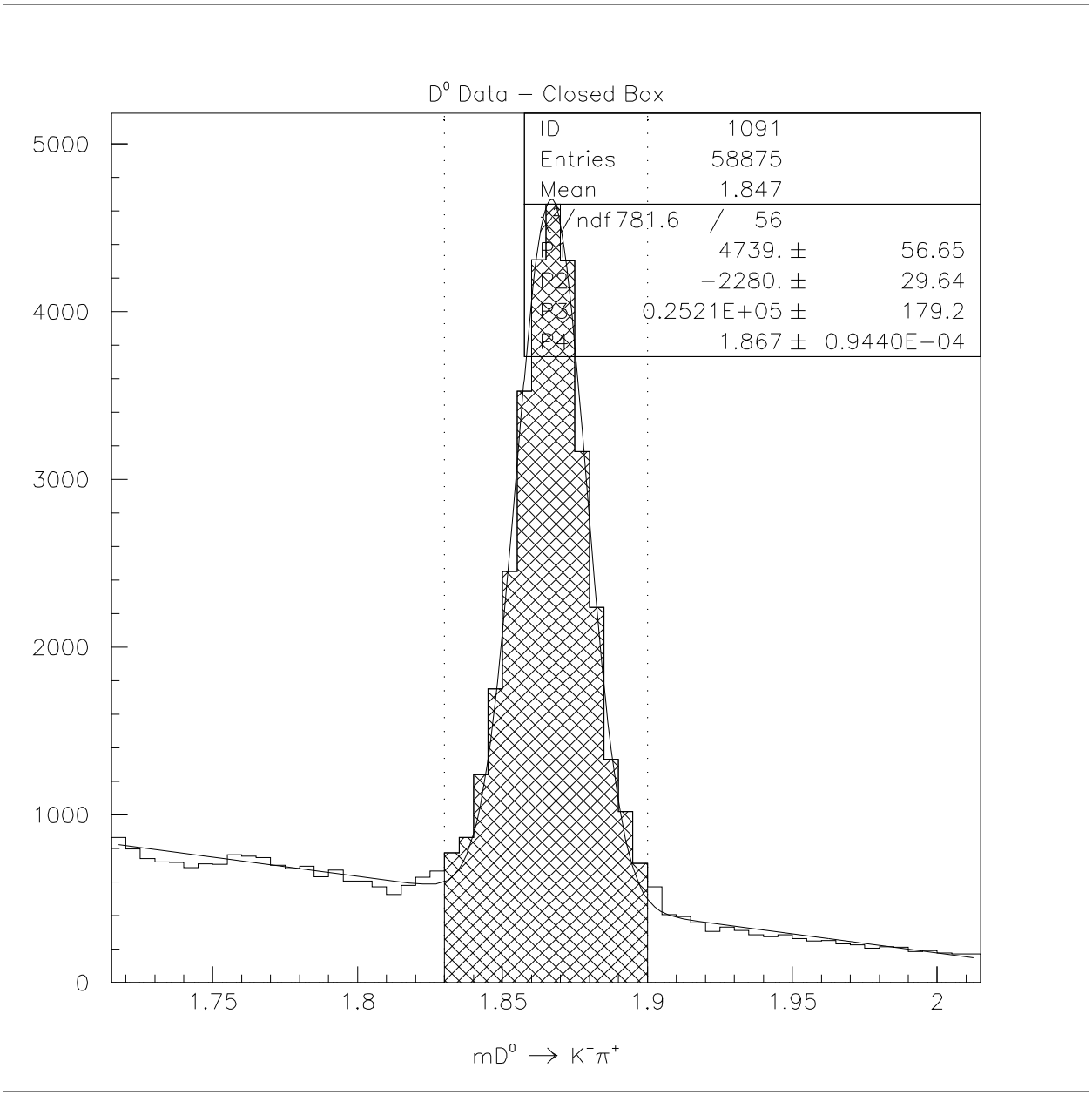

Figure 44:
Fitted data normalization $D^0 \to K^-\pi^+$. Width fixed at 12 MeV/c^2. Dotted lines are "box". Bin width = 5 MeV/c^2.

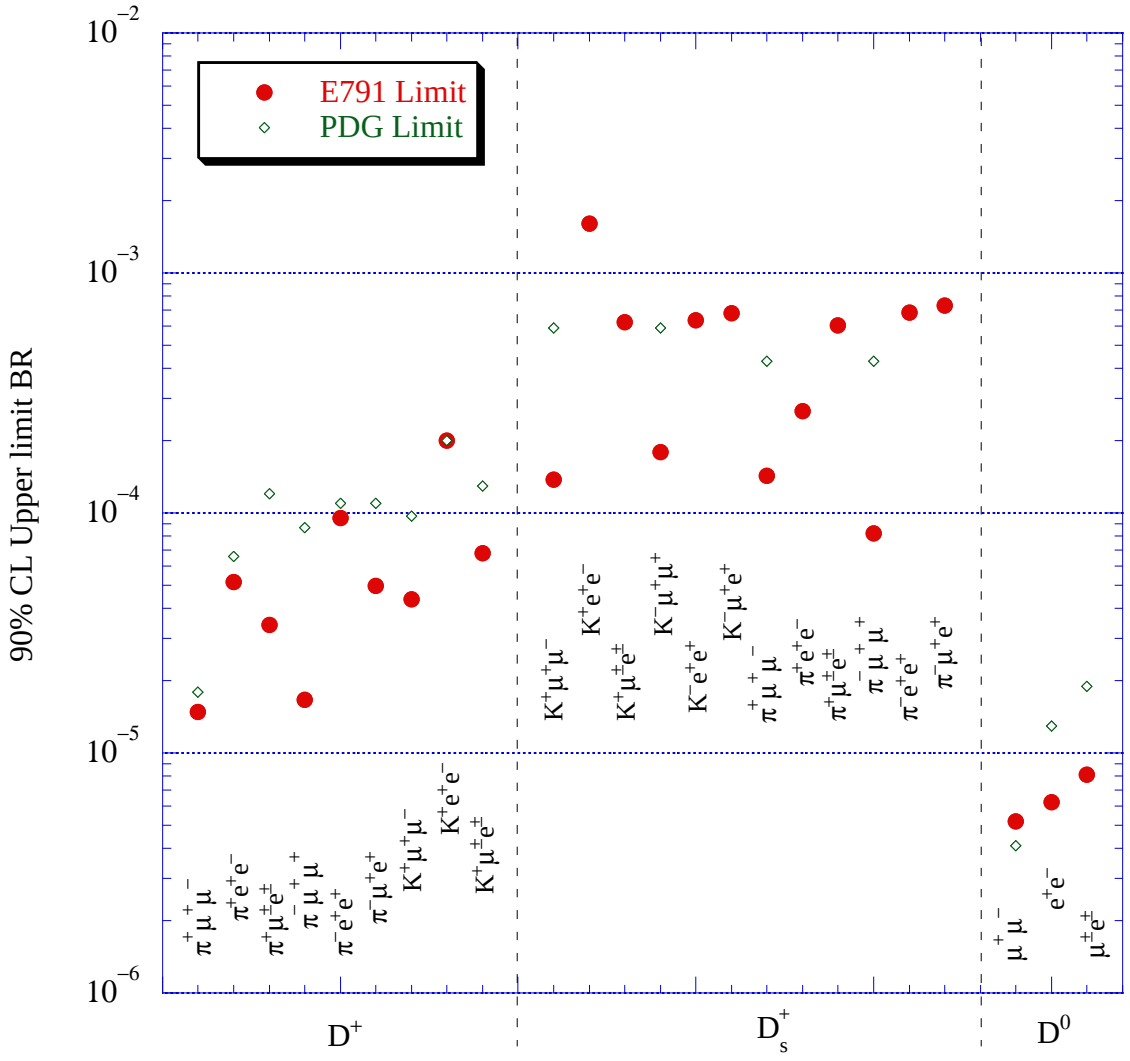

Figure 45:
The 90% CL Upper Limits of the branching ratios, corrected for systematic errors, are shown along with the 1998 PDG values.